

SYNTHESIS OF SILANE AND SILICON IN A NON-EQUILIBRIUM PLASMA JET

(NASA-CR-158374) SYNTHESIS OF SILANE AND SILICON IN A NON-EQUILIBRIUM PLASMA JET N79-20280
Final Report (AeroChem Research Labs, Inc.)
120 p HC A06/MF A01 CSCL 13H Unclas
G3/31 16664

FINAL REPORT

H.F. CALCOTE

OCTOBER 1978

The JPL Low-Cost Solar Array Project is sponsored by the U. S. Department of Energy and forms part of the Solar Photovoltaic Conversion Program to initiate a major effort toward the development of low-cost solar arrays. This work was performed for the Jet Propulsion Laboratory, California Institute of Technology by agreement between NASA and DoE.

AeroChem Research Laboratories, Inc.
Princeton, New Jersey



SYNTHESIS OF SILANE AND SILICON IN A NON-EQUILIBRIUM PLASMA JET

FINAL REPORT

H.F. CALCOTE

OCTOBER 1978

The JPL Low-Cost Solar Array Project is sponsored by the U. S. Department of Energy and forms part of the Solar Photovoltaic Conversion Program to initiate a major effort toward the development of low-cost solar arrays. This work was performed for the Jet Propulsion Laboratory, California Institute of Technology by agreement between NASA and DoE.

AeroChem **Research Laboratories, Inc.**
Princeton, New Jersey

FOREWORD AND ACKNOWLEDGMENTS

This is the final report on a program which started 20 July 1976.

The following people have made significant contributions to this program:

W. Felder, E.J. Louis, R.H. Mullen, R.L. Revolinski, and H.N. Volltrauer.

ABSTRACT

The original objective of this program was to determine the feasibility of high volume, low-cost production of high purity silane or solar cell grade silicon using a non-equilibrium plasma jet. The emphasis was changed near the end of the program to determine the feasibility of preparing photovoltaic amorphous silicon films directly using this method. The non-equilibrium plasma jet is produced by partially dissociating hydrogen to hydrogen atoms in a 50 to 100 Torr glow discharge and expanding the H/H₂ mixture through a nozzle. A high flux density of hydrogen atoms is thus produced at concentrations of about 3 mol % with about 30% energy utilization efficiency. The jet is mixed with a second reactant and the reaction proceeds at a temperature of 400 to 600 K to produce products. Yields of SiH₄, SiHCl₃, or SiH₂Cl₂ from SiCl₄ and SiHCl₃ were too low to be economically attractive. However, both amorphous and polycrystalline silicon films which strongly adhered to Pyrex, Vycor, aluminum, or carbon were prepared with either SiCl₄ or SiHCl₃ reactants. Preliminary doping experiments with PH₃ did not alter the electrical resistivity of these films. Strongly adhering films with SiH₄ reactant were more difficult to prepare; they were prepared by carefully cleaning the aluminum substrate, diluting the SiH₄ with about 90% argon, and forming the glow discharge between the mixing nozzle and the aluminum substrate. Doping such films with P by adding PH₃ reduced the electrical resistivity by two orders of magnitude. The non-equilibrium plasma jet should be further evaluated as a technique for producing high efficiency photovoltaic amorphous silicon films.

TABLE OF CONTENTS

	<u>Page</u>
ABSTRACT	iii
I. INTRODUCTION	1
II. PROGRAM CONCEPT	3
A. AeroChem Non-equilibrium Plasma Jet	3
B. Thermodynamic and Kinetic Considerations	4
III. APPARATUS	7
A. Experimental Parameters and Their Measurement or Control	7
1. Independent Parameters	7
2. Dependent Parameters	7
3. Apparatus Parameters	8
B. Apparatus Configuration	8
IV. CHARACTERIZATION OF HYDROGEN-ATOM SYSTEM	12
A. Electrical Discharge Stability	12
B. Measurement of Hydrogen-Atom Concentration	13
1. Energy Balance	13
2. Chemiluminescence Titration	16
3. Mass Spectrometer Titration	18
C. Hydrogen Atom Yields	19
V. SILANE, CHLOROSILANE, AND SILICON SYNTHESIS	21
A. Performance Limiting Conditions	21
B. In Situ Gas-Phase Analysis	26
C. Product Collection Experiments	26
VI. AMORPHOUS AND POLYCRYSTALLINE SILICON FILM PREPARATION	30
A. Films on Quartz Cylinders in Cross Flow	32
B. Film Preparation and Characterization	33
C. Water-Cooled Sample Holder Normal to Jet	39
D. Film Preparation with Restricted Recirculation	40
E. Film Preparation from Silane	41

PRECEDING PAGE BLANK NOT FILMED

	<u>Page</u>
VII. CONCLUSIONS	45
VIII. RECOMMENDATIONS	46
IX. NEW TECHNOLOGY	47
X. REFERENCES	48
APPENDIX A H-ATOM DECAY	107

LIST OF TABLES

<u>Table</u>		
I	COMPARISON OF EQUILIBRIUM CONSTANTS WITH HYDROGEN MOLECULES AND HYDROGEN ATOMS AS REACTANTS	51
II	EFFECT OF ELECTRON ENERGY ON THE CRACKING PATTERN OF CHLOROSILANES	51
III	HYDROGEN ATOM YIELD MEASUREMENTS	52
IV	CHARACTERIZATION OF NOZZLE NO. 6	54
V	MASS SPECTROMETRIC STUDY OF $H/H_2 + SiHCl_3$	55
VI	PRODUCT COLLECTION EXPERIMENTS	56
VII	CONDITIONS OF FIRST FILM DEPOSITION EXPERIMENTS	58
VIII	SUMMARY OF FIRST FILM DEPOSITION EXPERIMENTS FROM $SiCl_4$	59
IX	CONDITIONS FOR RUNS 116 TO 147	60
X	SOLID DEPOSITION EXPERIMENTS WITH VARIOUS REACTANTS	61
XI	CONVERSION EFFICIENCY OF REAGENT TO SILICON	63
XII	SOLID DEPOSITION EXPERIMENTS FOR $SiHCl_3$ REACTANT	63
XIII	SUMMARY OF NOZZLE NO. 6 FILM PREPARATION RUNS	64
XIV	SUCCESSFUL AMORPHOUS SILICON FILM DOPING EXPERIMENTS	67

LIST OF ILLUSTRATIONS

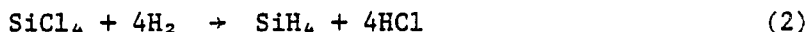
<u>Figure</u>		<u>Page</u>
1	NON-EQUILIBRIUM PLASMA JET FOR CHEMICAL SYNTHESIS	68
2	NON-EQUILIBRIUM PLASMA JET PROCESS FOR SYNTHESIS OF SILANE	68
3	NON-EQUILIBRIUM PLASMA JET APPARATUS	69
4	NON-EQUILIBRIUM PLASMA JET APPARATUS	70
5	NOZZLE ELECTRODES NO. 1, 2, AND 3 FOR NON-EQUILIBRIUM PLASMA JET GENERATION OF HYDROGEN ATOMS	71
6	FLOWER-PETAL NOZZLE (NOZZLE NO. 5)	72
7	COMPARISON OF DISCHARGE REGION GEOMETRY IN NOZZLES NO. 5 AND 2	73
8	ANNULAR NOZZLE NO. 6	74
9	RAKE INJECTOR	75
10	DISCHARGE STABILITY IN HYDROGEN Nozzle no. 1, cathode	76
11	DISCHARGE STABILITY IN HYDROGEN Nozzle no. 1, anode	77
12	DISCHARGE STABILITY IN HYDROGEN Nozzle no. 2, cathode	78
13	DISCHARGE STABILITY IN HYDROGEN Nozzle no. 2, anode	79
14	DISCHARGE STABILITY IN HYDROGEN Nozzle no. 3, cathode	80
15	DISCHARGE STABILITY IN HYDROGEN Nozzle no. 3, anode	81
16	DISCHARGE STABILITY IN HYDROGEN Nozzle no. 5, anode	82
17	CROSS SECTIONS AND ONSET ENERGIES IN H ₂	83
18	NO ₂ TITRATION CURVES	84

<u>Figure</u>	<u>Page</u>
19 DISCHARGE ENERGY EFFICIENCY AND HYDROGEN ATOM YIELD Nozzle no. 5, anode	85
20 DISCHARGE ENERGY EFFICIENCY AND HYDROGEN ATOM YIELD Nozzle no. 2, cathode	86
21 DISCHARGE ENERGY EFFICIENCY AND HYDROGEN ATOM YIELD Nozzle no. 2, anode	87
22 DISCHARGE ENERGY DISTRIBUTION	88
23 DISCHARGE ENERGY EFFICIENCY AND HYDROGEN ATOM YIELD Nozzle no. 5, anode	89
24 LIMITING PERFORMANCE CURVES $P_u = 50 \text{ Torr}, T_u = 300 \text{ K}; k_R = 1 \times 10^{-11} \text{ ml s}^{-1}$	90
25 LIMITING PERFORMANCE CURVES $P_u = 50 \text{ Torr}, T_u = 300 \text{ K}; k_R = 3 \times 10^{-10} \exp(-2500/T) \text{ ml s}^{-1}$	91
26 LIMITING PERFORMANCE CURVES $P_u = 50 \text{ Torr}, T_u = 1000 \text{ K}; k_R = 1 \times 10^{-11} \text{ ml s}^{-1}$	92
27 LIMITING PERFORMANCE CURVES $P_u = 50 \text{ Torr}, T_u = 1000 \text{ K}; k_R = 3 \times 10^{-10} \exp(-2500/T) \text{ ml s}^{-1}$	93
28 LIMITING PERFORMANCE CURVES $P_u = 300 \text{ Torr}, T_u = 300 \text{ K}; k_R = 1 \times 10^{-11} \text{ ml s}^{-1}$	94
29 LIMITING PERFORMANCE CURVES $P_u = 300 \text{ Torr}, T_u = 300 \text{ K}; k_R = 3 \times 10^{-10} \exp(-2500/T) \text{ ml s}^{-1}$	95
30 LIMITING PERFORMANCE CURVES $P_u = 300 \text{ Torr}, T_u = 1000 \text{ K}; k_R = 1 \times 10^{-11} \text{ ml s}^{-1}$	96
31 LIMITING PERFORMANCE CURVES $P_u = 300 \text{ Torr}, T_u = 1000 \text{ K}; k_R = 3 \times 10^{-10} \exp(-2500/T) \text{ ml s}^{-1}$	97
32 CALCULATED JET TEMPERATURES	98
33 EFFECT OF HEATING SEMICONDUCTOR GRADE SiCl_4 DEPOSIT TO 820 K FOR 22 HR	99
34 EFFECT OF EXPOSURE TIME ON SILICON FILMS DEPOSITED FROM SiCl_4	100

<u>Figure</u>		<u>Page</u>
35	X-RAY DIFFRACTION PATTERNS FOR SILICON FILMS	101
36	RATE OF SILICON DEPOSIT FROM SiHCl_3	102
37	WATER-COOLED SAMPLE HOLDER	103
38	RATE OF FILM DEPOSITION FROM SiCl_4	104
39	CONVERSION EFFICIENCY, SiCl_4 TO Si	105
40	SUBSTRATE HOLDER	106

I. INTRODUCTION

The hydrogenation of silicon halides and oxides to produce silanes or silicon using H_2 is difficult to achieve because of the considerable thermodynamic barriers involved. Reactions such as



and



are characterized by large positive free energy changes; equilibrium considerations therefore dictate small product yields or necessitate the use of expensive intermediates or exotic reaction conditions. However, when hydrogen atoms are substituted for hydrogen molecules in the above cases, the change in free energy becomes negative and equilibrium greatly favors the formation of desired products. The AeroChem non-equilibrium plasma jet is an efficient source of atomic species such as hydrogen atoms. In principle, therefore, this technique should permit work at lower temperatures with greater yields than are possible using hydrogen molecules.

This research program, designed to test the feasibility of this approach, began on 20 July 1976. Its specific objective was to determine the practicality of using the non-equilibrium plasma jet for the low cost, high volume production of silane and solar grade silicon. The chemical process of principal interest in this study was one based on the direct conversion of chlorosilanes to silane and/or silicon by reactions with hydrogen atoms. The non-equilibrium plasma jet provides the source of hydrogen atoms via the dissociation of hydrogen gas in an electrical discharge.

As the work progressed it became evident that the non-equilibrium plasma jet process would not meet the program objectives of low cost, high volume production of silane or solar grade silicon. At the same time it was observed that strongly adhering films of amorphous and polycrystalline silicon were being laid down on the reactor walls and that this process had considerable potential advantages over chemical vapor deposition (CVD) of polycrystalline silicon.¹ The substrate temperature with the non-equilibrium plasma jet can be low, a few hundred °C at most, compared to about 1000°C in other CVD processes. The lower temperature would mitigate the problems of substrate properties such as thermal stability and coefficients of expansion matching that of the deposited films. When compared to glow discharge deposition of photovoltaic amorphous silicon

films from silane,²⁻⁹ the non-equilibrium plasma jet increases the number of parameters available for manipulation to obtain a film with optimum qualities. This could be important since the mechanism by which the film is deposited is not understood. The present state-of-the-art indicates the need for methods of preparation which will lead to thin amorphous films with considerably greater efficiencies than the 6% realized to date. A process is envisioned in which the substrate is moved under a series of slot nozzles producing a wide ribbon of reactant jets directed at the substrate. The reactant would include dopants so that p or n type films could be laid down, one upon the other in a continuous process. Such a process could be very attractive for mass production. Of course, the problem of efficient photovoltaic energy conversion by amorphous or polycrystalline silicon, on which many others are working, must be solved for this to become a viable process.

The status of this effort is summarized in this report. In Section II the concept of the program is discussed with the arguments which led to its initiation. These arguments still seem valid although the ultimate results were disappointing in terms of the original objectives. It would take a more fundamental study than that carried out here to show where the rationale for the program's undertaking was wrong or where some important consideration was neglected. In the interest of understanding electrical discharge chemistry, this should be done. The apparatus and the complicated interaction of the various parameters are discussed in Section III. In Section IV the H/H₂ jet and electrical discharge system are characterized in terms of stable current-voltage-pressure regions in which the discharge can be operated, and the hydrogen atom concentrations and yields. The attempts to produce silane or chlorosilanes from SiCl₄ or SiHCl₃ are described in Section V. Experiments in which polycrystalline and amorphous silicon films were prepared and the characterization of these films are presented in Section VI where it is demonstrated that the process should be considered further for the direct preparation of photovoltaic amorphous silicon films. The main conclusions are presented in Section VII and recommendations are made in Section VIII. An appendix outlines the calculation of H-atom decay through the apparatus.

II. PROGRAM CONCEPT

A. AEROCHEM NON-EQUILIBRIUM PLASMA JET

Electrical discharges such as glows, coronas, and arcs have been studied for many years as tools for chemical synthesis and many compounds have been made in such devices.¹⁰⁻¹³ Nevertheless, they have not proven commercially useful except in a few instances (e.g., the production of ozone) because, generally, both the reactants as well as the products are exposed to the discharge, with the net effect of producing a wide distribution of products so that the yield of any specific product is very low. Separation costs then dominate the economics.

Discharges and discharge chemistry can be divided into low temperature systems and high temperature systems. In low temperature systems, which include glows, coronas, electrodeless discharges, and the so-called ozonator type discharges, the chemical reactions result from non-equilibrium production of ions and free radicals. In the high temperature discharge, where the discharge is produced by an arc, the gas temperature is raised to very high values (10,000 to 30,000 K is not uncommon) and one depends upon attaining a thermodynamic equilibrium favoring the desired product, e.g., acetylene, followed by rapid quenching to freeze out the desired product. Interest in MHD devices and re-entry problems stimulated considerable work in the sixties on arc or plasma jets.^{14,15} In these devices, a high temperature plasma is produced by an arc and the gases are caused to flow through a nozzle producing very high temperature jets in which the degree of dissociation is a result of the high temperature of the system.

A different approach¹⁶⁻¹⁸ is used in the AeroChem non-equilibrium plasma jet; one gas is passed through a low temperature glow discharge and expanded through a nozzle to produce a stream of highly ionized and dissociated gases at a relatively low temperature (300 to 1000 K). The degree of ionization and dissociation is very far out of equilibrium; in fact, to obtain the same degree of ionization and dissociation thermodynamically, the gas would have to be heated to several thousand degrees, e.g., 6000 K in a previously studied nitrogen system.¹⁸

The advantages for chemical synthesis of the AeroChem non-equilibrium plasma jet, Fig. 1, over conventional low temperature discharge systems and arc jet systems may be summarized as follows:

- (i) Energy is efficiently utilized; it is not wasted in heating the gas to a high temperature as in an arc jet.
- (ii) The actual reactant temperature can be very low, which frequently minimizes the occurrence of unwanted side reactions.
- (iii) Only one of the reactants is exposed to the discharge. This minimizes the products due to activation of the second reactant and, in addition, avoids destruction of the desired product by not exposing it to the discharge as in conventional low temperature discharge systems.
- (iv) A stream of highly reactive species is produced which can be utilized as reactants, e.g., atoms of oxygen, nitrogen, or hydrogen.
- (v) The low temperatures involved greatly minimize the materials problems encountered with arc jets.
- (vi) The high velocity possible in the exhaust stream stretches reaction time out in distance so that quenching at a particular stage of the reaction becomes feasible.
- (vii) Large throughputs are possible compared to conventional low temperature discharge systems.

The major disadvantage of the AeroChem non-equilibrium jet is that it must be operated at low pressure and thus requires vacuum pumps. Typically, in our experiments, pressures are held at 20 to 200 Torr in the discharge region and from 5 to 20 Torr in the downstream synthesis region. In addition, the concentration of reactant of interest, e.g., H atoms, is low, typically 3%. In any electrical discharge synthesis only high cost products should be considered. Silane and silicon are such products.

B. THERMODYNAMIC AND KINETIC CONSIDERATIONS

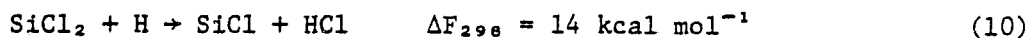
It can be easily demonstrated that starting with hydrogen atoms instead of hydrogen molecules greatly favors the production of SiH_4 and/or Si from SiO_2 or a chlorosilane. Equilibrium constants for some of the reactions involved are shown in Table I. It is apparent not only that hydrogen atoms favor the desired products over hydrogen molecules but also that the use of hydrogen molecules requires high temperatures and the use of hydrogen atoms requires low temperatures. This should impart a distinct advantage to the hydrogen

atom system because at low temperatures fewer side reactions are possible. When molecular hydrogen is used, high temperatures are in fact employed and many byproducts are obtained.

It is not easy to anticipate the kinetics of the system because reaction rate data are not available. However, the following set of reactions demonstrates that a thermodynamically favored path exists from reactant to product with no thermodynamic energy barriers.

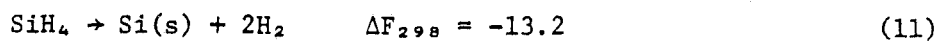
	ΔF_{298} kcal mol ⁻¹	
SiCl ₄ + H → SiCl ₃ + HCl	-16	(4)
SiCl ₃ + H → SiCl ₂ + HCl	-21	(5)
SiCl ₂ + H ₂ → SiCl ₂ H ₂	-27	(6)
SiCl ₂ H ₂ + H → SiClH ₂ + HCl	-14	(7)
SiClH ₂ + H → SiH ₂ + HCl	-18	(8)
SiH ₂ + H ₂ → SiH ₄	-27	(9)

Activation energies for all of the reactions would be expected to be low because they are free radical reactions and are also highly exothermic. Some obvious alternatives to the above set of reactions are not thermodynamically favored, e.g., the alternative to Reaction (6):



There are, of course, other possible paths from reactants to products; this scheme demonstrates that thermodynamically it is possible in a series of reasonable steps to get from reactant to product. There are also side reactions, e.g., radical recombinations which could give multisilicon molecules. Hydrogen atoms might be consumed by three-body recombination and wall reactions, but at the low pressures employed the three-body recombination will be slow and thus unimportant (see Appendix A) and the wall reaction can be minimized by increasing the reactor tube diameter.

The desired product, SiH₄, is thermodynamically unstable with respect to Si(s) and H₂ so the reaction could go all the way to silicon. This may not occur if the path from reactants to silicon is through SiH₄ because



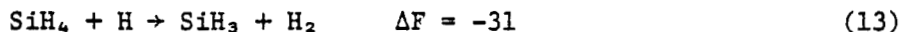
has an activation energy; SiH₄ is a stable molecule at ambient temperatures and must be heated to about 800 K to initiate decomposition. Further, if the

reaction goes through Si(g), the reaction



has $\Delta F_{298} = 83.9$ which probably accounts for the activation energy unless the reaction is carried out on a surface.

The presence of H atoms will, of course, initiate decomposition²⁰ via



If SiH₄ were the desired product the reaction might be quenched at that point by flooding with molecular hydrogen or quenching on a cold surface. On the other hand, silicon could be the desired product, e.g., as photovoltaic amorphous or polycrystalline silicon films.

It thus seemed reasonable to attempt to synthesize SiH₄ or Si by means of the non-equilibrium plasma jet. As stated by Jolly,²¹ "The art of predicting the course of discharge reactions is primitive and unreliable." Experiments must be performed.

A schematic of a possible process for carrying out either Reaction (2) or (3) in Table I is shown in Fig. 2.

III. APPARATUS

The apparatus in which this study was conducted, Figs. 3 and 4, has evolved during the course of this program. It consists of a glow discharge region in which hydrogen is partially dissociated into hydrogen atoms and the resulting H/H₂ mixture is then expanded through a nozzle where it is rapidly mixed with the second reactant and allowed to react. The products are identified in situ with a mass spectrometer, collected in cold traps, or deposited on solid surfaces. The important parameters in the experiment are discussed below followed by a detailed description of the apparatus.

A. EXPERIMENTAL PARAMETERS AND THEIR MEASUREMENT OR CONTROL

The experimental parameters to be measured and the means of measurement and control are:

1. Independent Parameters

- a. Current, I - measured with panel meter of power supply.
- b. Reagent flow rates, \dot{m}_{H_2} , \dot{m}_{SiCl_4} - measured with sonic orifice flow meters and varied by controlling the upstream pressure.
- c. Reaction section pressure, P_d - measured with Bourdon gauges or an electronic manometer and varied by a valve in the pump line.

2. Dependent Parameters

- a. Voltage, V - measured using power supply panel meters. The current setting and the physical conditions of the discharge section, including electrode/nozzle spacing, discharge pressure, and hydrogen flow rate, determine the voltage at which the discharge operates.
- b. Pressure in discharge section, P_u - measured with Bourdon gauges or an electronic manometer. The hydrogen flow rate, nozzle dimensions, and discharge conditions determine the discharge pressure. The pressure is measured with and without the discharge operating.
- c. Temperature in the reacting stream, T_d - estimated from increase in P_u on turning discharge on and the expansion ratio (see Section IV.B.1).
- d. Energy lost to the electrode and nozzle - obtained by measuring the temperature increase with mercury thermometers for water flowing at a known, fixed rate through these parts.

e. Hydrogen atom flow rate, \dot{m}_H - determined by a chemiluminescence titration (Section IV.B.2) or by an energy balance (Section IV.B.1).

3. Apparatus Parameters

The important apparatus parameters are:

a. Physical dimensions, and possibly electrode/nozzle materials, in the discharge section including electrode/nozzle distance and nozzle diameter. The nozzle diameter should be important in determining the energy loss to the nozzle and thus very important for scaling.

b. Means of mixing the second reactant with the partially dissociated hydrogen stream.

c. Type of discharge. Most experiments were carried out with dc glow discharges where the electrode was the cathode and the nozzle the anode. Preliminary experiments demonstrated this to be the most desirable configuration.

B. APPARATUS CONFIGURATION

The apparatus, Figs. 3 and 4, was designed with all of the above in mind so that changes could be made easily. The piping was originally 70 mm i.d. Pyrex pipe with standard pipe flanges so that any section could easily be removed for cleaning or replacement. Subsequently the reaction section was made of two 140 mm i.d. standard Pyrex pipe crosses for easy access, for example, to place substrates in the jet stream. The system was originally pumped by a 70 ℓ s^{-1} mechanical pump which was replaced by a 140 ℓ s^{-1} mechanical pump. The original Bourdon type pressure gauges were replaced with a single Pace Engineering capacitance pressure transducer module and a pressure measuring manifold so that pressures in various parts of the system could be measured alternately on the same pressure gauge.

The chlorosilane delivery system consists of a constant pressure boiler and reflux column. Nitrogen gas flows continuously over the top of the reflux column at ambient pressure, thus maintaining the pressure of chlorosilane on the upstream side of a needle valve at 1 atm. This needle valve is used to control the chlorosilane flow rate which is measured by measuring the upstream pressure of a critical flow orifice in the line. Any one or a combination of four orifices may be selected by toggle valves to give a large range of chlorosilane flows. The temperature of the critical flow orifice module is controlled by a thermostat to maintain the chlorosilane in the vapor

phase. Hot water from a separate thermostatically controlled water heater is flowed through the jacketed chlorosilane boiler to reflux the chlorosilane.

Electric power for the discharge is supplied by a Universal Voltronics "Labtrol" high voltage dc power supply, rated to ≈ 22 kVA with variable reactance current limiting. Maximum continuous output is 4 A at 4 kV adjustable in three ranges each; current: 0-0.6, 0-1.5, and 0-4 A; voltage: 0-0.5, 0-1.8, 0-4.0 kV. This is far more than adequate. The water-cooled electrode is a cylinder 1.75 cm diam and 30 cm long with a spherical end. The discharge takes place between this end and the nozzle walls so that any gas flowing into the nozzle must flow through the discharge. The "isolation tube," Fig. 3, simply helps define the gas flow path.

Several nozzles and reactant mixing schemes have been used, Figs. 5-8. In initial experiments with nozzles no. 1, 2, and 3 the chlorosilane was added to the H/H₂ jet by a single tube injection system, either countercurrent or with the stream. It is desirable that the injector give extensive, rapid mixing with minimum disturbance to the stream. These are conflicting requirements and are the same requirements encountered in chemical lasers.^{22*} Several techniques were tried. The rake injector, Fig. 9, has the virtue of simplicity so it was used while the flower-petal nozzle, Fig. 6, was being designed and constructed.

The flower-petal nozzle (no. 5) represents several compromises. The entrance section is smoothly contoured to minimize entrance flow disturbances but the expansion angle and length of the diverging section are somewhat arbitrary. Ideally, these should be tailored to each set of upstream and downstream conditions imposed, but since the experiments were carried out over a range of conditions, it was more expedient to accept some design compromises for savings in time and money. A large cone angle was chosen to allow flow separation within the nozzle during expansion. The nozzle material is brass, chosen for ease of machining. The nozzle is internally water-cooled and contains means of distributing SiCl₄ (or other reactant) to the four quartz reactant feed tubes which are held in the nozzle by epoxy cement. The placement of these tubes, either at an angle to the jet or parallel to it, is another compromise. Initial visual observations using the chemiluminescence arising

* The advice of Prof. Seymour Bogdonoff, Princeton University, with the problems discussed in this section is gratefully acknowledged.

from injecting NO into air and N₂ discharges indicated that the angled placement results in better mixing but more jet breakup than the parallel placement. In both cases, jet integrity was enhanced relative to the original, rather crude nozzles and reactant injection systems.

The placement of the injector tubes shown in Fig. 6 was determined from a calculation of the gas dynamic diameter of the jet stream. It was desired to assure that the four quartz reactant feed tubes were within the calculated diameter of the stream. The standard equation for the ratio of throat to exit areas of a supersonic nozzle (assuming isentropic perfect gas expansion) was employed:

$$\frac{A_t}{A_x} = \left(\frac{\gamma + 1}{2} \right)^{\frac{1}{\gamma-1}} \left(\frac{P_d}{P_u} \right)^{\frac{1}{\gamma}} \left(\frac{\gamma + 1}{\gamma - 1} \left[1 - \left(\frac{P_d}{P_u} \right)^{\frac{\gamma-1}{\gamma}} \right] \right)^{1/2} \quad (14)$$

where γ = ratio of specific heats of fluid, P_u = upstream pressure, and P_d = downstream pressure. For the nozzle in Fig. 6 with a throat diameter of 6.9 mm this gives

P_u/P_d	A_t/A_x	Jet Diameter mm
2	1.00	6.9
3	0.918	7.2
4	0.826	7.6
5	0.748	8.0
6	0.685	8.3
7	0.633	8.7

These values are much smaller than the apparent (visual) diameter which is certainly larger than calculated because of the mixing layer.* They also indicate that a unique spacing and placement of injectors should be used for optimum mixing for each pressure ratio. Again, for expediency, this error was accepted.

To further improve the mixing and still maintain the integrity of the jet, an annular subsonic flow nozzle, no. 6 (see Fig. 8) was designed and built. It

* The difference will be far less in a larger system.

was installed via a flange nozzle-holding plate (Fig. 8b). This nozzle design allows chlorosilane vapor to flow into the H/H₂ jet from a small annular opening. The expanding hydrogen stream should mix intimately with the outer ring of heavier chlorosilane and still maintain a reasonably well-defined jet for some distance. The nozzle is water cooled. The extent of mixing and the integrity of the jet produced were first tested by feeding NO₂, instead of a chlorosilane, through the annular orifice surrounding the H/H₂ jet core, because the reaction with NO₂ produces a visible jet and the chlorosilane does not. Good mixing was indicated by the luminosity near the nozzle exit. Over a range of conditions near Mach no. ≈ 1 (the conditions for which the nozzle was to be used) the jet was about 10 cm long before it broke up.

In operating the discharge it was found that alignment of the anode with the nozzle centerline was critical for reproducible operation. Therefore, a three-point alignment jig was attached externally to the cylinder electrode to allow centering the discharge.

A sample for mass spectrometric analysis is taken through a separately pumped, water-cooled sampling probe, which lies on the centerline of the H/H₂ jet in the reaction section. The probe is traversible from the nozzle exit plane to about 50 cm downstream. Samples are drawn through a 0.18 mm orifice at the tip of a 20° taper cone. This configuration was designed to minimize shock interference effects in the jet.

A simple magnetic type mass spectrometer was used with the in situ sampling probe, Fig. 3, and for analysis of products collected in the cold traps. Because this instrument was designed to operate at a fixed electron energy of 70 eV and it was suspected that some of the difficulty in observing products was due to the mass spectrometer, a more sophisticated quadrupole instrument was used to measure the cracking patterns of the three chlorosilanes, SiCl₄, SiHCl₃, and SiH₂Cl₂, as a function of electron energy. The cracking patterns were distinctively simplified as the electron energy was decreased, Table II. The magnetic instrument was thus modified so that the electron energy could be varied. However, experiments with reduced electron energies indicated that a severe loss in sensitivity accompanied such a reduction. A compromise electron energy of 50 eV provides both good selectivity between the masses of interest and satisfactory sensitivity.

IV. CHARACTERIZATION OF HYDROGEN-ATOM SYSTEM

Those aspects of the experiment which relate to the production of the H/H₂ jet are discussed in this section. This includes experiments to determine the discharge stability, techniques for determining the concentration of hydrogen atoms (which turned out to be a more difficult problem than originally envisioned), and determination of hydrogen atom yields, i.e., the efficiency of producing hydrogen atoms.

A. ELECTRICAL DISCHARGE STABILITY

Experiments were made to determine the stable regions with respect to the discharge current, voltage, and pressure in which a glow discharge can be maintained. The results are reported in Figs. 10-16. The reported pressures are those prevailing prior to initiating the discharge, with the hydrogen mass flows fixed.

The low current limit on the discharge stability diagrams, Figs. 10-16, is determined simply by the disappearance of the glow. This is noted on the stability curves as "extinction." In some cases the highest pressures and thus highest voltages were limited by the capability of the hydrogen flow system.

The most dramatic effects were observed at the high current limits. When the nozzle was the cathode, an increase in current produced an intense white glow within the nozzle. Occasionally, a local arc appeared on the downstream side of the nozzle plate -- frequently dancing around, and in and out, of the nozzle throat. When this occurred, the voltage dropped abruptly, as expected for the transition from a glow to an arc. This region is indicated on the stability curves as "nozzle arc." When the nozzle was the anode, the discharge was more stable and the maximum current was limited by overheating of the water-cooled cathode -- it glowed bright red. Better cooling of the cathode should allow these curves to be extended to higher discharge currents.

With the smaller nozzles, nos. 1 and 3, there was no marked difference in the stability regions for the nozzle in the cathode or anode mode, compare Fig. 10 with 11 and Fig. 14 with 15. There was, however, a marked difference between these modes with the larger nozzle (no. 2) as can be seen by comparing Figs. 12 and 13. For the larger nozzle, the glow discharge stability region

was larger in the nozzle as anode mode. The differences between the stability regions for the two different sized nozzles is probably due to differences in gas flow conditions at the nozzle entrance; this indicates that the stability curves, and presumably the H-atom concentrations, could be controlled somewhat by altering the gas flow in that region. It is also interesting that in either mode, the stainless steel nozzle, Figs. 14 and 15, operated at higher currents than did the brass nozzle, Figs. 10 and 11. This may be due to the somewhat different configuration of this nozzle, Fig. 5, or it may be due to the different material -- we are inclined to favor the latter view.

B. MEASUREMENT OF HYDROGEN-ATOM CONCENTRATION

1. Energy Balance

The hydrogen atom concentration was estimated from an energy balance, assuming the total electrical energy is distributed as follows:

Total energy input = Energy lost to electrodes + Energy
to heat the gas + Energy to excite the hydrogen to
non-equilibrium states

It is assumed that all of the energy that goes into non-equilibrium excitation of hydrogen is used to dissociate the hydrogen to produce hydrogen atoms. The total energy input is measured by measuring the discharge current and voltage; the energy lost to the electrodes is obtained by measuring the temperature increase of water flowing at a known, fixed rate through the cathode (electrode) and anode (nozzle) (Fig. 3). Generally, about 70% of the coolant energy loss is to the cathode and 30% to the anode.

The energy used in heating the gas was calculated from pressure measurements in the discharge section. It is assumed in making this calculation that, except for the energy going into dissociating the hydrogen, all the energy absorbed by the gas simply raises the gas temperature. This neglects any energy in non-equilibrium ionization, which probably ends up as dissociation, and any energy involved in non-equilibrium vibrational excitation (see subsequent discussion). The upstream temperature, actually the temperature at the entrance to the nozzle throat, is obtained from measurements of the rise in the discharge section pressure when the discharge is turned "on" relative to when the discharge is turned "off" by using the equations for mass flow through a choked (supersonic flow) nozzle:

$$\dot{m} = CPA \left(\frac{MW}{RT} \right)^{1/2} \Omega \quad (15)$$

where C = nozzle coefficient

P = upstream pressure, dyne cm²

A = area of orifice, cm²

MW = molecular weight of gas flowing through nozzle, g mol⁻¹

R = gas constant, erg mol⁻¹, -K

T = upstream temperature, K

Ω = function of specific heat ratio, γ , computed from

$$\Omega = \sqrt{\gamma(2/(\gamma + 1))} ((\gamma + 1)/2(\gamma - 1))$$

Writing this equation for the "discharge off" and "discharge on" conditions, assuming the nozzle coefficient is constant, and taking the ratio yields

$$T_u = \left(\frac{P_u}{P_o} \right)^2 \left(\frac{\Omega_u}{\Omega_o} \right)^2 \frac{MW_u}{MW_o} T_o \quad (16)$$

where the subscripts u and o pertain to discharge on and discharge off conditions, respectively. It should be noted that, with the discharge on, the molecular weight of the gas in the discharge section and the Ω of the gas are functions of the degree of dissociation, ϕ . Additionally, Ω is a function of the temperature. In terms of ϕ

$$MW_u/MW_o = \frac{1}{2}(2/(1 + \phi)) = (1 + \phi)^{-1} \quad (17)$$

Substituting Eq. (17) into Eq. (16) yields

$$T_u = (1 + \phi)^{-1} \left(\frac{P_u}{P_o} \right)^2 \left(\frac{\Omega_u}{\Omega_o} \right)^2 T_o \quad (18)$$

Calculations of the values of Ω as functions of ϕ and T_u show that for $0.0 \leq \phi \leq 0.05$ (i.e., up to 5% dissociation) and $300 \leq T_u \leq 2000$ K, the ratio

$$1.00 \leq (\Omega_u/\Omega_o)^2 \leq 1.05$$

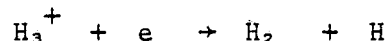
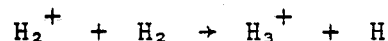
nearly cancels $(1 + \phi)^{-1}$ and thus, Eq. (18) is written:

$$T_u = \left(\frac{P_u}{P_o} \right)^2 T_o \quad (19)$$

The energy utilized in heating the gas is then calculated from the differences in enthalpy content at the two temperatures. On expansion through the nozzle, part of this energy will be converted to gas velocity, reducing the static gas temperature.

The above procedure assumes isentropic flow, i.e., flow through a smoothly converging-diverging nozzle. It also assumes no heat losses to the nozzle, which our measurements show to be appreciable, and further, it assumes that all the energy is added to the gas upstream of the nozzle entrance. Since the discharge appears to penetrate the nozzle throat, some unknown portion of the energy is added in the throat which would also increase the upstream pressure. The extent of errors introduced by these deviations from the ideal has not been evaluated.

The assumption that all of the unaccounted for energy is used in dissociating hydrogen was further considered. Figure 17 shows cross sections and onset energies for a number of processes^{23,24} which could contribute to the unaccounted for energy superimposed on the Maxwell-Boltzmann electron energy distribution for the present experimental system at $P_u^0 = 50$. The electron energy distribution was estimated using the method of von Engel.²⁵ Ionization processes would lead to hydrogen atoms via:



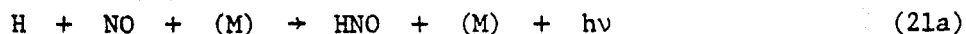
Processes such as direct vibrational excitation and radiative cascade from electrically excited states formed in the discharge will form vibrationally excited hydrogen. If the processes degrading this energy to rotation and translation are slow with respect to the time for the gas to expand through the nozzle, large concentrations of vibrationally excited H_2 should be found in the jet. Thus all of the unaccounted for energy is not used in dissociating hydrogen--some must end up as vibrationally excited H_2 and thus the H-atom concentration calculated by this technique must be an upper limit.

2. Chemiluminescence Titration

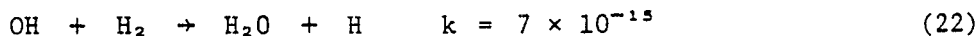
In this method increasing amounts of NO₂ are added to the discharge exhaust until the titration endpoint is reached (NO₂ flow equals H-atom flow) where the chemiluminescent glow is extinguished. Hydrogen atoms are removed by the titration reaction upon every collision²⁶



As long as the flow rate of NO₂ is less than that of H atoms, the NO formed in Reaction (20) goes on to react with a hydrogen atom in the indicator reaction to produce visible-ir light (600-800 nm)



The overall rate coefficient²⁷ ($k_{21a} + k_{21b}$) $\approx 6 \times 10^{-32} \text{ cm}^6 \text{ molecule}^{-2} \text{ s}^{-1}$ (proceeds about 1/10⁴ H/NO encounters under the conditions used). In our system these reactions result in a ≈ 75 cm long visible chemiluminescent glow. When sufficient NO₂ is added to consume all of the H atoms via Reaction (20) thus cutting off the supply for Reaction (21), the chemiluminescent glow is sharply reduced, shrinking back to within a few cm of the NO₂ inlet. This is taken as the endpoint of the titration, where the flow rates of NO₂ and H are equal. In the presence of a large excess of H₂, i.e., when the [H]/[H₂] ratio is much less than unity, the reaction^{24,28}



may become important unless observation times are short (i.e., linear flow velocity is large) and the production of H in Reaction (22) is far removed from the observation region.

The NO₂ titration is made with a photomultiplier (PMT) (RCA IP28) observing the light emitted perpendicular to the axis of the reaction tube. Intense background light reaching the PMT from the discharge itself gives a signal which is electrically "bucked-out"; the titration is performed by taking the endpoint where the chemiluminescent light intensity goes to zero. The bucked-out background signal generally registers about 5×10^{-8} A and the maximum light emitted in the titration generally registers about 10×10^{-8} A.

The above technique was also used in a modified form for convenience by measuring the relative light output for the chemiluminescent Reaction (21). For this experiment NO was added instead of NO₂ and a 1P28 PMT was placed

50 cm downstream of the nozzle. For each run the relative chemiluminescence intensity of the H/NO reaction was put on an absolute scale with an NO₂ titration. It was verified that, for small NO flow rates* ($f(\text{NO}) < f(\text{H}) \ll f(\text{H}_2)$), the chemiluminescence intensity is linearly proportional to the flow rate of NO and H. The flow rate of NO was chosen so that $f(\text{NO}) \leq 0.1 f(\text{H})$.

A set of tests was made in which the titration observation point, i.e., PMT location, was varied from 10 to 36 cm downstream of the nozzle to determine whether there is an effect of observation distance or downstream pressure on the observed H-atom concentration. The data qualitatively indicated that, at downstream pressures greater than about 30 Torr, measurement distance affects H-atom concentration determinations--lower values being measured at the larger distances (≥ 20 cm) than at the shorter distances. Quantitative interpretation of the data, however, was complicated by scatter ($\approx 30\%$) in the measurements. This scatter masked differences (if any) among measurements for distances < 20 cm and downstream pressure < 30 Torr.

To further check the titration technique two complete titration curves were generated, Fig. 18, with the endpoints indicated where the light intensity goes to zero. For comparison, theoretical curves, derived as follows, are also indicated: The relative intensity, I/I_{max} , of the chemiluminescent reaction is proportional to the flow rates (concentrations) of H atoms and NO, and is governed by Reactions (20) and (21a). When the flow rate of H atoms exceeds the flow rate of NO₂, each NO₂ will produce an NO molecule in the rapid²⁶ Reaction (20) by consuming an H atom. Thus, the H and NO flow rates will be related to the initial (no NO₂ addition) flow rate of H, f_{H_0} and the flow rate of NO₂, f_{NO_2} by:

$$\left. \begin{aligned} f_{\text{H}} &= f_{\text{H}_0} - f_{\text{NO}_2} \\ f_{\text{NO}} &= f_{\text{NO}_2} \end{aligned} \right\} \text{for } f_{\text{NO}_2} < f_{\text{H}_0}$$

The intensity emitted will be

$$I = k_{21a} f_{\text{H}} f_{\text{NO}} = k_{21a} (f_{\text{H}_0} - f_{\text{NO}_2}) f_{\text{NO}_2}$$

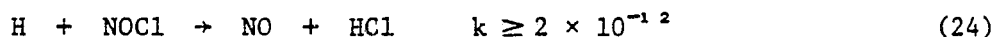
* $f(\text{X}) \equiv$ the flow rate of X.

Thus,

$$I/I_{\max} = \frac{k_{21a} (f_{H_0} - f_{NO_2}) f_{NO_2}}{k_{21a} (f_{H_0} - \frac{1}{2} f_{H_0}) \frac{1}{2} f_{H_0}} = 4 \frac{(f_{H_0} - f_{NO_2}) f_{NO_2}}{f_{H_0}^2} \quad (23)$$

The theoretical curves shown in Fig. 18 were obtained by normalizing the calculated values to the observed endpoints. The detailed differences in peak positions and shapes between the calculated and experimental curves are not considered significant.

Experiments using the NO₂ or NO technique turned out to be more complicated than expected; the endpoints were not distinct and the concentration of H atoms appeared to vary with distance more than expected. Thus an alternate titration reaction



followed by Reaction (21a) and (21b) was also used. In this system secondary reactions which complicate the interpretation are not present.²⁹ The results are compared in Fig. 19 in which excellent agreement with the NO₂ and NO titrations is shown. This indicates that the chemical assumptions are correct for the conditions of this experiment.

3. Mass Spectrometer Titration

Attempts near the end of this program at characterization of nozzle no. 6 by observing the endpoint of the chemiluminescent titration of H atoms with NO₂ were thwarted by difficulties in observing the endpoint. Consideration was then given to the possibility of determining the endpoint by use of a small sampling probe connected to a mass spectrometer. This method, in addition to its potential for determining the H-atom concentration, could also be used to determine the extent of mixing and rates of chemical reaction. The probe would be moved both across the stream and parallel to the stream flow to map out concentration contours. The first set of experiments would be used to determine the extent of mixing, using a reaction for which the kinetics are fairly well known, e.g., NO₂ + H, and then the technique could be used to study the rates of the H + SiCl₄, SiHCl₃, or SiH₄ reactions. Only one experiment (time limitation) was carried out in which the NO₂ concentration was monitored with the mass spectrometer; a very clean endpoint was obtained.

C. HYDROGEN ATOM YIELDS

Hydrogen atom yields were obtained for nozzles no. 1 and 2 for a number of conditions and the results are reported in Table III. The total energy input is divided among the electrode and nozzle "coolant," "gas heating," and dissociation of the hydrogen. The energy to dissociate the hydrogen was calculated from the H-atom concentration determined by the NO₂ titration or the NO relative light intensity measurement.

The data in Table III indicate that, for the specific physical configuration employed,* the power efficiency for H-atom production is greatest for the larger nozzle, with the nozzle as anode, (compare Figs. 20 and 21)[†] and at a pressure of 50 Torr (compared to 25 and 225 Torr). Higher H-atom concentrations were achieved with nozzle no. 1 (3.5% vol) but at a lower discharge energy efficiency, only 1.5 mol H/kWh. Assuming isentropic expansion through the nozzle and a downstream pressure of 30 Torr, the gas temperature in the H/H₂ jet would be about 420 K. For comparison, the gas would have to be heated to an equilibrium temperature of about 2200 K to attain the measured H-atom concentration of 2.7% for nozzle no. 2 at a 30% efficiency of energy utilization in producing hydrogen atoms. This clearly demonstrates the non-equilibrium nature of the jet. Because of the large number of as-yet-unstudied variables, these conditions are probably far from optimum. Yet the results were sufficiently encouraging to proceed to the chemical synthesis studies.

Measurements on H-atom production with the flower petal nozzle, no. 5, Fig. 6, with the angled quartz reactant feed tubes in and without these tubes indicated H-atom concentrations and discharge energy efficiencies about a factor of two less than those obtained with nozzle no. 2, cf., Figs. 19 and 21. The reasons for this are not understood.

In view of the lower H-atom concentrations and discharge energy efficiencies measured for nozzle no. 5 and the additional experience gained with the titration techniques, the nozzle no. 2 measurements were repeated to validate those data

* Physical configuration here means the combination of electrode distances, water-cooled electrode diameter, isolation tube diameter, and flow conditions at the entrance section of the nozzle. The results are probably dependent on these parameters.

[†] Some of the data in Fig. 21 were taken from subsequent runs.

and to further check the titration methods. The H-atom concentration and discharge energy efficiency are presented in Fig. 21. The points for H-atom concentration include the original data (Table III, runs 4 and 6), a new NO₂ titration (run 107), and an NO relative measurement normalized to the NO₂ titration curve at 1200 W (runs 108 and 109). While the data are somewhat scattered, the results confirm the original measurements of high H-atom concentrations and efficiencies.

The energy distribution for the nozzle no. 2 data is shown in Fig. 22. The fact that very nearly 100% of the energy is accounted for increases confidence in the validity of these results. Of course, the problem raised by these results is that the H-atom concentration and energy efficiency of the simple nozzle are greater than those of the more complex nozzle. Interestingly, at higher pressures both nozzles, no. 2 and no. 5,* show a trend of increasing yield and efficiency with increasing power (cf., Table III with Fig. 23). Comparing nozzles no. 5 and no. 2, a major difference can be seen in the nozzle entrance section geometry (Fig. 7) as well as a small difference in the electrode-nozzle spacing. Time limitations in the present work prevented study of such source geometry factors. These are known to be important from previous work (e.g., Refs. 17, 18, 30). A second difference was in the means of measuring the H-atom concentrations. For nozzle no. 2 the titrant was injected by a simple 1.5 mm i.d. (2.4 mm o.d.) alumina tube placed \approx 0.5 cm downstream from the nozzle exit plane with titrant flow countercurrent to the H/H₂ jet flow; for nozzle no. 5 the titrant flowed either through quartz feed tubes in the nozzle, Fig. 6, or through holes in the nozzle wall, Fig. 7. The different results obtained using these two injection methods with nozzle no. 5 indicate a possible mixing effect on the H-atom titration technique.

Hydrogen atom concentrations in the jet were determined for nozzle no. 6 over a range of operating conditions, by the energy balance technique. Measurements were made over a range of input powers from 800 to 2200 W and the distribution of energy between coolant, gas heating, and H-atom production showed very little variation with power input--probably within experimental error. Thus the results are summarized in Table IV by reporting at 1500 W input only. These results are consistent with previous results for nozzle no. 2 in that about 30% of the energy is utilized in H-atom production. The rather large portion of energy lost to the coolant should be reduced on scale-up because the surface to cross section area of the nozzle will be decreased.

* Only relative H-atom concentration measurements were made under these conditions.

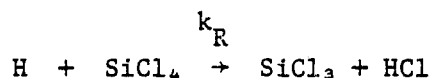
V. SILANE, CHLOROSILANE, AND SILICON SYNTHESIS

In this section attempts to increase the hydrogen content of chlorosilane starting materials will be discussed. Before describing the experiments some calculations of performance limiting conditions will be presented. These set the boundary conditions within which one might expect to synthesize the desired products and demonstrate the inter-relationships of the important experimental parameters.

A. PERFORMANCE LIMITING CONDITIONS

A set of calculations was made to define the limits within which gas-phase reactions between hydrogen atoms in the jet and the second reactant, e.g., silicon tetrachloride, injected into the jet would be most likely to proceed. These results are presented in Figs. 24-32. The jet velocity was calculated as a function of the synthesis region pressure subject to the following limiting conditions:

1. The half life, τ_{chem} , of the reaction rate of interest, e.g.,



was set equal to the characteristic flow time of the jet, τ_{flow} ; any jet velocity which produces a τ_{flow} greater than this limiting value allows the reaction to proceed.

2. The limiting loss of hydrogen atoms by three-body recombination (wall recombination was neglected) was taken to have a half life of one-tenth (very conservative) the characteristic flow time of the jet. For any jet velocity which gives a τ_{flow} less than this limiting value, the concentration of hydrogen atoms will have decayed very little from the original value.
3. An acceptable yield (mass throughput of product) is obtained. Assuming that the reaction is 100% efficient any jet velocity giving a throughput greater than this limit will give a higher yield than the value chosen as acceptable.

These calculations fix the boundary conditions within which the desired gas-phase reactions can be expected to occur. A system operating line is then

calculated from the input conditions; reaction will be expected on this line within the region bounded by the above limiting curves. It must be recognized that a number of assumptions had to be made to allow calculating these limiting conditions, but the assumptions required and their effect upon the results are instructive in guiding synthesis experiments.

The following discussion describes the details of calculating the performance limiting curves and the assumptions made.

The reaction rate requirement is that:

$$\tau_{\text{flow}} \cong \tau_{\text{chem}} \quad (25)$$

where

$$\tau_{\text{flow}} = \frac{d}{u} \quad (26)$$

d is the distance downstream from the point of mixing the second reactant with the hydrogen atom jet and u is the jet linear flow velocity. For a bimolecular reaction with both reactants in equal concentrations:

$$\tau_{\text{chem}} = \frac{1}{k_R C_0} \quad (27)$$

where k_R is the reaction rate coefficient and C_0 is the initial concentration of either reactant. (The equation is somewhat more complicated when the reactants are present in different concentrations, but, because the actual value for k_R is unknown, it is not worth pursuing here.) Because no value for k_R has been determined only one reaction step is assumed. Thus, from Eqs. (25) to (27)

$$u = dk_R C_0$$

and substituting

$$C_0 = X_H \left(\frac{P_d}{T_d} \right) L \left(\frac{T_0}{P_0} \right) = 9.658 \times 10^{18} X_H \left(\frac{P_d}{T_d} \right) \quad (28)$$

gives

$$u = 9.7 \times 10^{18} k_R d X_H \left(\frac{P_d}{T_d} \right) \quad (29)$$

where X_H = mole fraction of H atoms. Two limits $X_H = 0.02$ and 0.06 have been used to cover the extreme ranges expected to be practical.

P_d = downstream static pressure as measured, Torr.

T_d = downstream static temperature, K, calculated from the upstream temperature measurement, T_U (see Eq. (19)).

Assuming isentropic expansion:

$$T_d = T_u \left(\frac{P_d}{P_u} \right)^{\frac{\gamma-1}{\gamma}} \quad (30)$$

where γ = specific heat ratio C_p/C_v , T_o , P_o , and L are the STP temperature, the pressure, and the Loschmidt number, respectively. Two values for k_R were assumed, based on similar reactions, because no experimental values are available:

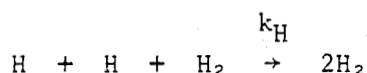
$$k_R = 1 \times 10^{-11} \text{ ml s}^{-1}$$

and

$$k_R = 3 \times 10^{-10} \exp(-2500/T_d) \text{ ml s}^{-1}$$

which corresponds to an activation energy of 5 kcal mol⁻¹. For d , a value of 10 cm has been chosen as consistent with the dimensions of the apparatus. For a larger apparatus a larger value would, of course, increase the range of jet velocity for which reaction would be expected. The limits imposed on u and P_d by these conditions are plotted in Figs. 24 through 31 as the band "Reaction Rate" limited.

The concentration of H atoms will be determined by the rate of the three-body recombination:



To establish limits for this recombination time we set the condition

$$\tau_{\text{flow}} \leq 0.1 \tau_{\text{recomb}}$$

It can be easily shown that

$$\tau_{\text{recomb}} = \frac{1}{k_H C_o C_{H_2}} \quad (31)$$

where C_o = the initial concentration of hydrogen atoms and C_{H_2} = the concentration of hydrogen molecules in the jet. These equations give, by arguments similar to those above:

$$u = 9.4 \times 10^7 k_H d X_H \left(\frac{P}{T_d} \right)^2 \quad (32)$$

k_H is given by Kaufman²⁷ as

$$9.5 \times 10^{-33} \left(\frac{300}{T_d} \right) \text{ ml}^2 \text{ s}^{-1}.$$

The ranges of limiting velocities and pressures that result from these calculations are plotted in Figs. 24 through 31 as the band "Recombination Rate" limiting.

To calculate the yield, Y , i.e., the rate of product production which will be considered acceptable, it is assumed that 100% conversion is obtained. Then, in g s^{-1}

$$Y = \dot{n}_{\text{product}} m = \left(\frac{P_d V_d}{R T_d} \right) \cdot m \quad (33)$$

where \dot{n}_{product} = moles product produced per s
 m = molecular weight of product, g mol^{-1}
 V_d = $X_H A$ (volume of product assuming 100% conversion)
 A = cross-sectional area of the jet

Thus

$$u = \frac{Y}{X_H A} \cdot \frac{R T_d}{P_d} \cdot \frac{1}{m} \quad (34)$$

or in terms of the jet diameter, D

$$u = \frac{4Y}{\pi X_H D^2} \cdot \frac{R T_d}{P_d} \cdot \frac{1}{m} \quad (35)$$

In calculating the "Yield" limiting curves, Figs. 24 through 31, the following were assumed:

$$Y = 1 \text{ kg per 8 hr day} = 0.035 \text{ g s}^{-1}$$

$$D = 1 \text{ cm}$$

$$m = 133 \text{ g mol}^{-1}, \text{ i.e., the product is SiCl}_3.$$

The operating line was calculated from the equation for the linear jet velocity after an adiabatic isentropic expansion³¹:

$$u = \left[\frac{2\gamma}{\gamma - 1} \frac{RT_u}{m} \left(1 - \frac{P_d}{P_u} \right)^{\frac{\gamma-1}{\gamma}} \right]^{1/2} \quad (36)$$

where γ = specific heat ratio, 1.4.

In making the calculation two extreme sets of upstream conditions were taken which could span the range of conditions to be expected (cf., Figs. 10 to 16 "Discharge Stability in Hydrogen" curves and Table III, "Hydrogen Atom Yield Measurements"). The extremes taken were the combinations of:

Upstream pressure, $P_u = 50$ and 300 Torr

Upstream (nozzle) gas temperature, $T_u = 300$ and 1000 K

The operating line is shown on curves 24 to 31 and the static jet temperature, corresponding to the synthesis region pressure, for the set of curves is shown in Fig. 32. A number of conclusions can be drawn from an examination of these curves:

1. The conditions of the experiment (upstream pressure, nozzle temperature, and downstream pressure) must be chosen with some care if a gas-phase reaction is to be realized.
2. If the synthesis reaction has an activation energy of as much as 5 kcal mol⁻¹ then a very low nozzle temperature, especially when coupled with a high upstream pressure is disastrous because of cooling of the gas on expansion, Fig. 32.
3. With a high upstream pressure the operating line is rather flat, i.e., the jet velocity is relatively independent of the downstream pressure.
4. The most attractive operating conditions, Figs. 26, 27, 30, and 31 are realistic.
5. The maximum synthesis region pressure is limited by the upstream pressure at which the discharge can be stably operated to yield high concentrations of hydrogen atoms.
6. The most poorly defined curves of the set are the reaction rate limiting curves; measurements in the present system could be used to derive these reaction rates.

7. To obtain any large change in jet velocity the upstream and downstream pressures must be very close, i.e., the flow must be subsonic.

B. IN SITU GAS-PHASE ANALYSIS

The mass spectrometer probe, Fig. 3, was used for in situ sampling of the reaction stream from nozzle no. 5 with SiCl_4 reactant. No indication of reaction was obtained, either as a reduction in the SiCl_4 concentration or as an increase in product concentration. Even when the mass spectrometer sample was taken through a 4.5 mm i.d. Teflon tube in the trapping section of the flow system, Fig. 3, about 150 cm from the nozzle exit, there was no indication of reaction. Yet when the flow stream was trapped for only a few minutes with liquid nitrogen in the traps, and the traps allowed to warm, product was easily observed in the mass spectrometer. These observations indicate that the products are produced on the walls of the cold traps.

In situ probe sampling was then carried out in the jet of a H/H_2 stream with SiHCl_3 injected in countercurrent flow. The results, Table V, while not directly reducible to product concentrations, indicate about 36% of the SiHCl_3 had reacted to form more highly hydrogenated products. Heavier coatings of solid product were regularly obtained with SiHCl_3 than with SiCl_4 .

In another experiment to confirm the above, a gas sample was collected in an evacuated 1 l flask \approx 150 cm downstream of the nozzle and taken to a more sensitive quadrupole mass spectrometer for analysis. The results again indicated 30 to 40% loss in SiHCl_3 reactant, consistent with an observed increase in HCl , but no indication of the formation of more highly hydrogenated gaseous chlorosilanes. It is assumed these were solid products deposited on the walls.

Further in situ mass spectrometric analyses were not carried out because at this time in the program the decision was made to concentrate on the feasibility of preparing photovoltaic silicon films.

C. PRODUCT COLLECTION EXPERIMENTS

A series of experiments was made with SiCl_4 reactant and the gaseous products collected in three cryogenic traps (Fig. 4) containing liquid nitrogen (-195°C). Solid products were collected in pre-weighed glass reaction zone liners. After an experiment, valves were closed to isolate the traps and they

were allowed to warm to room temperature. At this point, a visual estimate was made of the efficiency of the trapping system by observing the relative amounts of product condensed in the three traps. Condensed products were found to be distributed among the three traps in the ratio 3:2:1 indicating that each trap is $\approx 50\%$ efficient and that the overall efficiency of the trapping system is roughly 88%. It is conservatively assumed that all products are trapped equally efficiently; this will lead to an underestimate of high vapor pressure substances (e.g., SiH_4) for which the collection efficiency is less than that of, say, SiCl_4 . To determine the average molecular weight of the gaseous products, the pressure of the collected products was first determined at room temperature, T_r . These products were then recondensed into a sample flask and weighed. From the known volume of the collection section ($V_c = 3.69 \pm 0.06$ l) and the measured pressure, P_c , of the collected products, the number of moles of gas collected, n_c , was calculated assuming perfect gas behavior:

$$n_c = P_c V_c / R T_r \quad (37)$$

From the measured weight, w , the average molecular weight \bar{m} was calculated:

$$\bar{m} = w/n_c \quad (38)$$

To determine the composition of the collected products, the sample flask was then transferred to the mass spectrometer where a series of cold baths was applied and products fractionated into a known volume. As each bath was applied, the vapor pressure above the flask was determined in a closed system (≈ 1.0 l volume) at the mass spectrometer source. These gases were then admitted to the mass spectrometer and mass spectra obtained. From the pressure measurements and the assumption of perfect solutions, a set of linear equations was constructed which were used to determine the quantities of each gas-phase product collected:

$$P_T(T) = \sum a_i(T) X_i \quad (39)$$

where: $P_T(T)$ was the total pressure above the collected sample at temperature, T ,

X_i = mole fraction of species i in the liquid (solid) phase,

$a_i(T)$ = vapor pressure of substance i at temperature T .

Values of $a_i(T)$ at several temperatures were obtained from the Handbook of Chemistry and Physics and analytical expressions to fit the vapor pressure curves developed to fit these points. The $a_i(T)$ of SiH_2Cl_2 was interpolated

from the SiH_3Cl and SiHCl_3 expressions. The following expressions were obtained for species of interest (vapor pressure in Torr, T in K)

$$\begin{aligned}
 a_{\text{SiCl}_4} &= 9.9 \times 10^7 \exp(-3850/T) \\
 a_{\text{SiHCl}_3} &= 6.7 \times 10^7 \exp(-3470/T) \\
 a_{\text{SiH}_2\text{Cl}_2} &= 5.0 \times 10^7 \exp(-3120/T) \\
 a_{\text{SiH}_3\text{Cl}} &= 7.0 \times 10^7 \exp(-2770/T) \\
 a_{\text{SiH}_4} &= 8.5 \times 10^6 \exp(-1510/T) \\
 a_{\text{HCl}} &= 4.7 \times 10^8 \exp(-2450/T)
 \end{aligned}
 \tag{40}$$

Cold baths used include slushes of 2-methylbutane (114 K), ethanol (161 K), and water (273 K). Measurements were also obtained at room temperature.

The mass spectra of the products above each bath provided: (1) a confirmation of the species present and (2) a means for simplifying the solutions to the set of equations, e.g., by allowing certain products to be eliminated if their mass spectra were not observed.

The results are presented in Table VI. Due to the inefficiency of the three liquid nitrogen traps the product concentrations reported in Table VI have been corrected to total 100% of the input silicon; the correction factor required to accomplish this is given in the last column.

The following tentative conclusions were drawn. Greater percent conversion to products is obtained on the average with:

Larger equivalence ratios

$$\bar{\Sigma}(\text{runs 11, 14, 17}) = \frac{21 + 14 + 4.2}{3} = 13$$

$$\bar{\Sigma}(\text{runs 12, 15, 16}) = \frac{4.8 + 6.2 + 4.0}{3} = 5$$

Lower reaction zone pressure (or lower discharge pressure or higher H-atom concentration)

$$\bar{\Sigma}(\text{runs 11, 12, 14, 15}) = \frac{21 + 4.8 + 14 + 6.2}{4} = 12$$

$$\bar{\Sigma}(\text{runs 16, 17}) = \frac{4.0 + 4.2}{2} = 4$$

The present data do not indicate a significant difference in conversion efficiency with mixing geometry although a small preference might be given to parallel injector tubes:

Mixing geometry

$$\bar{\Sigma}(\text{runs 11, 12}) = \frac{21 + 4.8}{2} = 13$$

$$\bar{\Sigma}(\text{runs 14, 15}) = \frac{14 + 6.2}{2} = 10$$

The most surprising observation is that the use of electronic grade SiCl_4 (run 18) instead of technical grade SiCl_4 substantially decreased product yield and altered product distribution. This was checked in other experiments using electronic grade SiCl_4 , where it was observed that little or no solid product was deposited on the walls. Mass spectrometric analysis of the two reactants disclosed some SiHCl_3 in the technical grade SiCl_4 , which could account for the difference.

If the reaction is occurring in the liquid nitrogen traps as the data of the previous section indicate then the concentration of H atoms at the traps becomes important. It is calculated in Appendix A that, for the conditions of these experiments, the H-atom concentration has decreased to 10 to 20% of its original value by the time the trap is reached. Thus, if the reaction is occurring in the traps, moving them closer to the discharge nozzle should increase the yields.

These experiments were not pursued further because of the relatively low yields of any specific product and because other processes being pursued in the JPL/DoE Low-Cost Solar Array Project appeared to have a greater chance of meeting the program objectives of low cost, high volume production of silanes. The emphasis of the present study was, at this time, changed to concentrate on evaluation of the feasibility of preparing photovoltaic silicon surfaces directly.

VI. AMORPHOUS AND POLYCRYSTALLINE SILICON FILM PREPARATION

In the experiments reported in the previous section it was observed that heavy solid deposits were formed on the reactor walls and that under some conditions these films were very strongly adhering and gave the appearance of being either amorphous or polycrystalline silicon. For the conditions described in Table VII solid products were collected on 70 mm diam Pyrex tubing which lined the synthesis region for about 40 cm downstream of the nozzle. The data in Table VIII identified as "70 mm liner" were from the set of experiments in which the tentative identification of the deposited film was made from photomicrographs.

For condition 1 (Table VII) a yellowish-brown powder was rapidly deposited on the walls of the reaction zone liner. This coating was quite fragile and easily removed. It was partially water soluble and somewhat hygroscopic. These characteristics suggest that the powdery material is polymeric Si_xCl_y . There was no indication that deposits were denser at the bottom of the reaction tube than at the top. When various coatings such as silicone vacuum grease, HCl, HF, Teflon, and KOH were applied to the liner walls, the appearance and approximate density of deposits did not differ from the deposits obtained on clean Pyrex.

For condition 2, a dark brown glassy deposit formed on the walls; it was tentatively identified as amorphous silicon. The coating was quite rugged and could be removed only by using a razor blade to scrape it off. As was the case for the powder deposits, no directional preference for the deposit was found and the deposits collected on the various coatings were similar in appearance and approximate density to those collected on the clean Pyrex.

For condition 3, a dark brown (amorphous Si) glassy deposit rapidly formed. Within about 1.5 hr of running time, however, the deposit became opaque and was dark gray in color. After four hours of collection time, a coating several tenths of a millimeter thick with a smooth metallic appearance was obtained. This coating was more rugged than the glassy deposit, and could be removed only with considerable effort. No directional preference for the deposit was observed. The brown, glassy deposit was found at the farthest downstream end of the reaction zone liner (30-40 cm downstream of the SiCl_4 inlet). Even further downstream (≈ 50 cm from the SiCl_4 inlet) on the reaction tube centerline, solid product deposited on the mass spectrometer sampling probe (the

probe was fortuitously present--it had simply been pulled back to be out of the way). On the conical tip of the probe, the metallic deposit was found near the apex; this deposit graded into a mixture of the glassy deposit and the yellowish-brown powder. On the cylindrical body of the probe, only the powder was found.

Preliminary X-ray fluorescence analysis of the metallic material from run 3 showed it to be mainly Si, with some Cl and Ni present. The atomic ratio Si/Cl was $\approx 6/1$ (the starting material, SiCl_4 , is $1/4$) and the Ni was present at ppm levels. Conspicuously absent at ppm levels or higher were the heavy metals Fe, Cr, Pb, Sn, Cu, and Zn which are materials of construction of the plasma jet apparatus. It was subsequently shown that the nickel was from cathode sputtering. The Cl may be due to artifacts in the experimental procedure, e.g., exposing the liners to SiCl_4 flows in the absence of an H/ H_2 jet. X-ray fluorescence is not sensitive to the lighter elements, e.g., boron.

As a result of these observations and the recognition of the potential of preparing photovoltaic polycrystalline or amorphous silicon films directly, some effort was made to evaluate the conditions for preparation and the characterization of the films. Most of this work concentrated on film preparation from SiCl_4 or SiHCl_3 , but near the end of the program, when doping experiments were attempted to demonstrate that these films would accept dopants, it was recognized that the chance of demonstrating doping would be better with SiH_4 as starting material. Spear and LeComber^{2,3} demonstrated in 1975 that glow discharges in SiH_4 produced amorphous silicon films which could be doped to increase their electrical conductivity. Similarly, Carlson and Wronski⁴ in 1976 and subsequent workers all used SiH_4 . Several groups^{8,9} demonstrated that the difference between the glow discharge deposited films and previously studied vapor deposited films was the large H-atom concentration in the discharge deposited films from SiH_4 . Our attempts to deposit films from SiH_4 , using the non-equilibrium plasma jet to produce H atoms which were then mixed with SiH_4 , showed they were more difficult to prepare than from the chlorosilanes. We were finally successful in laying down doped films from SiH_4 which showed large decreases in resistivity from the undoped films but the experimental conditions were different from those in the plasma jet experiments.

In this section the experiments to prepare and characterize films deposited from SiCl_4 , SiHCl_3 , and SiH_4 will be described, essentially in the order in which they were done.

A. FILMS ON QUARTZ CYLINDERS IN CROSS FLOW

Solid products were collected for conditions 1 and 2 of Table VII on the outer surfaces of quartz cylinders (6 mm o.d.) placed perpendicularly across the centerline of the $H/H_2/SiCl_4$ stream and about 7 cm downstream of the $SiCl_4$ inlet. The stream diameter appeared visually to be approximately 1-2 cm. (Compare, however, the calculated jet diameters, Section III.B). To test whether the temperature of the collecting surface affected the characteristics of the solid deposits, the quartz cylinders were either heated with an internal nichrome resistance heater to about 750 K, water-cooled to maintain a temperature of about 300 K, or allowed to reach an equilibrium temperature. The cylinders were exposed to the synthesis region flows for 1/4-3/4 hr. The results of these tests, Table VIII, may be summarized as follows:

- (i) Heated cylinder samples, runs 6 and 7, appeared to be amorphous Si, for both flow conditions 1 and 2.
- (ii) Cooled cylinder samples, runs 4 and 5, had the same appearance under conditions 1 and 2 as samples collected on the synthesis region liners under these conditions. However, in run 5 the deposit did not adhere well to the surface.
- (iii) In all cases but one, the greatest density of a deposit was found on the upstream side of the cylinders (facing the H/H_2 jet and $SiCl_4$ addition inlet). The exception was the cooled probe with flow condition 1, run 4, which showed maximum buildup on the downstream side.
- (iv) Exposure of the polymer deposit to a stream of H atoms on an unheated cylinder (i.e., with no further $SiCl_4$ addition) resulted in no change in appearance of the deposit.
- (v) No products were deposited in the absence of the H_2 discharge.

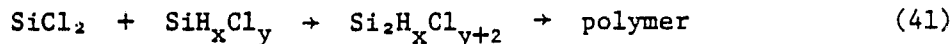
Interpretation of these observations is difficult because of their qualitative nature and because the categorization, as far as product identification, is not always clear, e.g., run 9. Higher gas stream temperature (also greater pressure and a longer flow time) for condition 1 appears to favor polymer formation, presumably due to the stability of intermediate $SiCl_2$ at high temperatures. In the case of run 7, this polymer may have been decomposed to amorphous silicon on the hot surface. The lower gas temperatures (also lower pressures and shorter reaction times) seem to favor the formation of silicon, either in the gas phase or on a surface. Why a polycrystalline silicon was

found in run 3 was not clear. The two distinct features of the run were higher equivalence ratio* and a longer run time.

Mechanistically, the above interpretation is consistent with low activation energies for H-atom reactions and high activation energies for polymerization reactions. One might also speculate that these results are consistent with a low activation energy for the reaction



while processes like



have high activation energies. Thus, in terms of the reaction scheme presented in Section II, Reaction (6) predominates at low temperature while at higher temperatures, the reactions initiating polymer formation. e.g., Reaction (41) reach competitive rates. Of course, even at high temperatures Reaction (6) still occurs, and this might account for the brown deposit (presumably amorphous silicon) formed on the cooled probe in run 4.

Although product buildup is greatest on the upstream sides of the cylinders (note the exception in (iii) above) consistent with deposition of particles formed in the gas phase, insufficient data are available to rule out direct surface reactions.

B. FILM PREPARATION AND CHARACTERIZATION

Experiments were carried out to determine the characteristics of the films, assumed to be amorphous or polycrystalline silicon, and to determine the effect on these films of the chlorosilane reactant and the exposure time. For the entire series of experiments, the H/H₂ jet conditions were fixed,

* Equivalence ratio, ϕ , defined as $\phi = \frac{(\text{chlorosilane or silane/H})_{\text{actual}}}{(\text{chlorosilane or silane/H})_{\text{stoic}}}$ where

it is assumed that the stoichiometric reactions are:

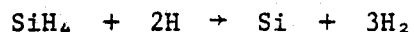
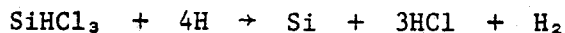
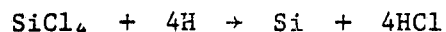


Table IX, and the downstream pressure was held essentially constant. Three or four ordinary microscope slides, 7.6 x 2.5 cm, were placed lengthwise along the bottom of the synthesis region section of the apparatus (70 mm i.d.). Both Pyrex and Vycor (quartz) slides were used. The chlorosilane was brought into the apparatus through a stainless steel tube (4.7 mm i.d., 6.4 mm o.d.) which was 2.9 cm off-center of the H/H₂ jet; thus a reactant jet of velocity varying from 160 cm s⁻¹ to 5800 cm s⁻¹, depending upon feed rate, impinged on the nozzle holder plate. This produced a turbulent diffusive mixing with the H/H₂ jet which visually extended up to about 30 cm downstream of the H/H₂ nozzle face plate. It was in this region that deposits were collected on the slides. The deposits seemed to be symmetrically distributed around the walls of the reaction tube.

In the first set of runs three Vycor slides were placed on the bottom of the reactor, the first against the nozzle plate, the second separated by 1.3 cm from the first and by 5.1 cm from the third. These runs, with some observations, are summarized in Table X. In all cases the maximum deposit was observed on the second, i.e., center slide. In this set of runs the weight of deposit was determined only for runs 116, 117, and 119. Results are summarized in Table XI.

In another set of experiments with SiHCl₃ feed instead of SiCl₄, the SiHCl₃ flow rate was varied over a large range to determine the effect of equivalence ratio on the nature and quantity of deposit. Four Pyrex slides were placed end on, butting against the nozzle plate and touching each other. The slides were prepared by washing in trichloroethylene, dipping in 20% HF solution for approximately 10 s, rinsing with distilled water, and drying with a paper towel. All other conditions were the same as in the above set of runs. The results were somewhat surprising in that, at least visually, the heaviest deposits occurred at the lower flow rates where a dark brown adhering film was formed. At intermediate flow rates the deposit appeared lighter and at the higher flow rates the character of the deposit was different, showing a gray metallic luster and strong adhesion to the surface. The basic data with descriptions of the observations are summarized in Table XII. Most of the coatings occurred on the central two slides (\approx 8-24 cm downstream), except at 5, 6, and 7.7 ml s⁻¹ where the light coatings observed were mostly deposited on the second slide (\approx 8-16 cm downstream). Interpretation of these data in terms of effect of composition is complicated by uncertainties in the flow pattern in the reactor.

The silane/H/H₂ reaction deposit (run 119) was heated in an oven with nitrogen flow for 26 hr at 830 K. Before heating the surface looked like a structureless fine powder. After heating the surface appeared as a white film and exhibited some microscopic structure. There was no significant weight change on heating.

A sample of solid product from the semiconductor grade SiCl₄/H/H₂ reaction (run 122) was heated to 820 K for 22 hr and the results are displayed in Fig. 33. Prior to heating, the coating had a lustrous metallic appearance which dulled on heating. Some parts of the slide showed small cracks on heating, others did not. Generally the number density of spheres, which we tentatively identify as polycrystalline silicon, appeared to increase on heating. Heating did not change the weight. Technical grade SiCl₄ deposits gave similar effects on heating. The dark brown deposits from SiHCl₃ (run 128, Table X, and run 136, Table XII) showed the same polycrystalline structure as in Fig. 33. The slide from run 136 was heated to 830 K for 24 hr and again very little change was noted. Heating the visually very light shiny metallic deposit from SiHCl₃ (run 133 Table XII) to 820 K for 24 hr again produced very little change when observed in photomicrographs.

Heat and/or a thick film produces fractures of the glassy films forming plates and eventually leads to peeling of the deposit. Strongly heating a thin deposit (9 min exposure to the reaction, Fig. 34) to 1220 K for 2.5 hr in an Ar atmosphere is sufficient to completely fracture the deposit into small plates probably due to the difference in thermal expansion coefficients between the film and slide. The small increase in optical density of the deposit on heating suggests a phase change to polycrystalline Si. The milder heating effect of the discharge/reaction begins to form small cracks by about 15 min exposure time. By 21 and 27 min exposure time fracturing is severe enough for the deposits to peel away from the slides. The cracks seem to propagate between particles; see, e.g., Fig. 34.

Samples of silicon deposits on Pyrex and Vycor substrates were chosen for X-ray fluorescence spectroscopy (XFS) from samples 122 through 143. (See Tables X and XII; runs 142 and 143 were with technical grade SiCl₄ at 0.34 mmol s⁻¹ and deposition times of 3 and 15 min, respectively.) The samples were chosen to represent variations in reagents used (technical and semiconductor grade SiCl₄, and SiHCl₃), in hydrogen flow rates, and in type of substrate (Pyrex or Vycor). XFS showed that all but two silicon samples contained up to

10 ppm nickel and chromium (the limit of detection is 5 ppm and the substrate itself contained no nickel or chromium). One sample contained no nickel or chromium and the other contained nickel only. These metal impurities come from the cathode. Chlorine in the samples varied from 1.7 mol % to 31 mol % with no apparent dependence on the reagent used, flow rate, exposure time, or sample handling methods.

Samples of silicon deposits on 25 x 25 mm slides were studied by X-ray diffractometry and were found to be amorphous or polycrystalline with preferred alignment in one or more crystal planes. Figure 35 shows experimental curves for intensity of x-radiation vs. angle 2θ (where θ is the angle of refraction), for three different samples. The normal relative intensities for polycrystalline randomly distributed powder should be³²:

<u>Plane</u>	<u>Angle, 2θ</u>	<u>Relative Intensity</u>
111	28.4	100
220	47.3	55
311	56.2	30

An estimate of intensities for sample 143-3, Fig. 35 is 100:30:36 for the 111:220:311 planes. Within the limits of estimated intensities this sample appears to be polycrystalline silicon with some preferred growth in both the 111 and 311 planes.

Sample 143-2, on the other hand, has a 220 plane reflection at 47.3° which is much more intense than the 111 plane reflection at 28.4° . The estimated intensities are 76:100:32 for the 111:220:311 planes. This indicates substantial preferred growth of the silicon 220 plane parallel to the substrate surface. The broad reflection for all three samples around 22° is due to the Vycor. The X-ray pattern for sample 124-2, shows no reflection at 28.4° , 47.3° , or 56.2° , and is therefore not crystalline. These silicon deposits thus vary from amorphous to preferred growth polycrystalline material.

A Beckman Instruments IR-5A spectrometer which has a range of 5000 cm^{-1} to 625 cm^{-1} was used for infrared spectroscopic studies. Samples were prepared by grinding a bit of the material to be analyzed with anhydrous reagent grade KBr with an agate mortar and pestle and pressing the mixture into a pellet at 20,000 to 25,000 psi for 20 min under vacuum. Three silicon samples were studied: (1) the yellow deposit from run no. 158, (2) scrapings of the dark brown shiny deposit from run 128, and (3) scrapings of a strongly adhering silicon film from run 143.

The material from run 158 was a loose yellow powder that could easily be rubbed off the substrate. Strong absorption at 3300 and 3500 cm^{-1} and a broad intense band at 830-910 cm^{-1} indicated the presence of Si-OH groups. There was an Si-O-Si band at 1000-1110 cm^{-1} and Si-H peaks at 2150 cm^{-1} and 2260 cm^{-1} . The broadness of the Si-O-Si and Si-OH absorption indicates a complex structure, as in a polymer. The yellow to orange color of the material is characteristic of Si_xH_y , $(\text{SiOH})_x$, and $\text{Si}_x\text{H}_y\text{Cl}_z$ polymers.³³ The Si-Cl stretch has been reported at 600 cm^{-1} for $\text{Si}_5\text{Cl}_{12}$ and $\text{Si}_6\text{Cl}_{14}$ ³⁴ and at 800 cm^{-1} for other chlorosilanes, including SiCl_4 .³⁵ There was no discernible peak at 800 cm^{-1} although a small peak could be hidden by the broad Si-OH peak at 830 cm^{-1} ; any peak at 600 cm^{-1} would not be registered on the IR-5A.

Scrapings from sample 128 which looked like gray silicon were found by XFS to have 31 mol % chlorine content and showed no definite IR bands except for a small unassignable broad band at 1000 to 1250 cm^{-1} . Sample 143, a thick gray deposit, showed a spectrum of very broad peaks at 1400, 1100, 910, and 830 to 770 cm^{-1} .

The rate of silicon deposit and conversion efficiency from the SiHCl_3 runs (Table XII) were plotted as a function of SiHCl_3 flow rate, Fig. 36, assuming the deposit to be silicon. These curves yield a rate of film deposition of 4 $\mu\text{m min}^{-1}$ at a conversion efficiency of about 17% and an equivalence ratio of 0.2. One implication of the low equivalence ratio is that the H atoms are not being efficiently utilized, or that the reaction requires more than four H atoms per molecule of SiHCl_3 reacting as assumed in defining the equivalence ratio.

A set of experiments (runs 142-147) was carried out in which the time the slides were exposed to SiCl_4 reactant was varied. Samples were collected and handled as in the above tests. The discharge conditions in these experiments were as given in Table IX and the flow rate of SiCl_4 (technical grade) was fixed at 0.34 mmol s^{-1} ($\phi = 0.84$). Exposure times of clean sets of slides to the reaction were varied from 3 to 27 min. In addition to these runs, some exposed slides were heat treated, re-exposed to the reaction, or exposed only to the discharge.

The rate of solid deposition was observed to be constant with the deposits symmetrically distributed about the center of the four slides, with slides 1 and 4 and slides 2 and 3 being equivalent. The deposition rates were 0.27 mg min^{-1} for slides 1 and 4 and 0.72 mg min^{-1} for slides 2 and 3. Assuming that the deposits on slides 2 and 3 are uniform in thickness, the films

collected range in thickness from 0.5-4.5 μm . These data yield a rate of film deposition of 0.2 $\mu\text{m min}^{-1}$, assuming the deposit has the density of silicon. The thinner films, when seen with the naked eye (3 and 6 min runs), show interference fringes. At least two green fringes are apparent on the 3 min exposure and five on the 6 min exposure slide. Classical theory gives

$$\text{thickness} = \frac{(\text{no. of fringes} + 1/2) \cdot \text{wavelength}}{2 \cdot \text{refractive index}}$$

Taking the wavelength $\approx 5.5 \times 10^{-5}$ cm (green light) and refractive index ≈ 1.5 gives a film thickness of 0.5 μm for the 3 min exposure and 1.1 μm for the 6 min exposure, consistent with the above calculation based on uniform film thickness.

Again assuming that the deposits are pure Si, and using the observation that solid deposits in the synthesis region are cylindrically symmetric about the H/H₂ jet axis, the yields of solid are estimated for the runs in which no peeling was observed. The solid product yield from SiCl₄ for these conditions is only between 3 and 4%.

Two types of deposit are observed, a glassy film (assumed to be amorphous Si) and metallic particles (assumed to be polycrystalline Si). From the photomicrographs, Fig. 34, the presence of many small particles can easily be seen. The glassy film is more evident when cracks appear in it at the longer exposure times. At short exposure times very few particles and many small holes (bright spots on photomicrographs--see Fig. 34) can be seen. This suggests that the particles are embedded in the films. It appears on observation with a metallurgical microscope that the particles fall onto the surface from the gas stream and are slightly mobile until they are covered by the glassy film. Indeed, separate experiments, in which surfaces were made "stickier" by coating the slides with vacuum grease, clearly showed the presence of many particles after only 3 min exposure. We tentatively conclude that both types of Si are being formed simultaneously at all reaction times. It should also be noted that the buildup of deposits with time can be seen from the progressive darkening of the constant exposure photomicrographs of Fig. 34.

Qualitatively the metallic particles are uniform in size (≈ 0.5 to 1.0 μm) independent of exposure time. The number density of deposited particles increases with time, see Fig. 34. Larger particles appear to result from agglomeration on the surface.

The samples were sent to an outside laboratory that specializes in particle size and number distribution measurements but electron micrographs showed the substrate used (Vycor slides) to be inappropriate for this type of analysis because of surface roughness. In addition, the extremely small size of many of the deposited particles did not allow their examination except at very high electron energies at which interfering secondary radiation from the Vycor substrate resulted in poor resolution.

C. WATER-COOLED SAMPLE HOLDER NORMAL TO JET

To better define the position of the substrate with respect to the jet and to control the temperature of the substrate, a water-cooled sample holder, Fig. 37, was built to hold a substrate plate 25 x 25 mm and up to 3.2 mm thick. The substrate plate is sealed to the holder by an O-ring so that the cooling water impinges on the back where the temperature is measured with a thermocouple. The support tube is passed through a vacuum seal at the downstream end of the reactor, allowing the substrate to be placed at variable distances from the nozzle on the reaction tube centerline. At the same time that this was done the reaction chamber diameter was increased from 70 to 140 mm so that the sample holder would not block the gas flow and so the reactor wall deposits would be displaced further downstream of the nozzle.

In this series of experiments (runs 191 to 240) the reactants were SiCl_4 , SiHCl_3 , or SiH_4 with flow rates over the range of 0.08 to 0.5 mmol s^{-1} ; H_2 flows were 31 or 52 mmol s^{-1} ; discharge pressures were 40 to 70 Torr; reactor pressures were 15 to 40 Torr, and discharge powers were between 1200 to 2400 W.

The deposits were generally loose powders which resembled previously analyzed polymers. Often the powders exhibited a strong odor of HCl , presumably from atmospheric H_2O reacting with Si-Cl bonds in the polymer. The powder, in some cases, also appeared to have been blown off the substrate by the jet. Samples tested from several runs all showed Si-OH and Si-O-Si bonds by infrared absorption and some samples showed Si-H bonds. X-ray fluorescence analysis of several samples indicated the presence of 15 to 60 mol % Cl .

Of the several possible explanations of why the strongly adhering silicon films of previous runs were not obtained, the most rational appears to be based on recirculation. In previous experiments the jet was confined by a 70 mm diam tube, while in this series of runs the jet was in a 140 mm diam tube.

Large recirculation was visually observable with the jet in the larger tube. With a smaller diameter tube surrounding the jet, recirculation is suppressed. Thus it appears that recirculation of some of the product back into the reacting jet stream favors polymer formation over silicon formation. This is supported by other observations. In one run the aluminum substrate was placed on the bottom of the reaction tube and a yellow-brown powder was obtained. While in most of the earlier successful runs, the samples for study were placed on the bottom of the tube so that the jet axis was parallel to the substrate, in several experiments the substrate was placed so the jet was normal to it (e.g., see Section VI.A with quartz cylinders in cross flow) and this also resulted in a strongly adhering film. In other cases strongly adhering films were observed on the mass spectrometer water-cooled probe. Thus the explanation cannot be sought in the direction of the jet with respect to the substrate.

Experiments were then carried out with a smaller diameter reacting tube surrounding the jet.

D. FILM PREPARATION WITH RESTRICTED RECIRCULATION

A series of experiments (runs 244 to 274) with SiCl_4 reactant was carried out, repeating the older procedure, i.e., the substrate was placed on the bottom of a reactor tube of 64 mm i.d. diam. In all runs strongly adhering silicon films were obtained. The results, including two previous runs (128 and 143), are summarized in Table XIII. The number affixed to the run number (-X) represents the substrate slide that was evaluated, the slides being numbered from the nozzle. As before, four or five slides were placed on the bottom of the reactor and generally the thickest deposit was on slide no. 3. In several runs substrates other than those reported in the table were also included. Thus run 246 included a graphite test sample and run 260 included a graphite and aluminum test sample. A strongly adhering film was also observed on each of these. The sample thickness was determined by weight increase, assuming the films have the density of silicon. Figure 38 shows a maximum rate of film deposition at an equivalence ratio of about 0.6. Compare experiments with SiHCl_3 , Fig. 36.

The conversion efficiency of SiCl_4 to Si, Fig. 39, decreases with increasing SiCl_4 flow rate, consistent with previous results for SiHCl_3 , Fig. 36. Because the data reported in Fig. 39 were made at different power inputs they have all been normalized to 1400 W, assuming the conversion efficiency is

directly proportional to power input. Of the three points which are far off the curve, run 261 had an abnormally low power input, 390 W; runs 251 and 266 were not unusual.

The formation of polycrystalline films seems to be associated with higher temperatures in conjunction with:

- (1) high power input, run 143
- (2) long exposure time, runs 245, 249, 251
- (3) subsequent heating, run 257.

Electrical resistivity and activation energy for conductivity, E_A , were measured for some samples by the four probe technique.^{36,37} They were in the range of 0.5 to 20×10^8 ohm cm at room temperature and 0.5 to 1.1 eV which is in the range of photovoltaic undoped amorphous films reported in the literature.^{5,9,38} The significance of the variation of these quantities with conditions is not clear. The measurement is difficult because of the thin films and the large resistance, approximately 10^{11} ohms, which must be measured. Such measurements are extremely sensitive to surface contamination and humidity. Resistivities for the BCl_3 and PH_3 doped samples, runs 267, 269, and 274 were in the same range and suffered from the same experimental errors.

Infrared absorption analysis of the films prepared in runs 128-2, 252-3, 253-3, and 264-3 gave evidence for Si-Cl covalent bonds but no evidence for the presence of Si-H bonds.

It is clear from the above that amorphous films of silicon which strongly adhere to Vycor, Pyrex, aluminum, and carbon can be prepared by the non-equilibrium plasma jet with SiCl_4 or SiHCl_3 reactant and that such films have electrical properties comparable to those of undoped photovoltaic amorphous silicon films. The next step is to demonstrate that such films can be doped to greatly reduce their electrical resistivity.

E. FILM PREPARATION FROM SILANE

Attempts to prepare adhering amorphous silicon films on Pyrex or Vycor slides (runs 275-289) placed on the bottom of the reactor, as above, from SiH_4 were unsuccessful. Brown, presumably amorphous, powders were obtained. In these experiments: the H/H_2 flow was 32 or 63 mmol s^{-1} ; SiH_4 flow was 0.01, 0.1, and 0.33 mmol s^{-1} ; the discharge pressure varied from 10 to 75 Torr; and the reactor (downstream) pressure varied from 2 to 40 Torr. Nozzle no. 6 was used.

The chemistry in our system and in the glow discharge method, as used by RCA and others to prepare photovoltaic amorphous silicon films, would be expected to be very similar. The major differences seem to be that the glow discharge processes operate at several Torr and, in many cases, the substrate is one of the electrodes. These conditions would favor ionic processes as well as higher levels of dissociation. We thus modified our apparatus to work at conditions more closely approximating the glow discharge conditions of others; our aim was to produce doped films at conditions approaching those of the glow discharge process and use this as a benchmark from which we would gradually alter conditions toward those of the non-equilibrium plasma jet to determine whether it could be used with advantage to prepare photovoltaic amorphous silicon films.

Toward this end, a substrate holder was built, Fig. 40, which could be electrically heated to 550 K and to which an electric field could be applied. Three experiments were then carried out with the non-equilibrium plasma jet and the substrate holder about 80 mm from the nozzle, using an aluminum substrate in one experiment and Pyrex substrates in the other two. With the substrate heated to about 500 K only an extremely thin film was obtained on Pyrex after a 3 hr run. The conditions were: $0.43 \text{ mmol s}^{-1} \text{ H}_2$ through the discharge nozzle; $0.001 \text{ mmol s}^{-1} \text{ SiH}_4$ through the annulus (nozzle no. 6); 560 V and 0.22 A through the discharge; and a reactor chamber pressure of 2.5 Torr.

In the next series of runs (306 to 321) with the discharge between the nozzle and the substrate holder, simulating the glow discharge experiments, some amorphous silicon films were prepared but they peeled off rather easily on handling, e.g., to measure electrical resistance. Doping with 0.1 and 1% PH_3 did not give significant changes in electrical resistivity, although because of the fragile nature of the deposits these measurements were difficult and highly uncertain. In these experiments the substrates were Pyrex or aluminum. Resistivities of films on Pyrex were measured by the four probe technique and on aluminum by pressing an indium sheet against the film and measuring the resistance between the indium sheet and the aluminum. The conditions for this set of experiments were: $0.33 \text{ mmol s}^{-1} \text{ H}_2$ flow; 0.001, 0.003, and $0.004 \text{ mmol s}^{-1} \text{ SiH}_4$ flow, with PH_3 dopant concentrations of 0.1, 0.3, and 1.0 mol %; the pressure was varied from 0.2 to 2.3 Torr and the discharge voltage varied from about 700 to 1100 V.

In the above experiments the aluminum substrate was washed with trichloroethylene. In an attempt to improve film adherence to aluminum the aluminum was washed in KOH solution, rinsed in distilled water, washed in HCl solution, and again rinsed in distilled water. Four runs (322-325) within the above conditions gave strongly adhering films on aluminum. PH_3 doping did not appreciably change the electrical resistivity of the film.

In a series of ten runs, Table XIV, successful doping with PH_3 was obtained with an argon carrier gas. The aluminum substrate was the cathode and was heated to approximately 550 K in the substrate holder, Fig. 40, which was placed about 20 mm from the nozzle. Argon with about 10 mol % H_2 was fed through the central section of the nozzle and the SiH_4 was fed through the annular section. For the doping experiments, the hydrogen contained a fixed, 975 ppm, concentration of PH_3 , so the PH_3 concentration in the reaction was varied by varying the H_2 flow rate. The amount of amorphous silicon deposited on the aluminum, 25 mm on a side and 0.89 mm thick, was determined by weighing the aluminum before and after the experiment. The resistance at local points through the deposited film was determined by means of a simple electrical probe constructed by wrapping the eraser of a standard pencil with indium metal foil. The surface was divided into nine rectangles and the probe was manually placed at a position approximately in the middle of each of these. The resistance was measured with a Keithley 616 Digital Electrometer. The resistance varied from area to area on the surface but was reproducible from day to day indicating that the surface is not uniform. Two to three replica tests on different days were made on most samples.

The data in Table XIV are ordered for increasing relative electrical resistance. The relative resistance was derived by first averaging the replicas for each section of the sample then summing these and dividing by nine (number of areas measured) and dividing by the deposited mass. This assumes that the resistance is proportional to the film thickness and corrects for what were rather wide variations in resistances in the nine areas of the surface. The values were then normalized to make the lowest resistance equal to one. A simple averaging procedure gave the same order except for one point, but increased the relative range of resistance.

It is immediately apparent in Table XIV that the resistance of the group of doped films is less than that of the undoped films. The ratio doped/undoped = 58/1. The maximum ratio is 950/1 and the minimum ratio is 14/1.

It is tempting to look for other trends in the data reported in Table XIV. The resistance appears to be decreased by reducing the pressure, run 329, and by reducing the concentration of dopant. Except for run 332 there seems to be a trend with deposited mass; for undoped films the resistance decreases with increasing mass, i.e., film thickness. Just the opposite occurs for doped samples, possibly counterbalancing the dopant effect above, so the dopant trend might be much greater were the mass effect (film thickness) not operative. The reason for the variation in deposited mass is not clear and it would be stretching the data to try to pull an explanation out of the variables especially without "current" data. It is also not clear why run 332 does not follow the trend; the nozzle was cleaned just prior to this run, the only time for this set of data. Run 336 has an abnormally high resistance compared to the other undoped samples which is surprising considering the low mass which would give a thin film where chances of shorting are greatest. The film was poorly distributed and only showed high resistances over about 2/3 of the film.

The data in Table XIV clearly demonstrate that doping with P from PH₃ decreases the electrical conductivity of amorphous silicon films as prepared in these experiments.

VII. CONCLUSIONS

The main conclusions from this study are:

1. Strongly adhering films of either amorphous or polycrystalline silicon can be prepared on Pyrex, Vycor, aluminum, or carbon by reacting the H/H₂ jet with SiCl₄ or SiHCl₃. The electrical resistivity and activation energy for electrical conductivity of such films are in the range of undoped amorphous silicon films prepared in glow discharges for use in photovoltaic devices.
2. P-doped strongly adhering amorphous silicon films with greatly increased electrical conductivities over similarly prepared undoped films can be prepared from SiH₄ in Ar when the discharge is between the mixing nozzle and an aluminum substrate cathode heated to about 500 K.
3. Yields of SiH₄ or SiH₂Cl₂ from SiCl₄ or SiHCl₃ reacting with the H/H₂ jet are too small (less than 20%) to be of commercial interest.
4. The non-equilibrium plasma jet produces large fluxes of hydrogen atoms at concentrations of about 3 mol % H atoms at an energy utilization efficiency of about 30%, with discharge pressures of about 50 to 150 Torr, and with the temperature of the jet ranging from about 400 to 600 K depending upon the downstream pressure.
5. A conical, annular nozzle with the H/H₂ stream through the center and the other reactant through the annular section gives good mixing with minimum disruption of the jet integrity.

VIII. RECOMMENDATIONS

1. It is recommended that the present program be continued to determine the feasibility of preparing photovoltaic amorphous silicon in the non-equilibrium plasma jet from SiH_4 , SiCl_4 , and SiHCl_3 . A part of the proposed program should be directed to understanding the mechanism of the process to distinguish between that involved in the glow discharge preparation and in the plasma jet preparation and to shed light on the glow discharge mechanism. This program should include studies with a thermal H-atom source to distinguish between ionic and neutral species mechanisms and should include films laid down from chlorosilanes and then bombarded with H-atoms from the plasma jet and from a thermal source.
2. It is recommended that a program be initiated to understand the potential of the non-equilibrium plasma jet as a chemical synthesis tool and as a device for studying reaction kinetics. The first reaction to be studied in detail should be the $\text{H} + \text{NO}_2$ reaction for which the mechanism and reaction kinetics are known. After this study the reactions of H atoms with SiCl_4 and SiHCl_3 to produce higher hydrogen homologs should be studied. These studies would build upon the results summarized in this report and should consider the use of a thermal hydrogen atom source to supplement the results obtained in the plasma jet.

IX. NEW TECHNOLOGY

The new technology reported herein includes:

1. A means of producing large fluxes of hydrogen atoms at a high energy utilization efficiency.
2. A means of mixing the plasma jet with a second reactant while maintaining the integrity of the jet.
3. A means of producing higher hydrogen homologs of SiCl_4 or SiHCl_3 by reaction with a non-equilibrium hydrogen plasma jet.
4. A means of preparing strongly adhering amorphous silicon films on simple substrates such as Pyrex, Vycor, and aluminum from SiCl_4 and SiHCl_3 .
5. A means of preparing strongly adhering amorphous silicon films on aluminum from SiH_4 .
6. A means of doping films prepared from SiH_4 with P to increase the electrical conductivity.

X. REFERENCES

1. Rockwell International, "Chemical Vapor Deposition Growth," ERDA/JPL 954372, Quarterly Reports.
2. Spear, W.E. and LeComber, P.G., "Substitutional Doping of Amorphous Silicon," *Solid State Commun.* 17, 1193-1196 (1975).
3. Spear, W.E. and LeComber, P.G., "Electronic Properties of Substitutionally Doped Amorphous Si and Ge," *Phil. Mag.* 33, 935-949 (1976).
4. Carlson, D.E. and Wronski, C.R., "Amorphous Silicon Solar Cell," *Appl. Phys. Lett.* 28, 671-673 (1976).
5. Carlson, D.E. Ponkove, J.J., Wronski, C.R., and Zanzucchi, P.J., "Hydrogenated Amorphous Silicon - A Solar Cell Material," *Thin Solid Films* 45, 43-46 (1977).
6. Carlson, D.E., "Semiconductor Device Having a Body of Amorphous Silicon," U.S. Patent 4,064,521, Dec. 20, 1977.
7. Carlson, D.E., "Amorphous Silicon Solar Cells," *IEEE Trans. on Electron Devices* ED24, 449-453 (1977).
8. Malhotra, A.K. and Neudeck, G.W., "Effects of Hydrogen Contamination on the Localized States in Amorphous Silicon," *Appl. Phys. Lett.* 28, 47-49 (1976).
9. Fritzsche, H., Tsai, C.C., and Persons, P., "Amorphous Semiconducting Silicon-Hydrogen Alloys," *Solid State Techn.* 21 (1), 55-60 (1978).
10. Glockler, G. and Lind, S.C., eds., The Electrochemistry of Gases and Other Dielectrics (John Wiley and Sons, New York, 1939).
11. Baddour, R.F. and Timmins, R.S., The Application of Plasmas to Chemical Processing (MIT Press, Cambridge, 1967).
12. McTaggart, F.K., Plasma Chemistry in Electrical Discharges (Elsevier Publishing Co., New York, 1967).
13. Venugopalan, M., ed., Reactions Under Plasma Conditions, Vols. I and II (Wiley-Interscience, New York, 1971).
14. Mannal, C. and Mather, N.W., eds., Engineering Aspects of Magnetohydrodynamics (Columbia University Press, New York, 1962).
15. Mather, N.W. and Sutton, G.W., eds., Engineering Aspects of Magnetohydrodynamics (Gordon and Breach, New York, 1964).
16. Fenn, J.B., "Electrical Discharge Jet Stream," U.S. Patent 3,005,762, 24 October 1961.

17. Rosner, D.E. and Calcote, H.F., "Generation of Supersonic Dissociated and Ionized Nonequilibrium Streams," AeroChem TM-10, DDC AD 207 590, October 1958.
18. Rosner, D.E., "Generation of Supersonic Dissociated and Ionized Nonequilibrium Streams. II. Energy Utilization and the Determination of Atom Concentrations," AeroChem TP-31, DDC AD 264 973, July 1961.
19. JANAF Thermochemical Tables, Dow Chemical Co., Midland, MI (continuously updated).
20. Austin, E.R. and Lampe, F.W., "Hydrogen-Atom Initiated Decomposition of Monosilane," J. Phys. Chem. 80, 2811-2817 (1976).
21. Gould R.F., ed., Chemical Reactions in Electrical Discharges, Advances in Chemistry Series 80 (American Chemical Society, Washington, DC, 1969) p. 156.
22. Gross, P.W.F. and Bott, J.F., eds., Handbook of Chemical Lasers (John Wiley and Sons, New York, 1976).
23. Massey, H.S.W., Electronic and Ionic Impact Phenomena, Vol. II. Electron Collisions with Molecules and Photoionization (Oxford Univ. Press, London, 1969) Chaps. 11, 12.
24. McDaniel, E.W., Collision Phenomena in Ionized Gases (Wiley, New York, 1964) Chap. 5
25. von Engel, A., Ionized Gases (Oxford Univ. Press, London, 1955) Chap. 8.
26. Thrush, B.A., "Reactions of Hydrogen Atoms in the Gas Phase," Prog. React. Kin. 3, 65-95 (1965).
27. Kaufman, F., "Elementary Gas Reactions," Ann. Rev. Phys. Chem. 20, 45-90 (1969).
28. Clyne, M.A.A., "Reactions of Atoms and Free Radicals Studied in Discharge Flow Systems," Physical Chemistry of Fast Reactions, Vol. 1, B.P. Levitt, ed. (Plenum Press, New York, 1973) pp. 247-329.
29. Clyne, M.A.A. and Stedman, D.H., "Reactions of Atomic Hydrogen with Hydrogen Chloride and Nitrosyl Chloride," Trans. Faraday Soc. 62, 2164-2174 (1966).
30. Rosner, D.E., "Summary of Low Temperature Plasmajet Research; Energy Transport in Chemically Active, Nonequilibrium Supersonic Streams," Final Report, AeroChem TP-39, DDC AD 273 889, February 1962.
31. Rotty, R.M., Introduction to Gas Dynamics (Wiley, New York, 1962) Chap. 5.
32. Powder Diffraction File No. 27-1402, Joint Committee on Powder Diffraction Standards, International Center for Diffraction Data, 1601 Park Lane, Swarthmore, PA 19081.

33. Rochow, E.G., Comprehensive Inorganic Chemistry (Pergamon Press, New York, 1973) Chap. 15.
34. Nuss, J.W. and Urry, G., "On the Structures of Pentasilicon Dodecachloride, $\text{Si}_5\text{Cl}_{12}$ and Hexasilicon Tetradecachloride, $\text{Si}_6\text{Cl}_{14}$," J. Inorg. Nucl. Chem. 26, 435 (1964)
35. Bellamy, L.J., The Infra-red Spectra of Complex Molecules (John Wiley and Sons, New York, 1954) p. 280.
36. Coleman, L.B., "Technique for Conductivity Measurements on Single Crystals of Organic Materials," Rev. Sci. Instrum. 46, 1125-1126 (1975).
37. Montgomery, H.C., "Method for Measuring Electrical Resistivity of Anisotropic Materials," J. Appl. Phys. 42, 2971-2975 (1971).
38. Chittick, R.C., Alexander, J.H., and Sterling, H.F., "The Preparation and Properties of Amorphous Silicon," J. Electrochem. Soc. Solid State Sci. 116, 77-81 (1969).
39. Ferguson, E.E., Fehsenfeld, F.C., and Schmeltekopf, A.L., "Flowing After-glow Measurements of Ion-Neutral Reactions," Adv. Atom. Molec. Phys. 5, 1-56 (1969).
40. Reid, R.C. and Sherwood, T.K., The Properties of Gases and Liquids (McGraw Hill, New York, 1966).
41. Kaufman, F., "Reactions of Oxygen Atoms," Prog. React. Kin. 1, 1-39 (1961).

TABLE I
COMPARISON OF EQUILIBRIUM CONSTANTS WITH HYDROGEN MOLECULES
AND HYDROGEN ATOMS AS REACTANTS^a

	log K _p					
	Molecules			Atoms		
	298 K	1000 K	1500 K	298 K	1000 K	1500 K
(1) SiO ₂ (s) + 2H ₂ → Si(s) + 2H ₂ O or 4H	-60.9	-18.1	-10.9	72.3	23.8	14.9
(2) SiCl ₄ + 4H ₂ → SiH ₄ + 4HCl or 8H	-52.1	-13.0	-7.73	233	56.4	30.3
(3) SiCl ₃ H + 3H ₂ → SiH ₄ + 3HCl or 6H	-36.3	-9.40	-5.79	178	42.6	22.8

^a The thermodynamic data were taken from JANAF tables.¹⁹

TABLE II
EFFECT OF ELECTRON ENERGY ON THE CRACKING PATTERN
OF CHLOROSILANES^a

	Electron Energy (eV)	Relative Intensity at Mass			
		170 SiCl ₄ ⁺	133 SiCl ₃ ⁺	98 SiCl ₂ ⁺	63 SiCl ⁺
SiCl ₄	73	0.35	1.00	0.13	0.55
	26	1.00	0.98	0.04	0.18
	18	1.00	0.55	---	---
SiHCl ₃	73	---	1.00	0.14	0.95
	26	---	1.00	0.37	0.04
	18	---	1.00	0.28	0.03
SiH ₂ Cl ₂	73	---	---	0.42	1.00
	26	---	---	1.00	0.48
	18	---	---	1.00	0.16

^a The 73 eV data were taken with the magnetic mass spectrometer and the 26 and 18 eV data were taken with the quadrupole mass spectrometer.

TABLE
 HDYROGEN ATOM

No.	Nozzle Polarity	Run No.	Pressure (Torr)		Voltage (V)	Current (A)	\dot{m}_{H_2} (10^{-3} mol s $^{-1}$)	H Conc. (mol %)
			P _o Off	P _u On				
1	-	5	50	56	780	0.18	15.5	0.2
				62	720	0.30		0.6
				66	680	0.50		1.1
				83	700	1.0		1.4
1	+	1	50	64	760	0.3	15.5	0.9
				91	740	1.0		2.5
				113	740	1.8		3.5
1	+	2	225	285	1600	0.55	69.2	0.2
				302	1540	0.85		0.3
				313	1500	1.1		0.7
2	-	3	50	58	755	0.5	54.3	0.4
				64	720	1.0		0.6
				68	705	1.5		1.0
				73	710	2.0		1.4
2	+	4	50	57	625	0.5	54.3	0.5
				63	610	1.0		1.0
				67	600	1.5		2.0
				72	580	2.0		2.8
2	+	6	50	58	930	0.35	54.3	0.2
				64	850	1.0		2.3
				77	870	2.0		2.8
				82	870	2.5		0.9
2	+	7	25	25	635	0.1	27.2	0.05
				29	700	0.5		1.0
				37	690	1.0		2.1
				38	670	1.5		2.0
				43	700	2.0		1.4
				47	715	2.5		1.1

III

YIELD MEASUREMENTS

Nozzle Gas Temp. (K)	Energy Distribution					Efficiency (mol H/kWh)
	Total (W)	Coolant (%)	Gas Heat (%)	Dissoc. (%)	Unacc. (%)	
360	137	68	20	6	6	0.8
460	216	--	17	9	--	1.6
510	340	55	28	11	6	1.8
815	700	34	33	8	25	1.1
485	228	40	36	13	11	2.2
1000	740	37	43	11	9	1.9
1540	1330	33	45	9	13	1.5
470	880	29	39	4	28	0.6
530	1310	30	36	4	30	0.6
570	1650	22	33	7	38	1.2
395	378	40	40	12	8	2.1
485	720	42	41	10	7	1.6
540	1060	39	21	11	29	1.8
630	1420	21	37	12	30	1.9
380	313	29	41	17	13	3.1
470	610	32	44	20	4	3.2
525	900	31	30	23	16	4.3
610	1160	33	43	29	-5	4.7
400	326	46	49	8	-3	1.2
490	850	41	35	32	-8	5.3
710	1730	38	39	20	3	3.2
800	2175	36	40	5	29	0.8
300	64	--	0	5	--	0.8
400	350	50	23	18	9	2.8
640	690	49	39	18	-6	3.0
700	1000	46	32	12	10	2.0
890	1400	--	34	9	--	1.0
1060	1790	--	34	4	--	0.6

TABLE IV
CHARACTERIZATION OF NOZZLE NO. 6^a

\dot{m}_{H_2} (mmol s ⁻¹)	Upstream Pressure P_u (Torr)	Down- stream Pressure P_d (Torr)	P_u/P_d	Energy Distribution (%)			H-Atom Conc. (%)
				Coolant	Gas Heating	H Atoms	
32	28	10	2.8	45	23	32	3.2
44	35	15	2.3	43	29	28	1.9
52	40	17	2.4	38	32	30	2.1
32	34	26	1.3	51	20	29	2.6
44	41	31	1.3	44	34	32	2.0
52	50	39	1.3	42	36	32	1.4
32	46	40	1.1	45	25	30	3.3
44	68	62	1.1	41	38	21	1.6
52	71	65	1.2	38	48	14	0.8

^a Results pertain to an input electrical power of 1500 W.

TABLE V
 MASS SPECTROMETRIC STUDY OF H/H₂ + SiHCl₃
 Runs 112-113
 Nozzle no. 2, P_o = 50 Torr, P_d = 20 Torr

SiHCl ₃ Flow (ml s ⁻¹)	Discharge Power (kW)	Probe Distance (cm)	Change in Signal from Discharge "Off" to Discharge "On" (%)			
			SiCl ₃ ⁺	SiCl ₂ ⁺	SiCl ⁺	Si ⁺
1.2	1.2	21	-50	-20	-50	+100
5.9	1.0	29	-40	-60	-40	---
		51	-10	-10	-10	---
	2.0	29	-70	-80	-70	---
		51	-60	-50	-50	---
6.1	1.2	21	-30	-30	-20	+100
		51	-50	-40	+10	+100
12.2	1.2	21	-30	-10	-30	+60
		36	-30	-20	-30	+10
		51	-60	-40	-30	-10
Averages			-43	-36	-32	+36

TABLE
PRODUCT

Nozzle no. 5, anode; Discharge Power = 1000 W,

<u>Run No.</u>	<u>Injector Tubes</u>	<u>P_d (Torr)</u>	<u>H-Atom Conc. (%)</u>	<u>Equivalence Ratio</u>
11	Parallel	23	1.0	2.6
12	Parallel	23	1.0	0.4
14	Angled	24	1.0	2.6
15	Angled	27	1.0	0.4
16 ^c	Angled	50	0.2	1.8
17 ^c	Angled	50	0.2	13.1
18 ^d	Angled	28	1.0	2.6

^a Assumed to be solid Si.

^b Not measured.

^c Discharge pressure = 72 Torr, T_d = 440 K.

^d Used electronic grade SiCl₄; technical grade used for all other runs.

VI

COLLECTION EXPERIMENTS

Discharge Pressure = 62-65 Torr, $\dot{m}_{\text{H}_2} = 64 \text{ mmol s}^{-1}$, $T_d = 380 \text{ K}$

% of Input Si Recovered						Total Products	Correction Factor
<u>SiCl₄</u>	<u>SiHCl₃</u>	<u>SiH₂Cl₂</u>	<u>SiH₃Cl</u>	<u>SiH₄</u>	<u>Solid^a</u>		
79	15	4.6	< 0.1	0.5	1.2	21	1.3
95	1.5	1.5	< 0.1	0.2	1.6	4.8	1.7
86	10	2.7	< 0.1	1.3	--- ^b	14	1.6
94	2.2	3.7	< 0.1	0.3	--- ^b	6.2	1.4
96	0.6	1.2	< 0.1	1.9	0.3	4.0	1.9
97	2.8	1.0	< 0.1	0.4	< 0.1	4.2	1.4
99	< 0.1	< 0.1	0.7	0.2	< 0.1	0.9	1.5

TABLE VII
 CONDITIONS OF FIRST FILM DEPOSITION EXPERIMENTS

	Experimental Conditions ^a		
	1	2	3
Upstream pressure, Torr	60-65	65	65
Synthesis region pressure, Torr	56-60	15-18	15
H ₂ flow, mmol s ⁻¹	18	43	43
Jet temperature, ^b K	850	350	350
Jet velocity, ^b m s ⁻¹	180	2300	2300
H-atom concentration, %	3	2.5	2.5
Equivalence ratio ^c	0.010-0.016	0.025	0.83

^a Measurements were made using the stainless steel, 6.1 mm i.d. nozzle no. 4 in the nozzle-as-anode and using the rake injector, Fig. 9.

^b Values of the jet temperature, T_d , and jet velocity, u , are calculated assuming isentropic expansion at the pressure ratio. The upstream temperature was obtained as described previously. H-atom measurements were obtained by NO₂ titration.

^c For definition see footnote page 33.

TABLE VIII
SUMMARY OF FIRST FILM DEPOSITION EXPERIMENTS FROM SiCl_4 ^a

Run No.	Collection	Experimental Condition ^b	Collector Temperature (K)	Duration of Runs (Hrs)	Comments in addition to text
<u>Polymer (tentative)</u>					
1	70 mm liner	1	equil. ^c	1.0	----
4	6 mm cooled probe	1	290	0.17	Densest deposition on downstream side of probe; hydrolyzed to white (SiO_2) coating with dull brown remaining upstream in center of probe.
<u>Amorphous Si (tentative)</u>					
2	70 mm liner	2	equil.	1.5	----
6	6 mm heated probe	2	790	0.75	Densest upstream; iridescent brown.
7	6 mm heated probe	1	790	0.17	Densest upstream; iridescent brown.
5	6 mm cooled probe	2	290	0.75	Densest upstream; translucent brown, poorly adhered to probe.
9	6 mm steady-state probe	1	equil.	0.17	Densest upstream; dull brown similar to run 4.
<u>Polycrystalline Si (tentative)</u>					
3	70 mm liner	3	equil.	4.0	----

^a Without H/H_2 discharge, no solid product is collected.

^b As listed in Table VII, reaction time at 10 cm downstream is 0.6 ms for condition 1 and 0.04 ms for conditions 2 and 3.

^c Temperature not regulated, collection surface allowed to come to thermal steady-state.

TABLE IX
 CONDITIONS FOR RUNS 116 TO 147
 Nozzle No. 2

Hydrogen flow rate, mmol s^{-1}	54
H-atom concentration, % H_2	3
Upstream discharge pressure, P_u , Torr	75
Downstream reaction chamber pressure, P_d , Torr ^a	18
Discharge voltage, V	780
Discharge current, A	2.1
Discharge power, W	1600
H/ H_2 jet temperature, K	
Static	440
Stagnation	670
H/ H_2 jet velocity, m s^{-1}	2.6×10^3

^a Some variation in downstream pressures was observed because the 70 l s^{-1} vacuum pump was on its last legs. This pump was replaced by a new 140 l s^{-1} pump.

TABLE X

SOLID DEPOSITION EXPERIMENTS WITH VARIOUS REACTANTS

Runs 116-131, see Table IX for conditions.

Chlorosilane or Silane Feed at 7.7 ml s⁻¹, Vycor Slides

Run No.	Reactant	Equivalence Ratio	Run Time (min)	Relative Deposit ^a	Observations
119	SiH ₄	0.43	5	3	Jet white with some green for ≈ 15 cm, orangish-brown talc like deposit, rubbed off easily, not hygroscopic.
124	SiCl ₄ (Technical)	0.85	15	3	Dull brown with gray cast strongly adherent.
126			30	4	Shiny gray-brown deposit which flaked away, appeared to be dull gray deposit over a glassy brown deposit.
125			60	4	Flaky deposit like run 126, but more flaky.
116			90	4	Flaky deposit.
120	SiCl ₄ (Semiconductor)	0.85	15	2	Glassy brown strongly adherent.
123			15	1	Very little coating compared to run 120. New package of slides with finger smudges, cleaned with trichloroethylene. ^b
122			30	3	Brown with dull gray cast strongly adherent.
121			60	4	Similar to run 122 but appears less dense, strongly adherent.

(continued on next page)

TABLE X (continued)

<u>Run No.</u>	<u>Reactant</u>	<u>Equivalence Ratio</u>	<u>Run Time (min)</u>	<u>Relative^a Deposit</u>	<u>Observations</u>
129	SiHCl ₃	0.85	3.3	1	Brown deposit, not very adherent.
128			7.5	3	Dark brown shiny deposit which flaked off.
130			7.5	2	Slide exposed in center of tube, end on to jet.
131			7.5	2	Similar to run 128 but more flaky.
127			15	3	Similar to run 128 but more flaky.

^a Visual inspection. 1-4 for light to heavy.

^b Prior to run 123 slides were cleaned with a paper towel; after this run they were cleaned with trichloroethylene and wiped with a paper towel.

TABLE XI
CONVERSION EFFICIENCY OF REAGENT TO SILICON

<u>Reactant</u>	<u>Run No.</u>	<u>Total Weight^a of Deposit (g)</u>	<u>Rate of Deposit (mg s⁻¹)</u>	<u>Conversion Efficiency (mol %) Reagent as Silicon</u>
SiCl ₄ (Technical)	116	4.2	0.79	8
SiCl ₄ (Semiconductor)	117	1.4	0.25	3
Silane	119	0.21	0.70	7

^a Estimating the weight deposited between the slides and assuming the deposit on the reactor tube has the same density as that on the slide.

TABLE XII
SOLID DEPOSITION EXPERIMENTS FOR SiHCl₃ REACTANT
Runs 132-141, see Table IX for conditions.

5 min Runs

<u>Run No.</u>	<u>SiHCl₃ Flow (ml s⁻¹)</u>	<u>Equivalence Ratio</u>	<u>Observations</u>
141	0.5	0.06	Heavy brown adhering deposit.
139	1.0	0.11	Heavy brown adhering deposit.
136	2.0	0.23	Less heavy brown deposit with tendency to flake.
134	3.9	0.43	Heavy brown adhering deposit.
140	5.0	0.55	Very light deposit, flaky.
137	6.0	0.66	Slightly heavier brown deposit than run 140.
132	7.7	0.85	Somewhat heavier brown deposit.
135	10	1.10	Metallic appearing thin deposit.
133	15	1.65	Light shiny thin metallic deposit appearing with large variation in density.
138	18	1.98	Similar to run 133.

TABLE
SUMMARY OF NOZZLE NO. 6

Run No. ^a	Substrate	Reactant Flow (mmol ⁻¹ s ⁻¹)		Operating Pressure (Torr)	
		H ₂	SiCl ₄ ^d	Discharge	Reactor
128-2 ^c	Vycor	49.7	0.3444 ^d	73	18
143-3 ^f	Pyrex	52.0	0.344	78	16
244-2	Pyrex	31.5	0.076	40	13
245-3	Pyrex	31.5	0.076	40	12
246-3	Aluminum	31.5	0.076	40	12
249-3	Pyrex	31.5	0.076	40	13
250-3	Pyrex	52.0	0.117	56	16
251-3	Pyrex	52.0	0.117	55	17
252-3 ^h	Pyrex	31.5	0.134	40	13
253-3 ^h	Pyrex	31.5	0.223	40	13
255-3 ^h	Pyrex	31.5	0.326	40	11
256-3	Pyrex	31.5	0.134	40	11
257-2	Pyrex	31.5	0.076	41	13
257-3	Pyrex	31.5	0.076	41	13
258-3	Pyrex	31.5	0.076	40	13
259-3	Pyrex	31.5	0.029	40	13
260-4	Pyrex	31.5	0.156	40	13
261-3	Aluminum	31.5	0.029	30	13
263-3	Aluminum	31.5	0.029	41	12
264-3	Aluminum	31.5	0.326	41	12
265-3	Aluminum	31.5	0.076	41	12
266-4	Pyrex	52.0	0.117	55	14
267-4 ^j	Pyrex	52.0	0.117	55	14
268-4	Pyrex	31.5	0.029	46	14
269-4 ^j	Pyrex	31.5	0.029	42	14
273-2	Pyrex	31.5	0.134	34	12
274-2 ^k	Pyrex	31.5	0.34	33	12

XIII

FILM PREPARATION RUNS

Discharge Power			Run Time (min)	Film Characterization		
(A)	(V)	(W)		Thick- ness (μm)	Morphology ^b	Chlorine (mol %)
2.0	800	1600	7.5	---	amorphous	25 ^e
2.2	770	1694	15.0	3.1	polycrystalline	4.4 ^e
2.0	710	1420	---	0.46	polycrystalline	---
2.0	700	1400	60.0	6.2	polycrystalline	---
2.0	700	1400	30.0	---	---	0.9 ^g
2.0	690	1380	60.0	5.7	polycrystalline	0.68 ^e
2.0	800	1600	20.0	2.4	amorphous	---
2.0	800	1600	60.0	4.5	polycrystalline	---
2.0	700	1400	20.0	3.5	amorphous	1.2 ^e
2.0	700	1400	31.0	4.8	amorphous	1.2 ^e
2.0	700	1400	22.0	3.0	amorphous	1.1 ^e
2.0	700	1400	---	1.7	polycrystalline	2.0 ^e
2.0	700	1400	20.0	1.5	amorphous	---
2.0	700	1400	20.0	2.9	amorphous ⁱ	---
2.0	700	1400	6.0	0.80	amorphous	---
2.0	700	1400	15.0	0.80	amorphous	1.1 ^e
2.0	700	1400	60.0	9.7	---	---
0.5	780	390	30.0	0.16	---	---
2.0	720	1440	30.0	---	---	1.8 ^g
2.0	720	1440	30.0	---	---	8.6 ^g
2.0	720	1440	30.0	---	---	0.9 ^g
2.0	770	1540	13.0	1.3	amorphous	---
2.0	770	1540	13.0	0.99	amorphous	---
2.0	690	1380	20.0	1.0	amorphous	---
2.0	680	1360	20.0	1.2	polycrystalline	---
2.0	730	1460	20.0	4.2	amorphous	---
2.0	740	1480	20.0	3.9	amorphous	---

TABLE XIII (continued)

Footnotes

- a The cathode was: copper through run 260 and for runs 273 and 274; nickel plated stainless for runs 261-265; and Elkonite for runs 266-269.
- b By X-ray diffraction.
- c With nozzle no. 2, see Tables VII and X.
- d SiHCl_3 .
- e Chlorine analysis by X-ray fluorescence spectroscopy (XFS).
- f With nozzle no. 2, see Table VII.
- g Chlorine analysis by particle induced X-ray emission (PIXE).
- h Electrode arcing during run.
- i Material changed from amorphous to polycrystalline upon heating to 500°C for 24 hrs under 1 atm of N_2 gas.
- j 1900 ppm of BCl_3 added to SiCl_4 gas stream.
- k 740 ppm of PH_3 added to SiCl_4 gas stream.

TABLE XIV
 SUCCESSFUL AMORPHOUS SILICON FILM DOPING EXPERIMENTS

Aluminum Substrate

Run No.	Reactant Composition				Pressure (Torr)	Voltage (V)	Current (MA)	Time (min)	Deposit	
	Ar (mmol s ⁻¹)	H ₂ (μmol s ⁻¹)	SiH ₄ (μmol s ⁻¹)	PH ₃ (mol % SiH ₄)					Mass (mg)	Relative Resistance
329	0.33	0.04	2.5	2.0	1.20	500	10	45	12.0	1
338	0.37	0.004	2.5	0.2	1.45	420	10	60	2.8	4.8
333	0.33	0.04	4.4	1.0	1.30	450	10	60	8.9	6.8
335	0.33	0.04	2.5	2.0	1.40	420	10	60	7.3	7.4
328	0.33	0.04	1.1	4.0	1.30	400	20	90	12.0	7.7
330	0.37	0	4.4	0	1.30	460	10	60	16.0	110
326	0.37	0	4.4	0	1.45	520	20	50	9.3	130
337	0.33	0.04	2.5	0	1.35	420	20	60	4.3	140
332	0.37	0	4.4	0	1.35	450	10	60	11.0	290
336	0.37	0	2.5	0	1.40	420	10	60	3.1	950

67

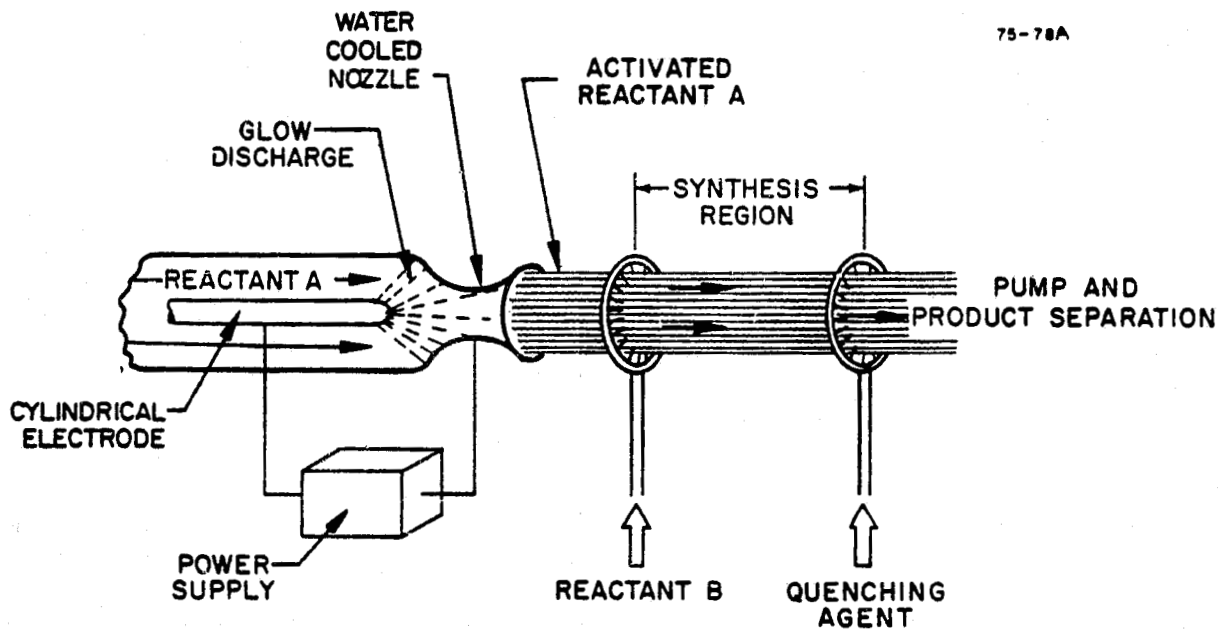


FIGURE 1 NON-EQUILIBRIUM PLASMA JET FOR CHEMICAL SYNTHESIS

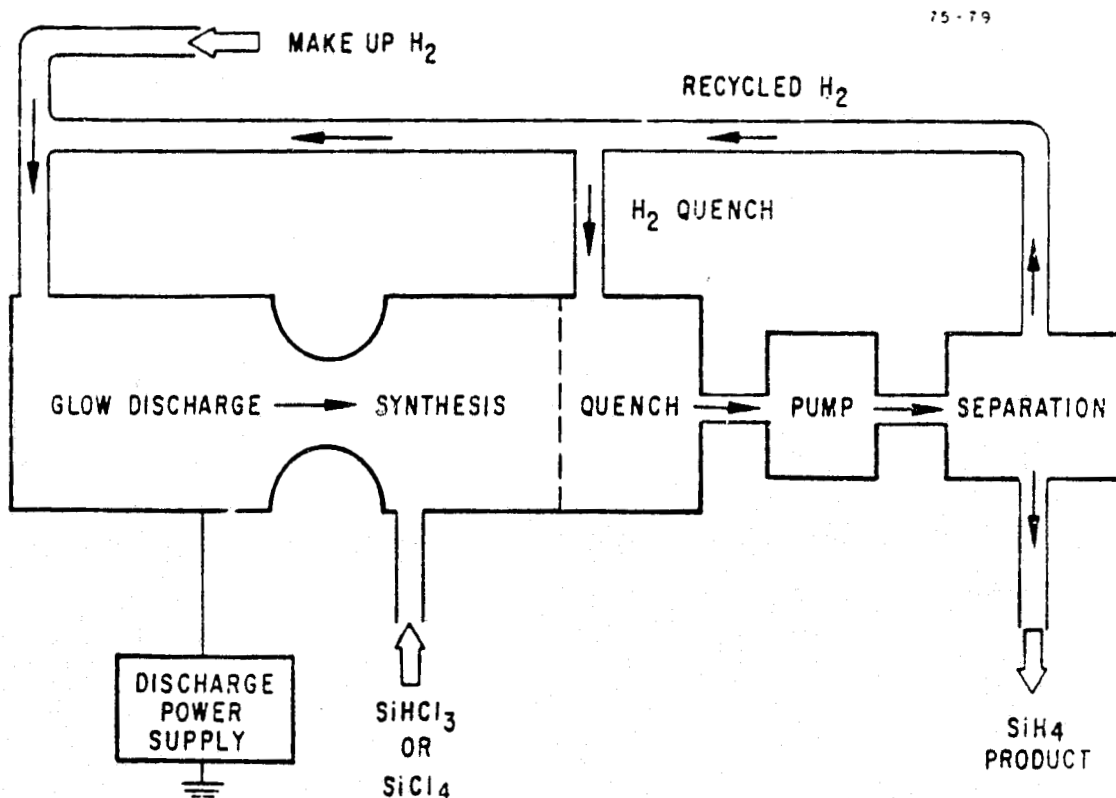
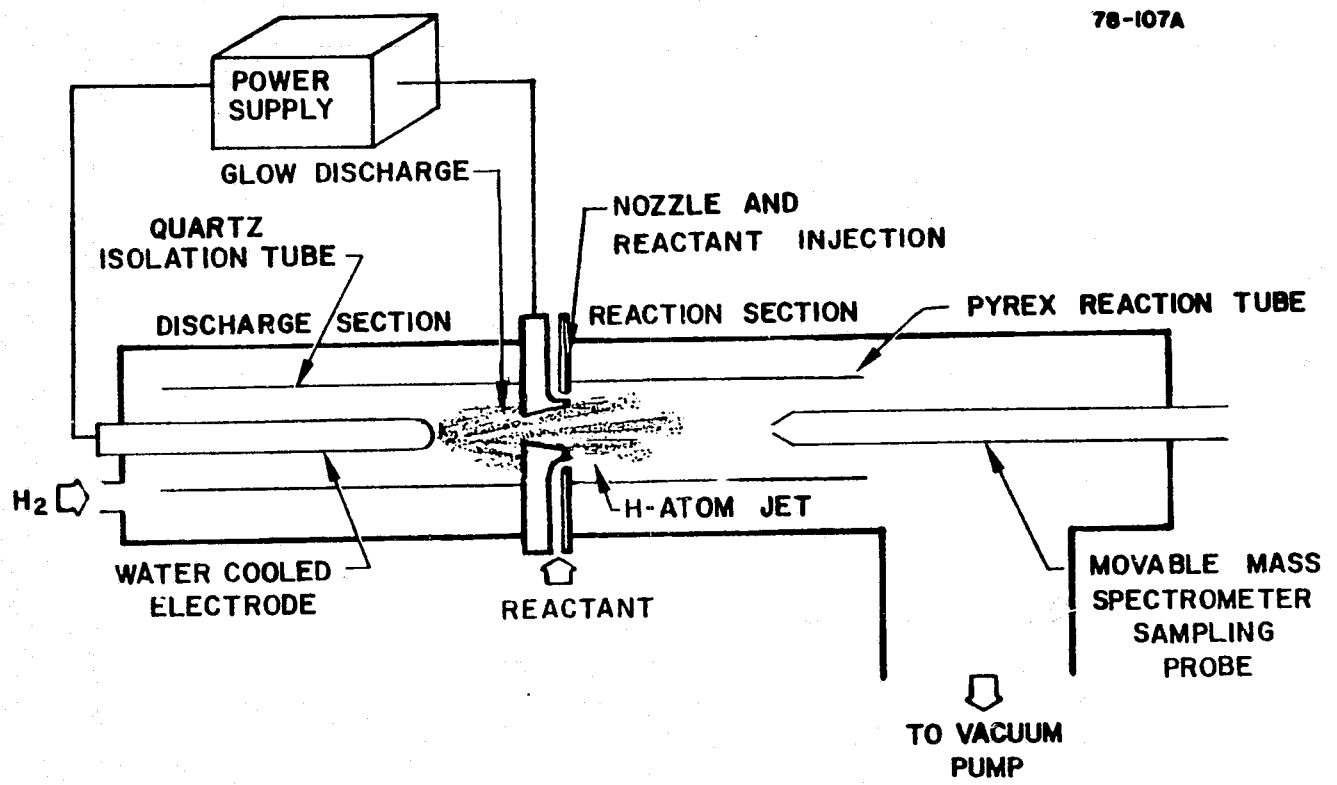


FIGURE 2 NON-EQUILIBRIUM PLASMA JET PROCESS FOR SYNTHESIS OF SILANE

76-107A



69

FIGURE 3 NON-EQUILIBRIUM PLASMA JET APPARATUS

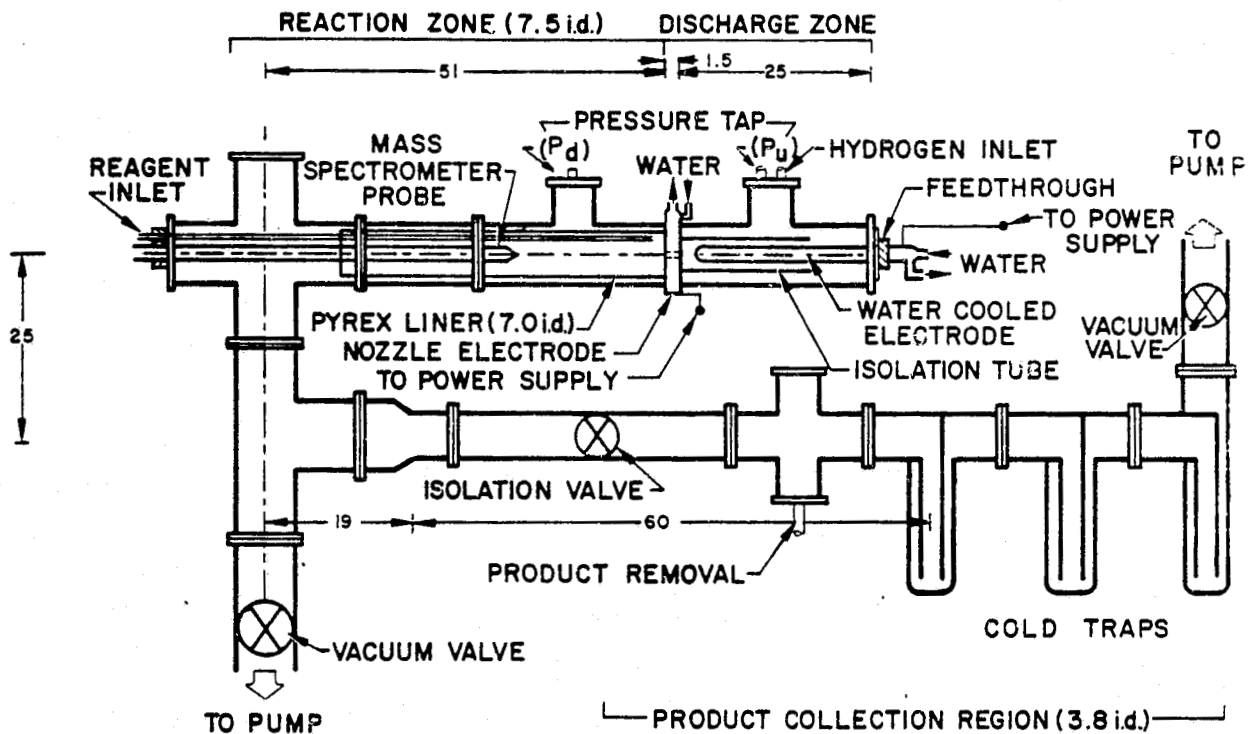
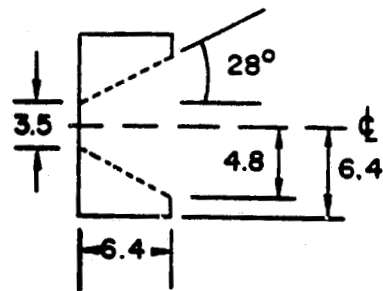
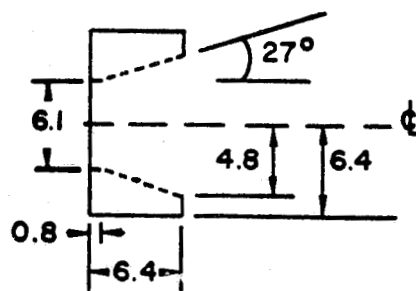


FIGURE 4 NON-EQUILIBRIUM PLASMA JET APPARATUS

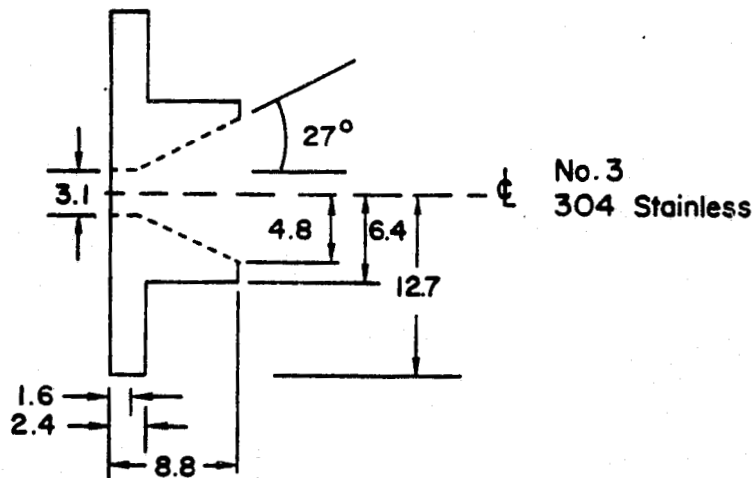
Dimensions in cm.



No. 1
Brass



No. 2
Brass



No. 3
304 Stainless

FIGURE 5 NOZZLE ELECTRODES NO. 1, 2, AND 3 FOR NON-EQUILIBRIUM PLASMA
JET GENERATION OF HYDROGEN ATOMS

Dimensions in mm.

77-14A

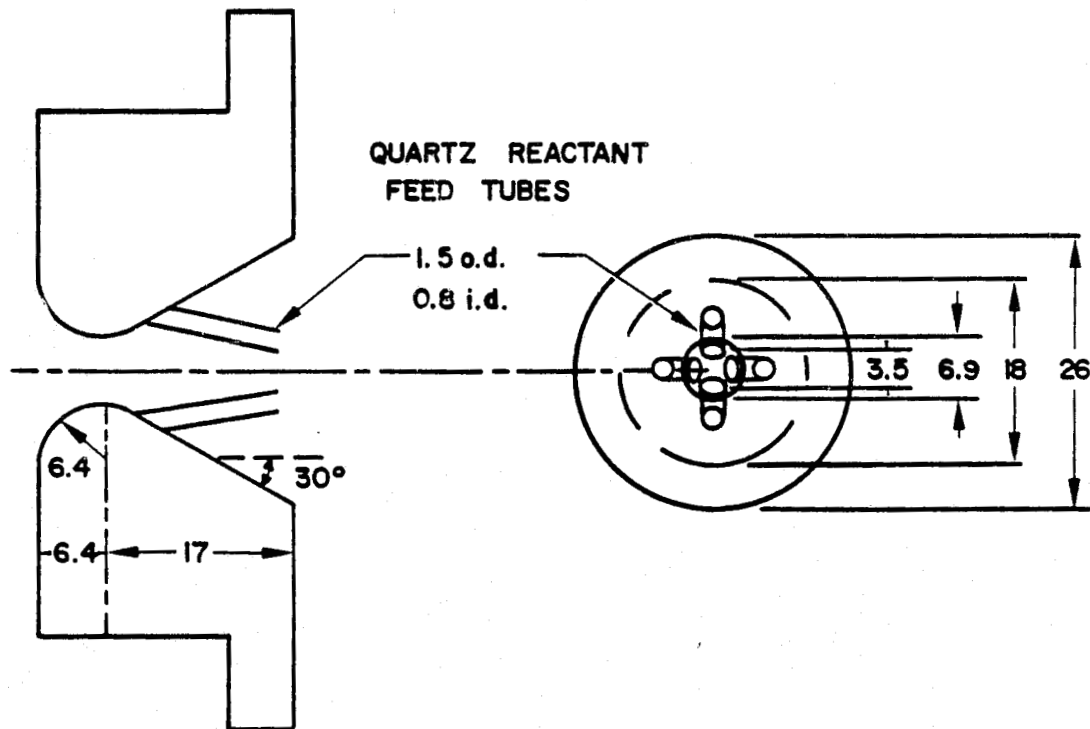


FIGURE 6 FLOWER-PETAL NOZZLE (NOZZLE NO. 5)
 Dimensions in mm.

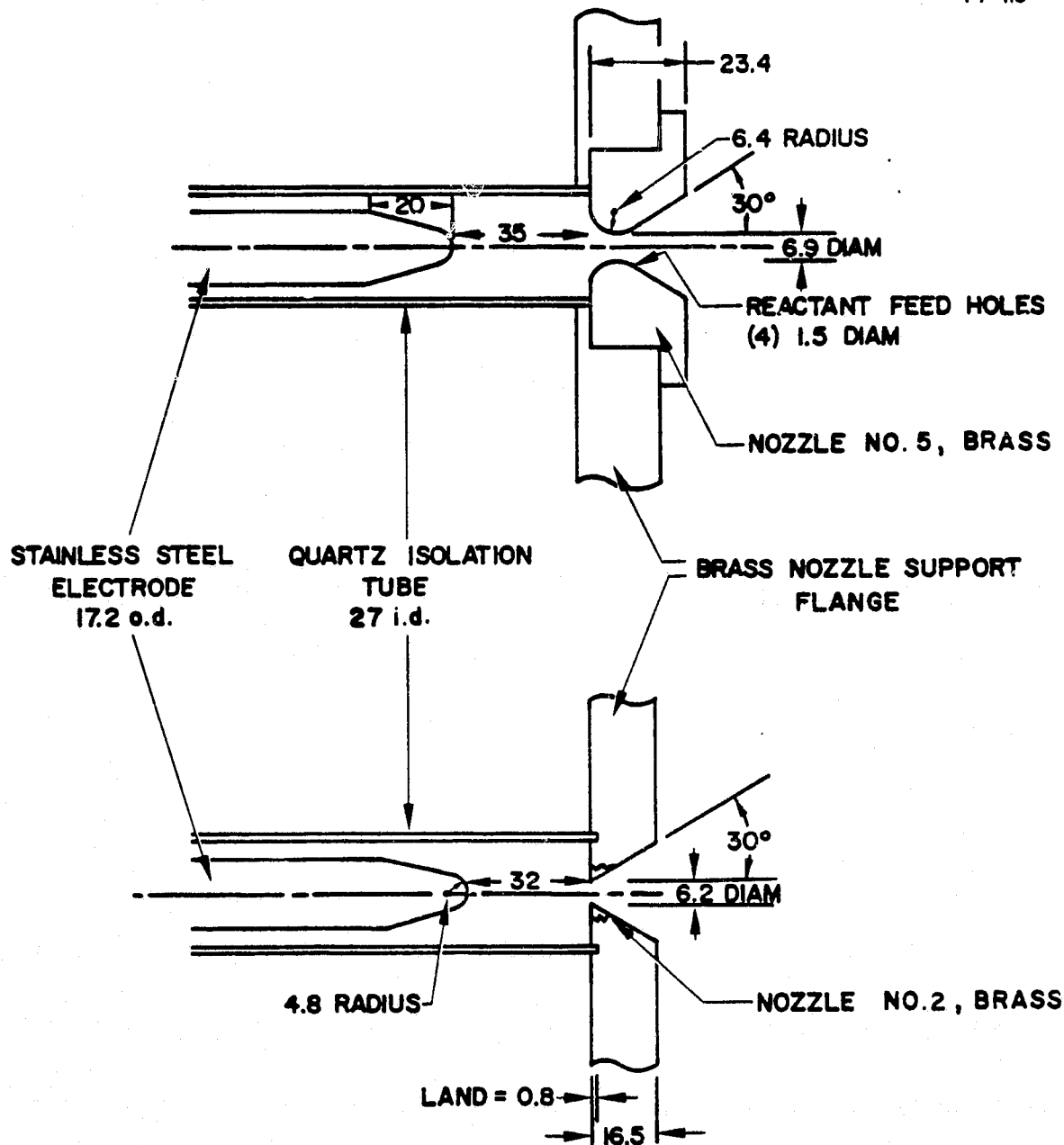
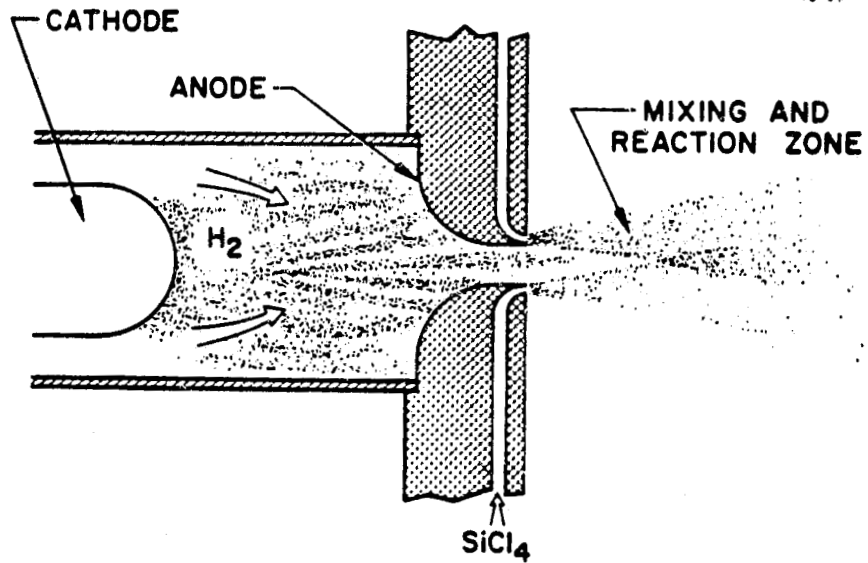


FIGURE 7 COMPARISON OF DISCHARGE REGION GEOMETRY IN NOZZLES NO. 5 AND 2

Dimensions in mm.



(a) SCHEMATIC

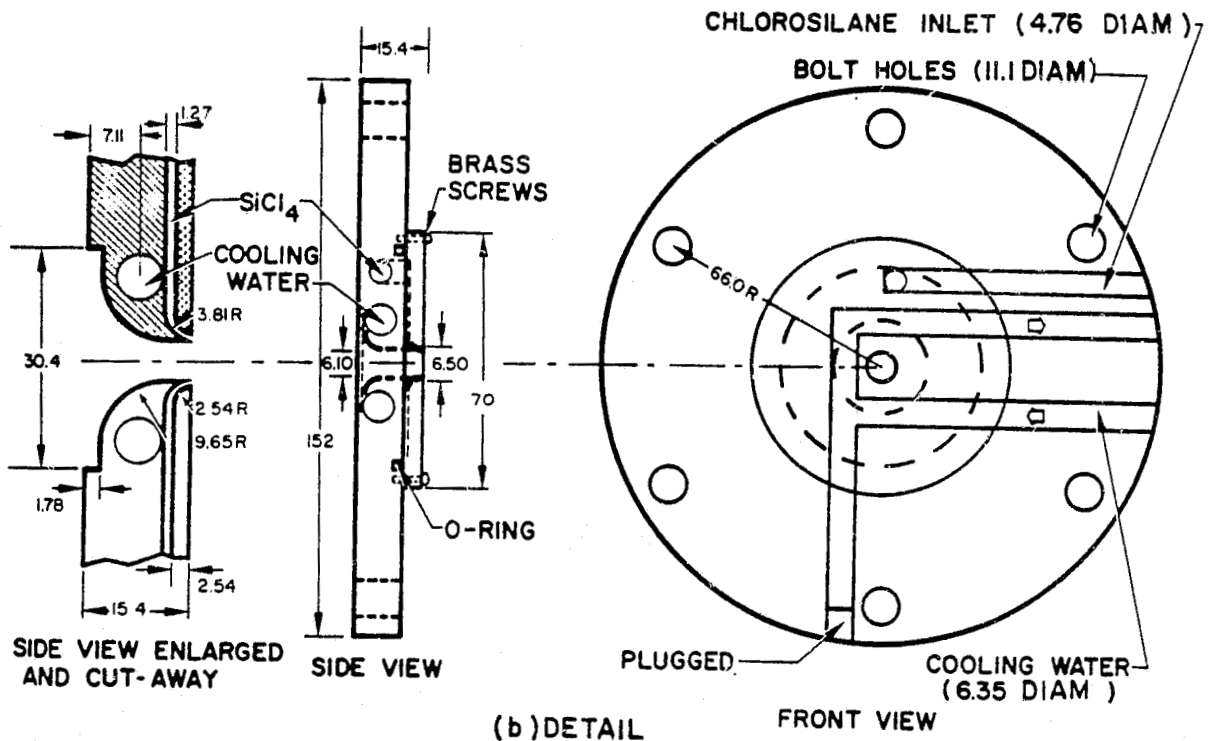


FIGURE 8 ANNULAR NOZZLE NO. 6

Dimensions in mm.

77-18A

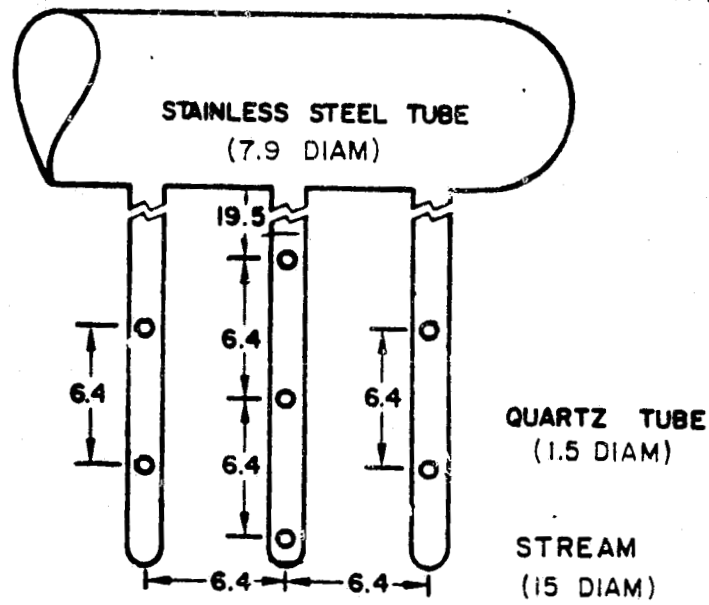


FIGURE 9 RAKE INJECTOR
Dimensions in mm.

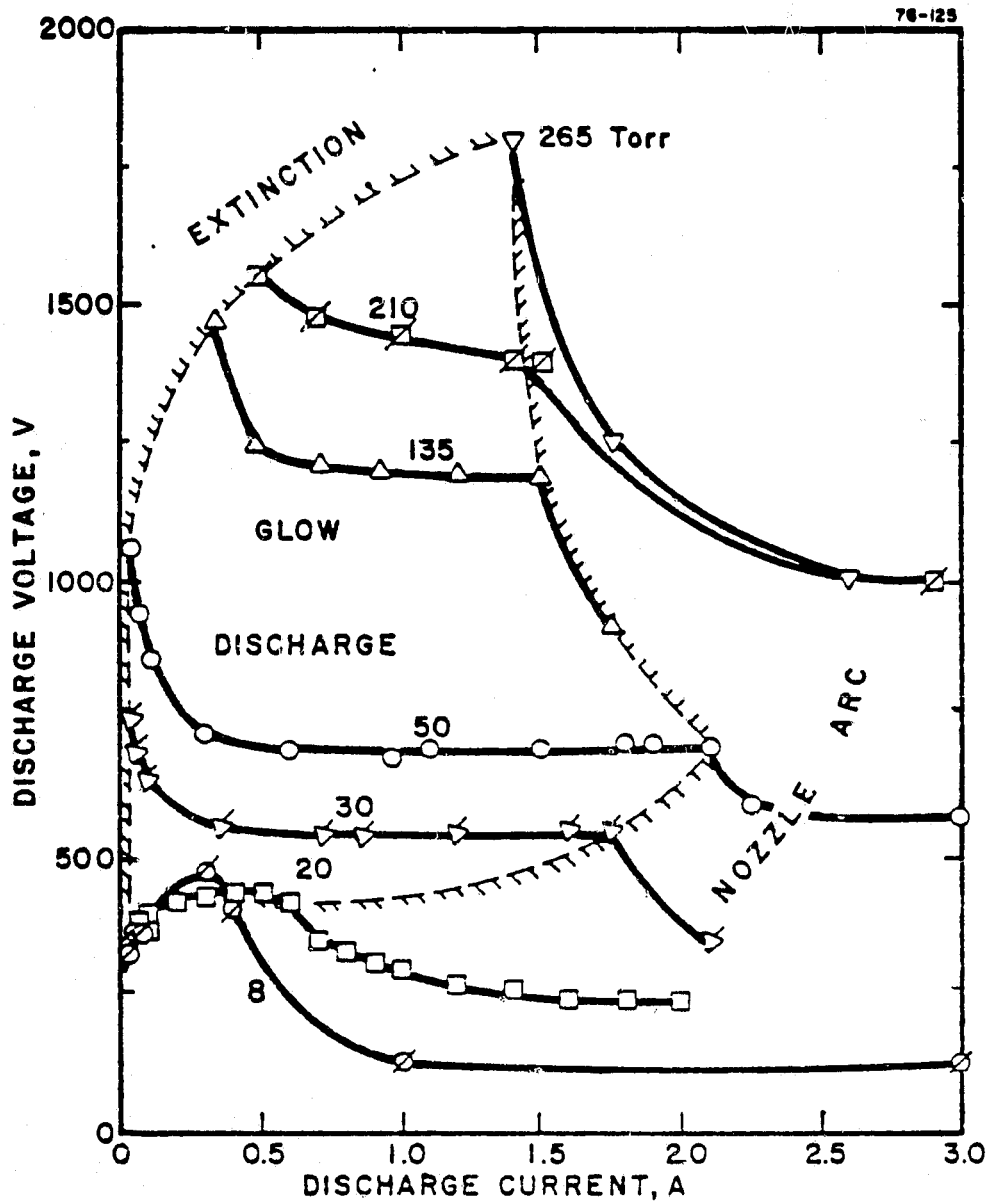


FIGURE 10 DISCHARGE STABILITY IN HYDROGEN

Nozzle no. 1, cathode, throat diam = 3.2 mm; electrode/nozzle distance = 3.2 cm. Pressure indicated with discharge off. Molar H_2 flow rates: 8 Torr - 1.6 mmol s^{-1} ; 20 - 4.3; 30 - 7.1; 50 - 12.3; 135 - 34.1; 210 - 53.0; 265 - 67.5.

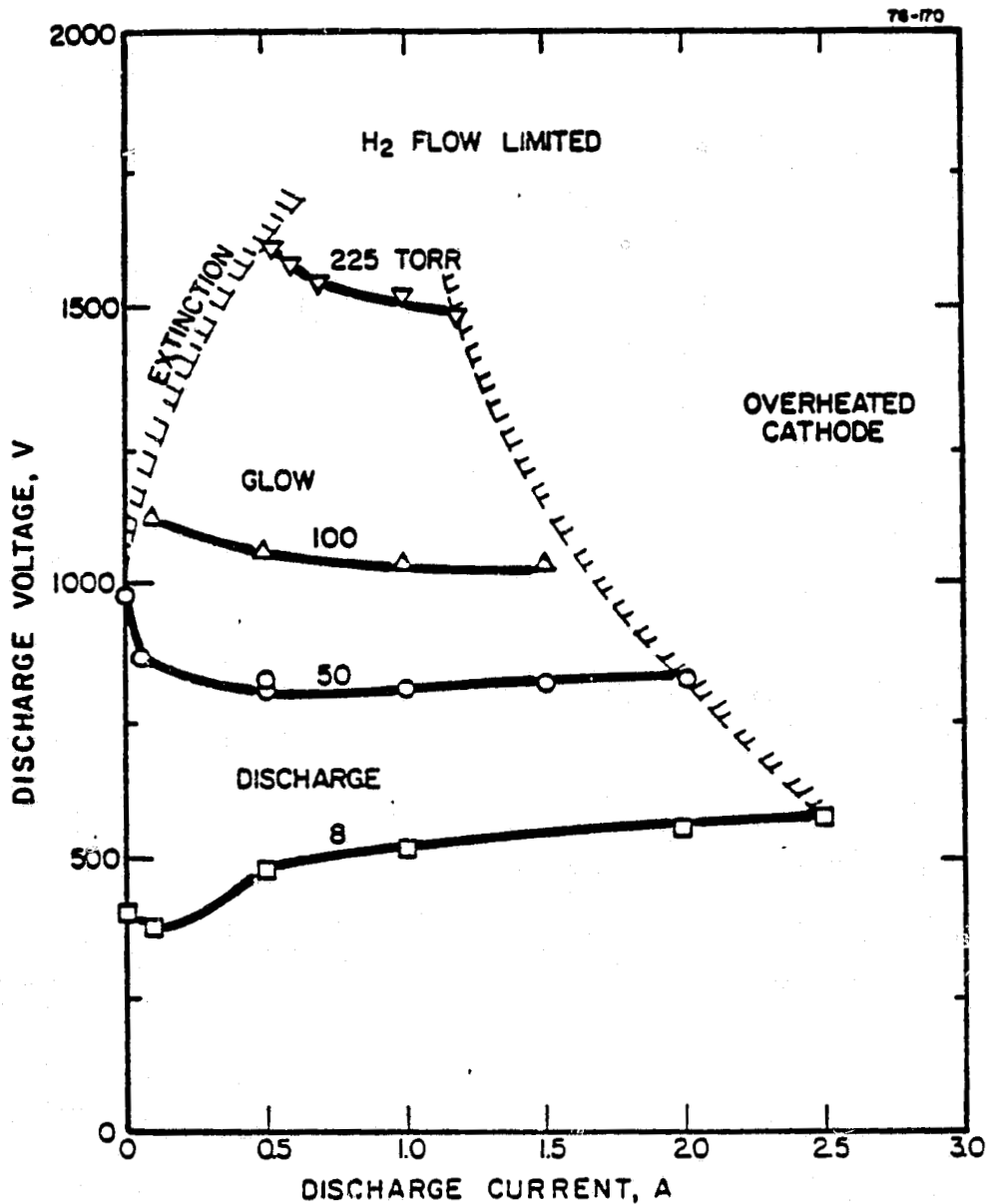


FIGURE 11 DISCHARGE STABILITY IN HYDROGEN

Nozzle no. 1, anode, throat diam = 3.5 mm; electrode/nozzle distance = 3.2 cm. Pressure indicated with discharge off. Molar H₂ flow rates: 8 Torr - 2.0 mmol s⁻¹; 50 - 15.5; 100 - 31.5; 225 - 69.2. Note change in flow rates from Fig. 10 due to nozzle erosion.

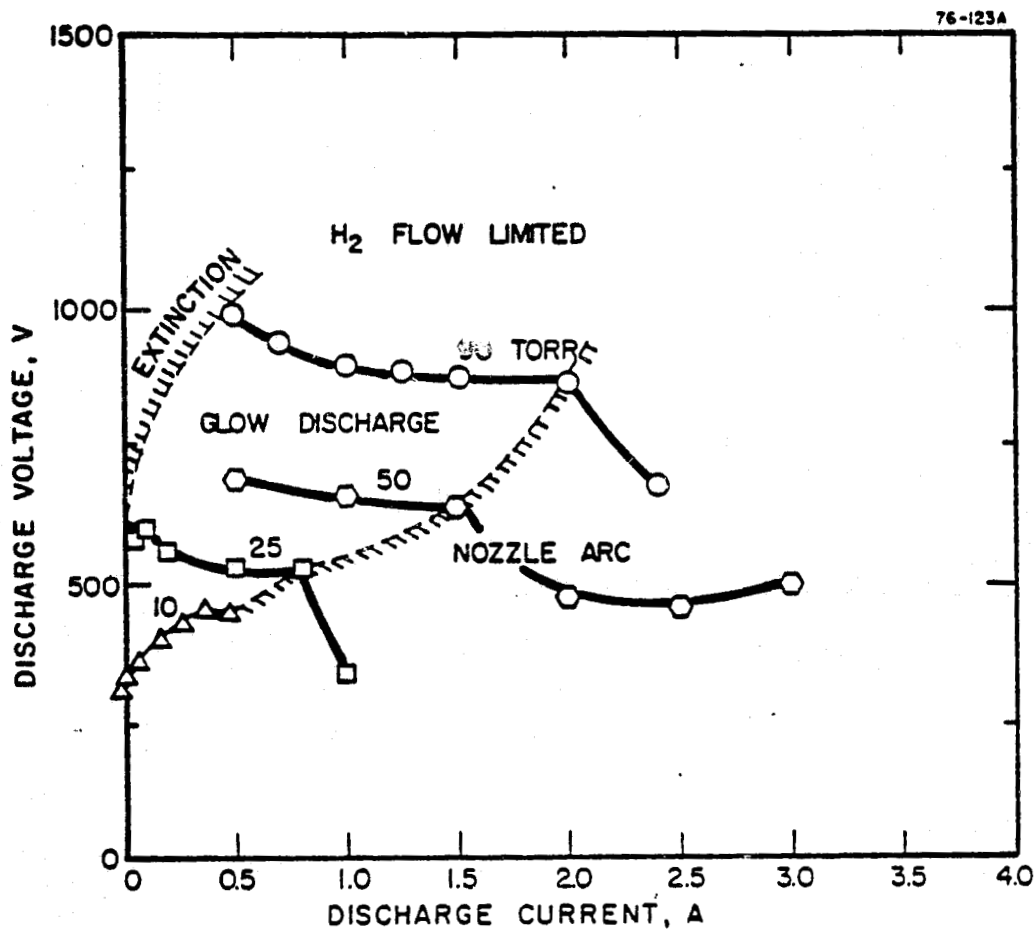


FIGURE 12 DISCHARGE STABILITY IN HYDROGEN

Nozzle no. 2, cathode, throat diam = 6.1 mm; electrode/nozzle distance = 3.2 cm. Pressure indicated with discharge off. Molar H₂ flow rates: 10 Torr - 27.2 mmol s⁻¹; 25 - 23.5; 50 - 49.8; 90 - 82.0.

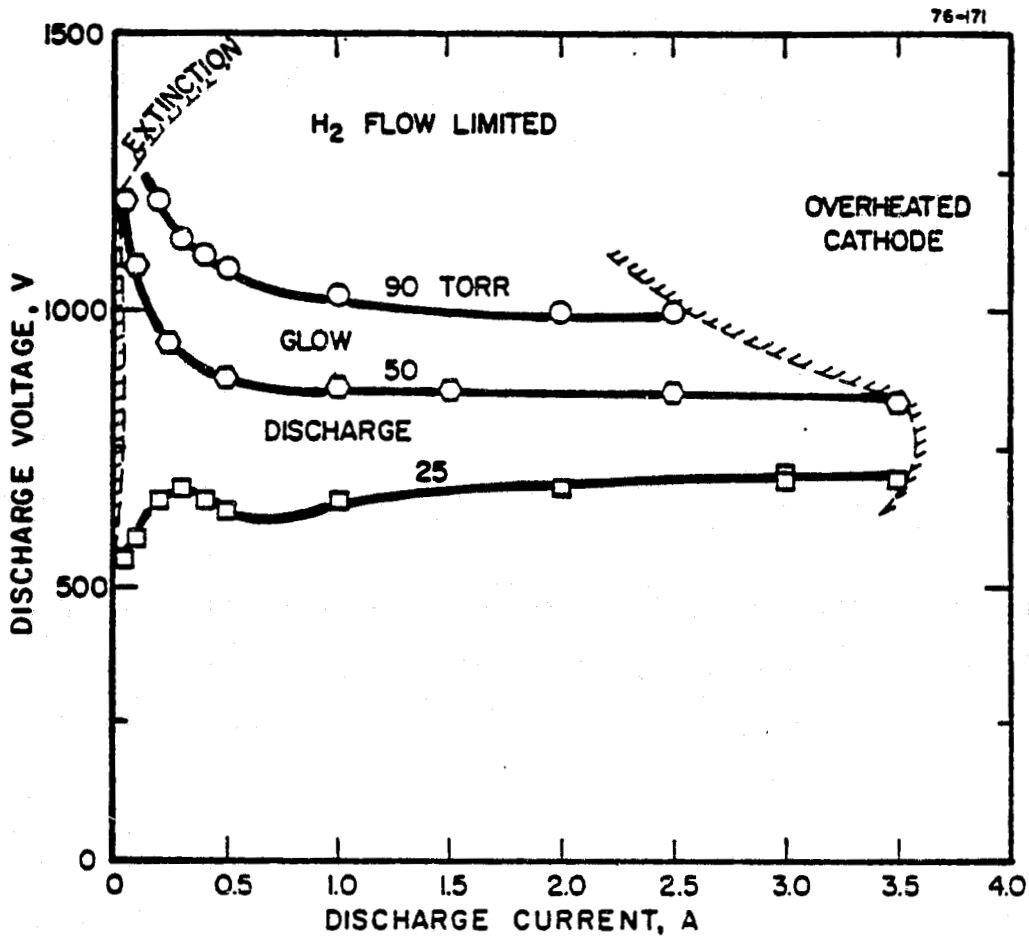


FIGURE 13 DISCHARGE STABILITY IN HYDROGEN

Nozzle no. 2, anode, throat diam = 6.1 mm; electrode/nozzle distance = 3.2 cm. Pressure indicated with discharge off. Molar H₂ flow rates: 25 Torr - 27.2 mmol s⁻¹; 50 - 54.3; 90 - 95.2.

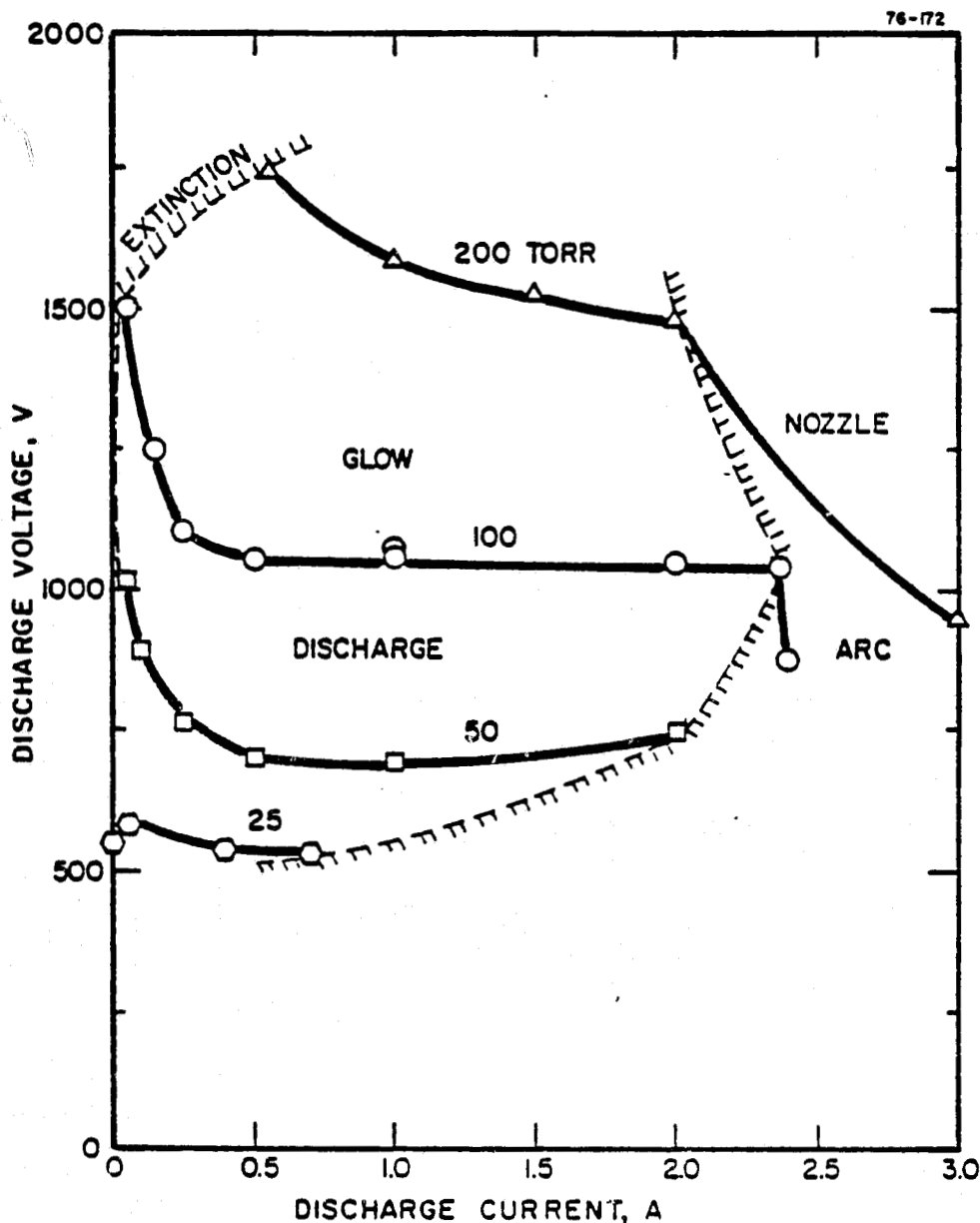


FIGURE 14 DISCHARGE STABILITY IN HYDROGEN

Nozzle no. 3, cathode, throat diam = 3.1 mm; electrode/nozzle distance = 3.2 cm. Pressure indicated with discharge off. Molar H₂ flow rates: 25 Torr - 5.9 mmol s⁻¹; 50 - 12.3; 100-24.3; 200 - 48.1.

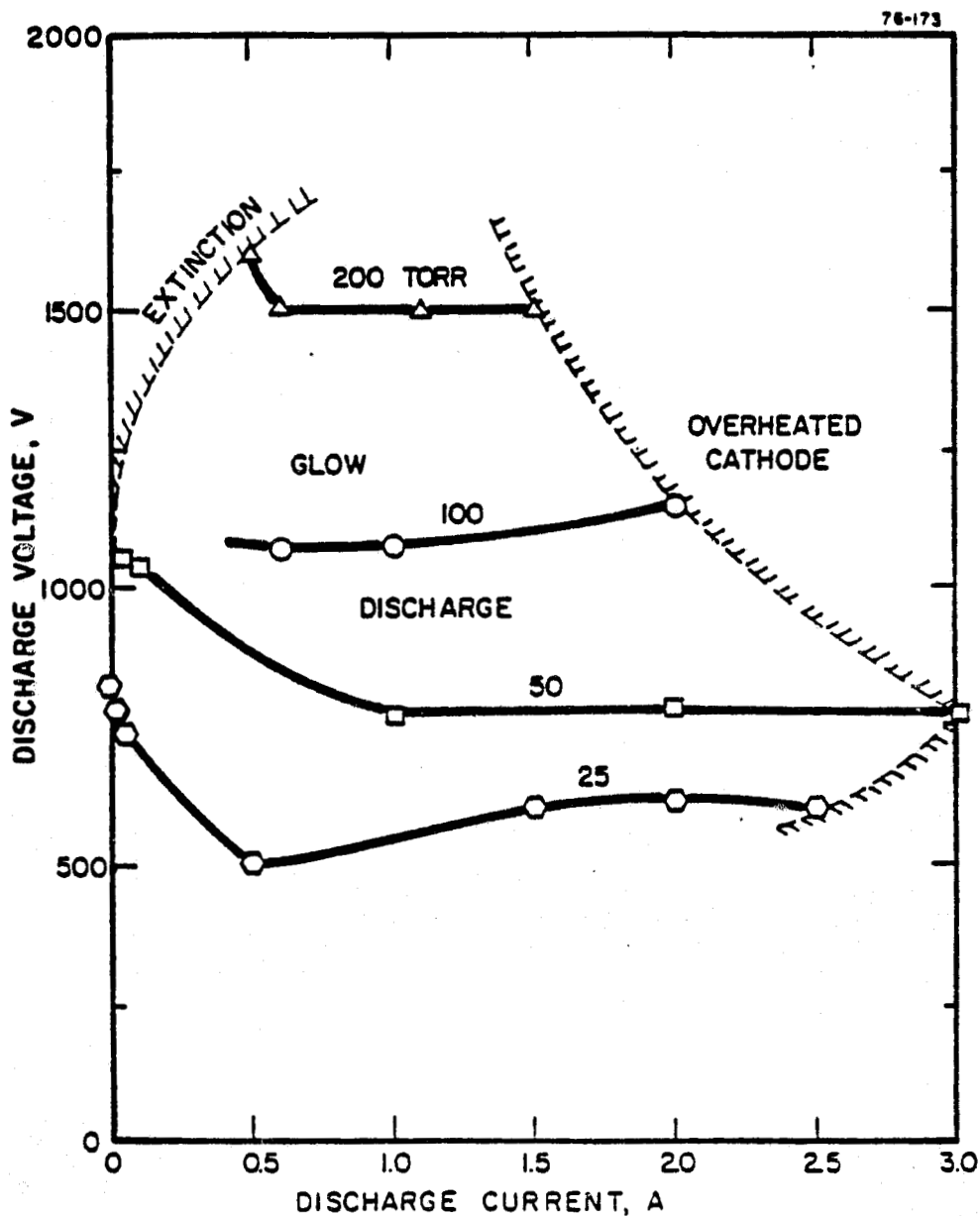


FIGURE 15 DISCHARGE STABILITY IN HYDROGEN

Nozzle no. 3, anode, throat diam = 3.1 mm; electrode/nozzle distance = 3.2 cm. Pressure indicated with discharge off. Molar H_2 flow rates: 25 Torr - 5.9 mmol s^{-1} ; 50 - 12.3; 100 - 24.3; 200 - 48.1.

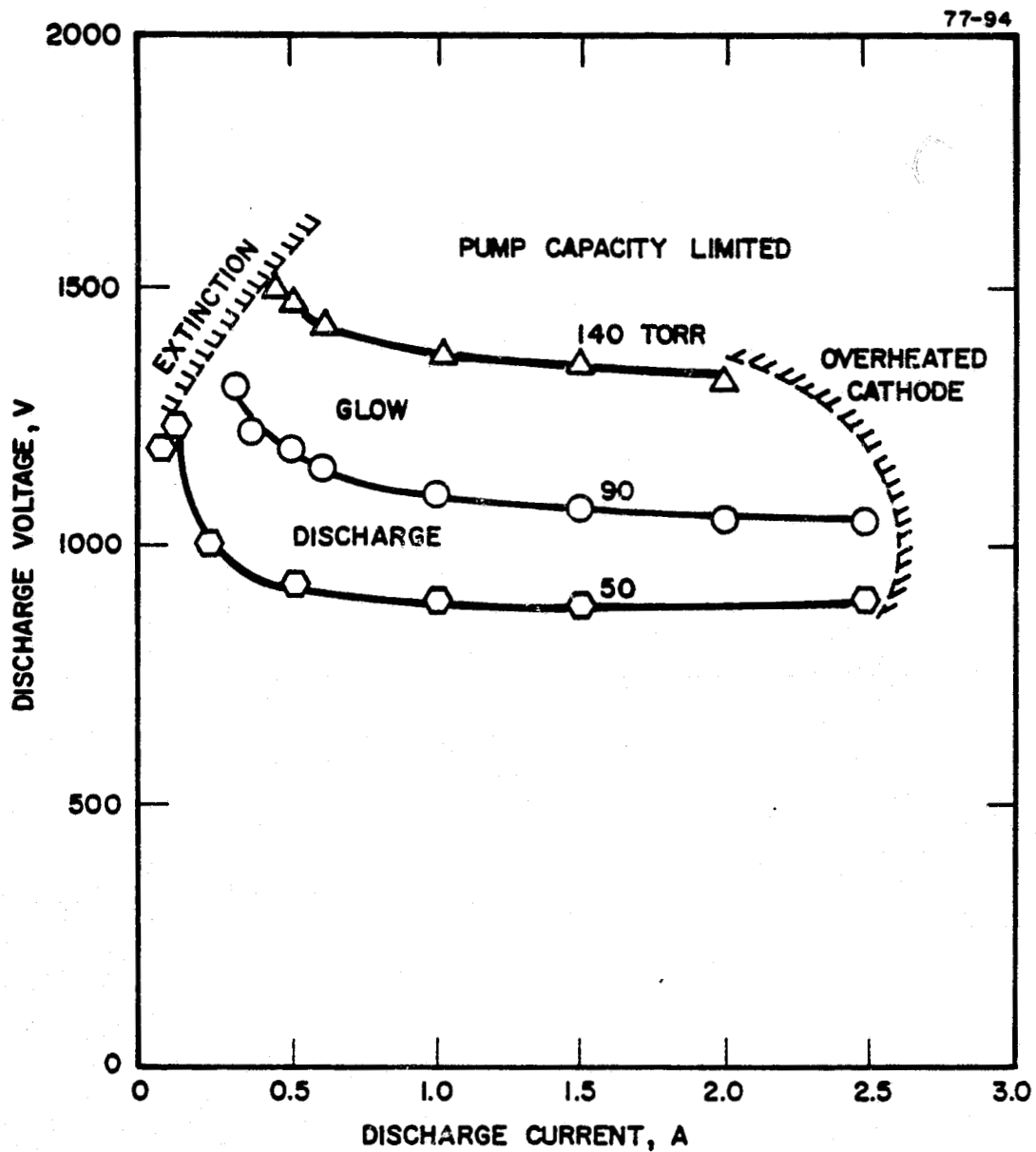


FIGURE 16 DISCHARGE STABILITY IN HYDROGEN

Nozzle no. 5, anode, throat diam = 6.9 mm; electrode/nozzle distance = 3.5 mm. Pressure indicated with discharge off. Molar H_2 flow rates: 50 Torr - 64 mmol s^{-1} ; 90 - 114; 140 - 183.

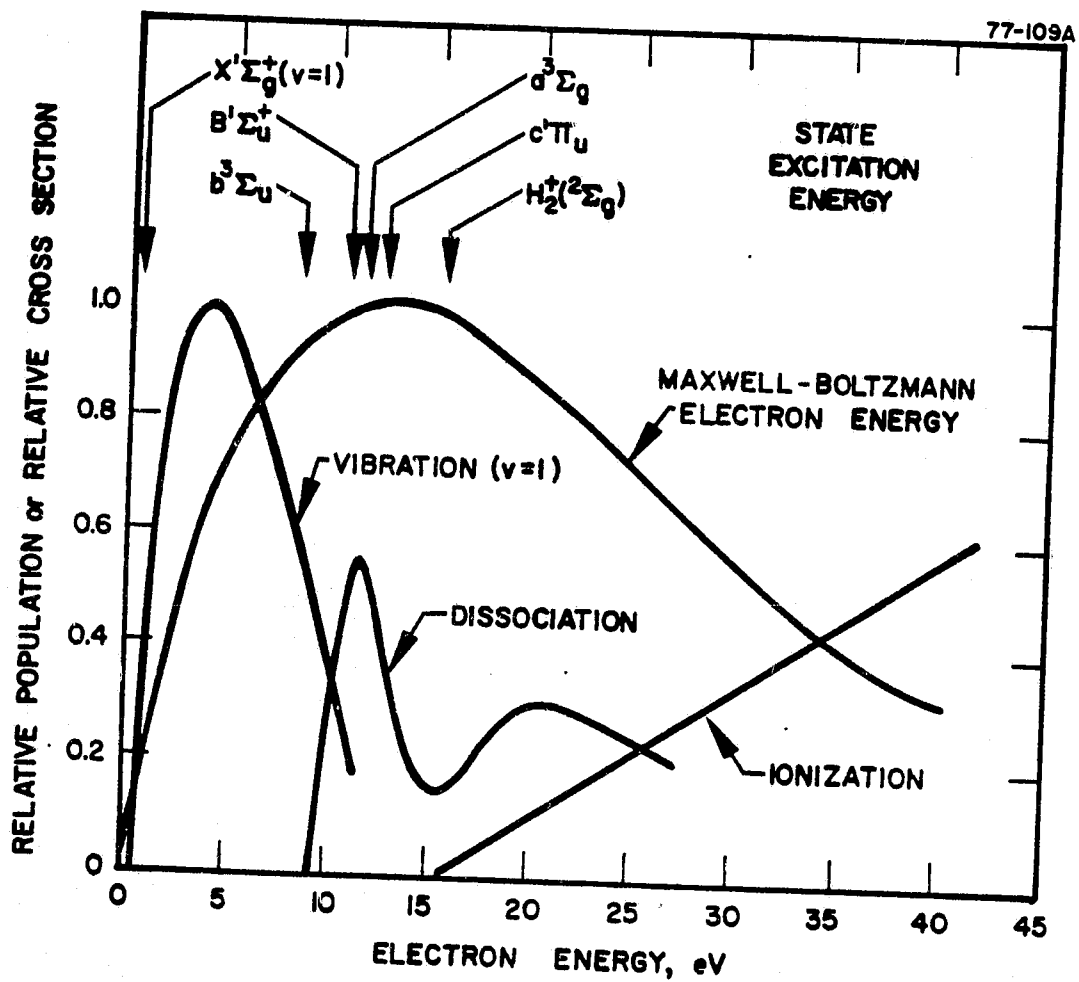
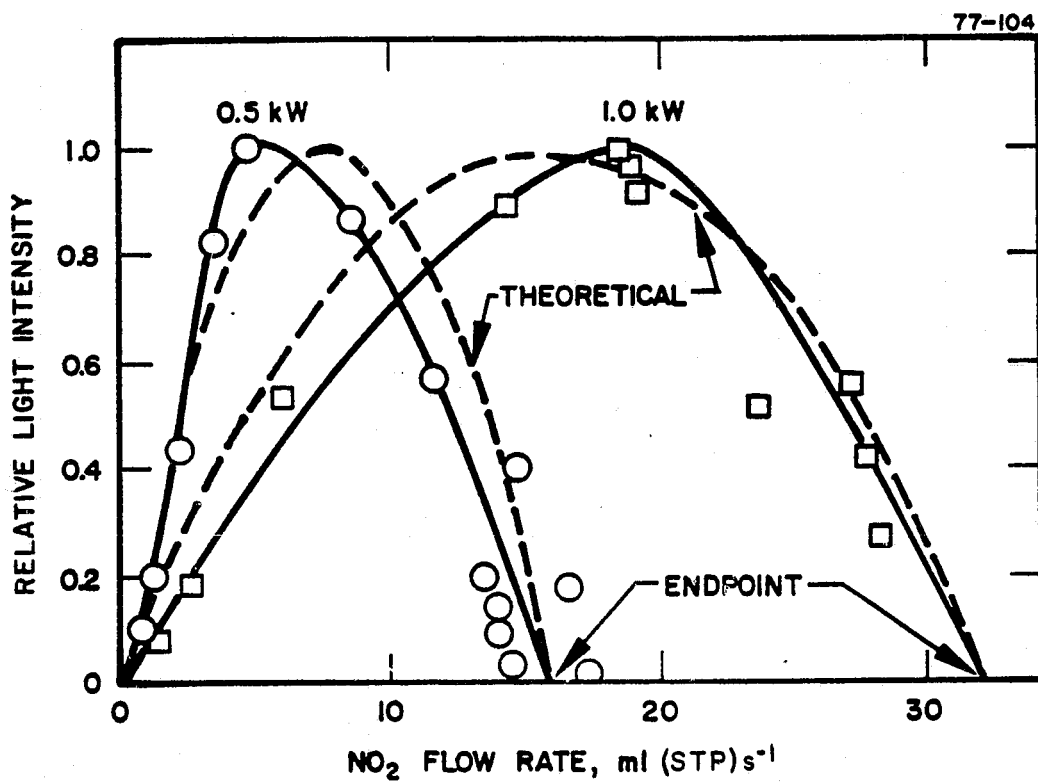


FIGURE 17 CROSS SECTIONS AND ONSET ENERGIES IN H₂

FIGURE 18 NO₂ TITRATION CURVES

Nozzle no. 5, anode, no injector tubes, $P_u = 50$ Torr;
 $P_d = 24$ Torr; $\dot{m}_{H_2} = 64$ mmol s⁻¹.

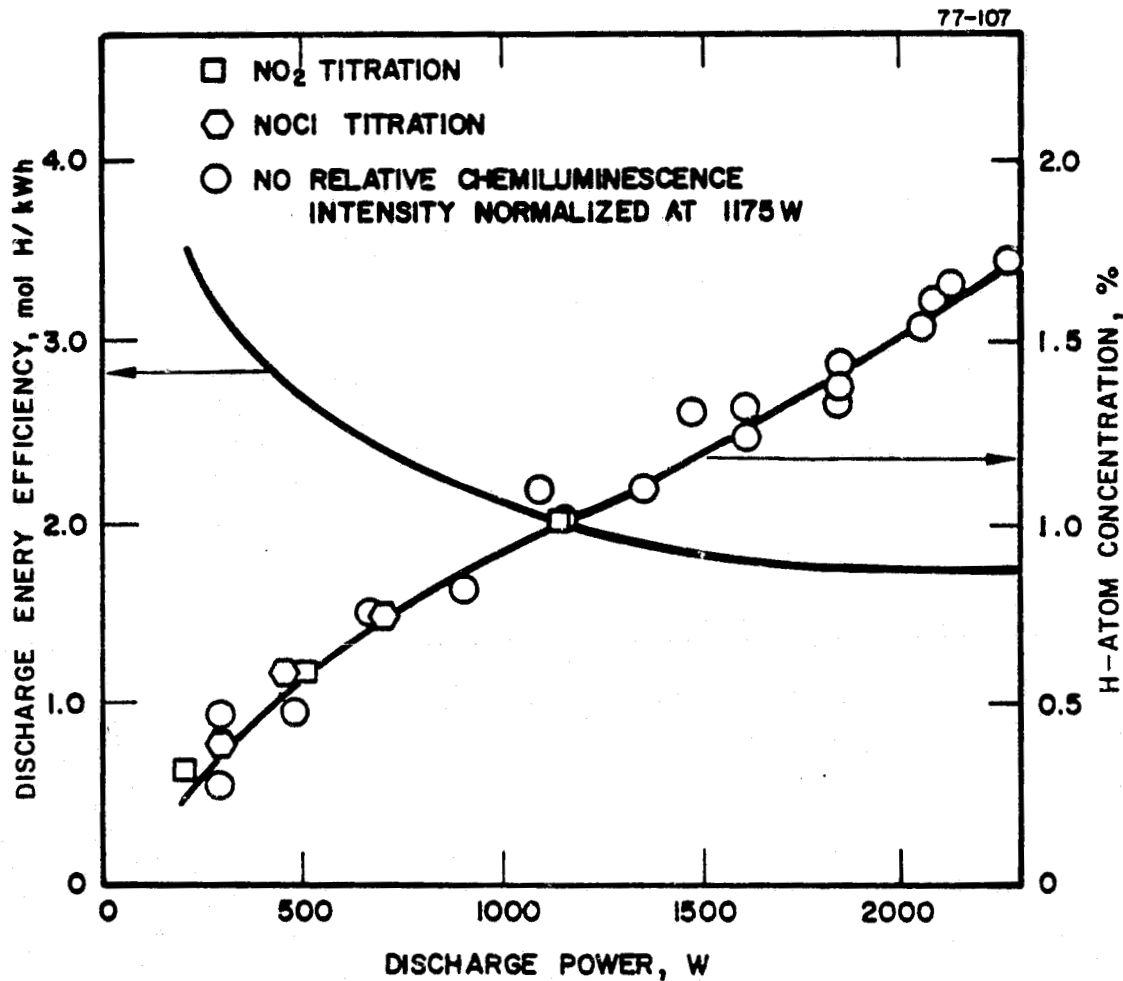


FIGURE 19 DISCHARGE ENERGY EFFICIENCY AND HYDROGEN ATOM YIELD

Nozzle no. 5, anode, angled injector tubes, $P_u = 50$ Torr;
 $P_d = 25$ Torr; $\dot{m}_{H_2} = 64 \text{ mmol s}^{-1}$.

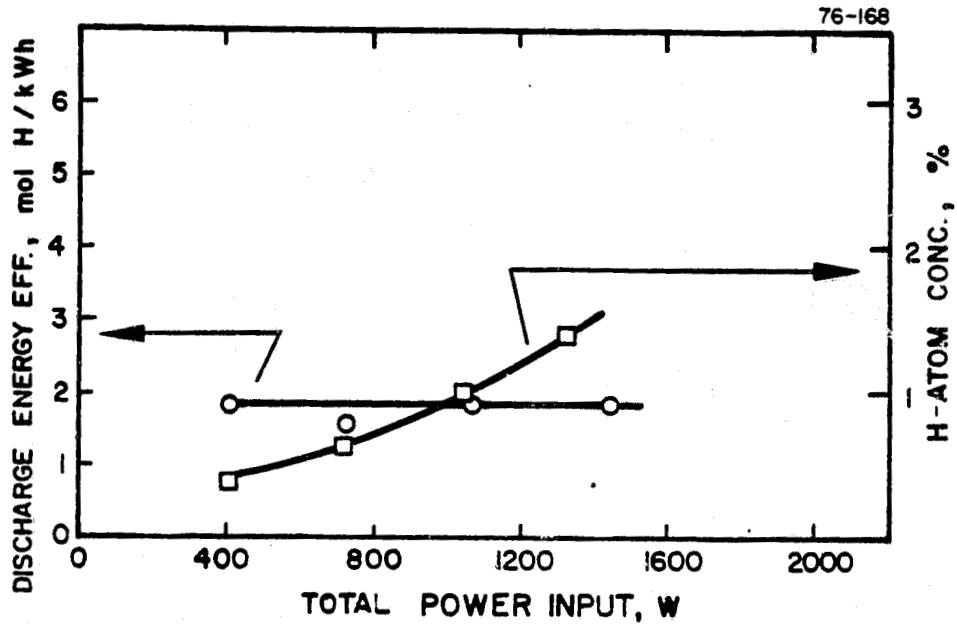


FIGURE 20 DISCHARGE ENERGY EFFICIENCY AND HYDROGEN ATOM YIELD

Nozzle no. 4 cathode -- data of run 3.

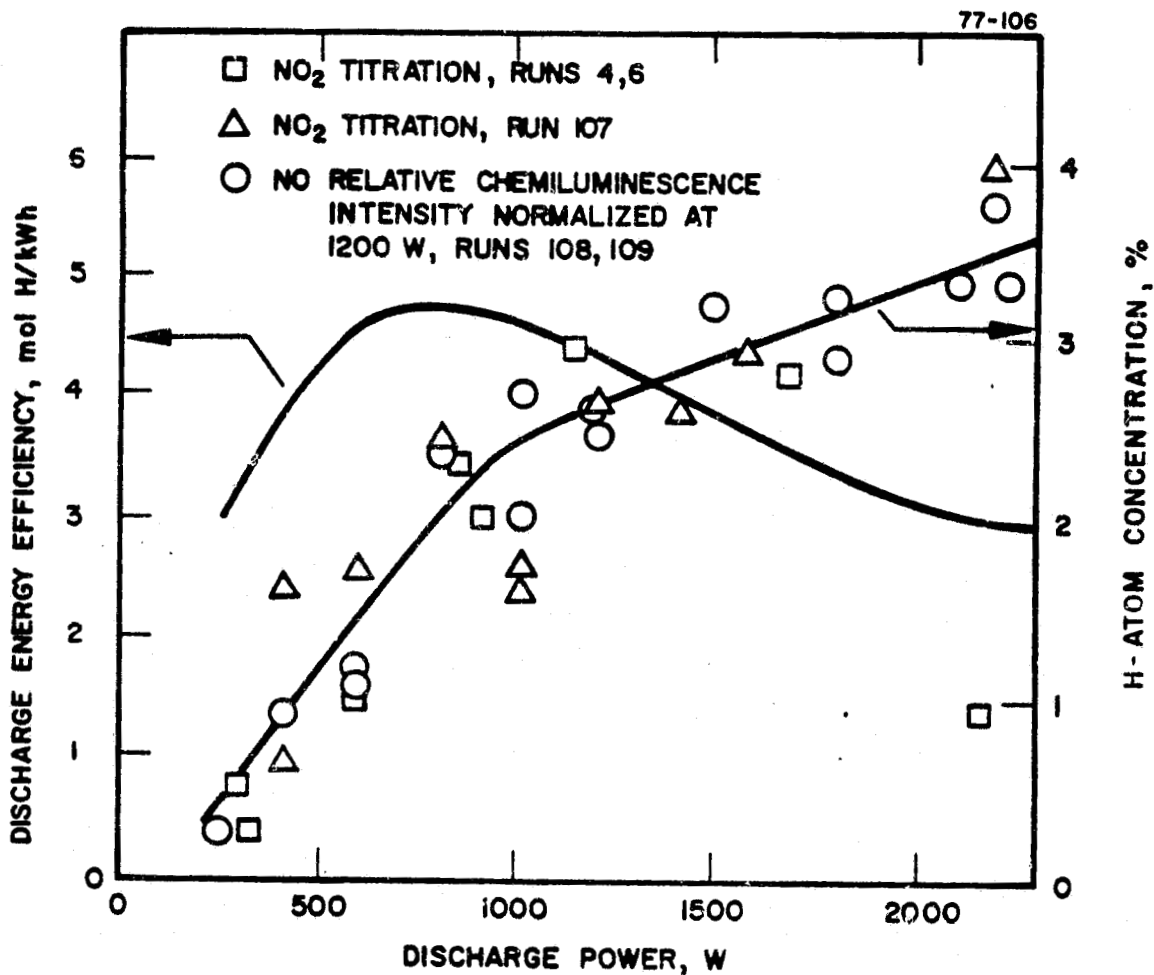


FIGURE 21 DISCHARGE ENERGY EFFICIENCY AND HYDROGEN ATOM YIELD

Nozzle no. 2, anode, $P_u = 50$ Torr; $P_d = 22$ Torr;
 $\dot{m}_{H_2} = 54 \text{ mmol s}^{-1}$.

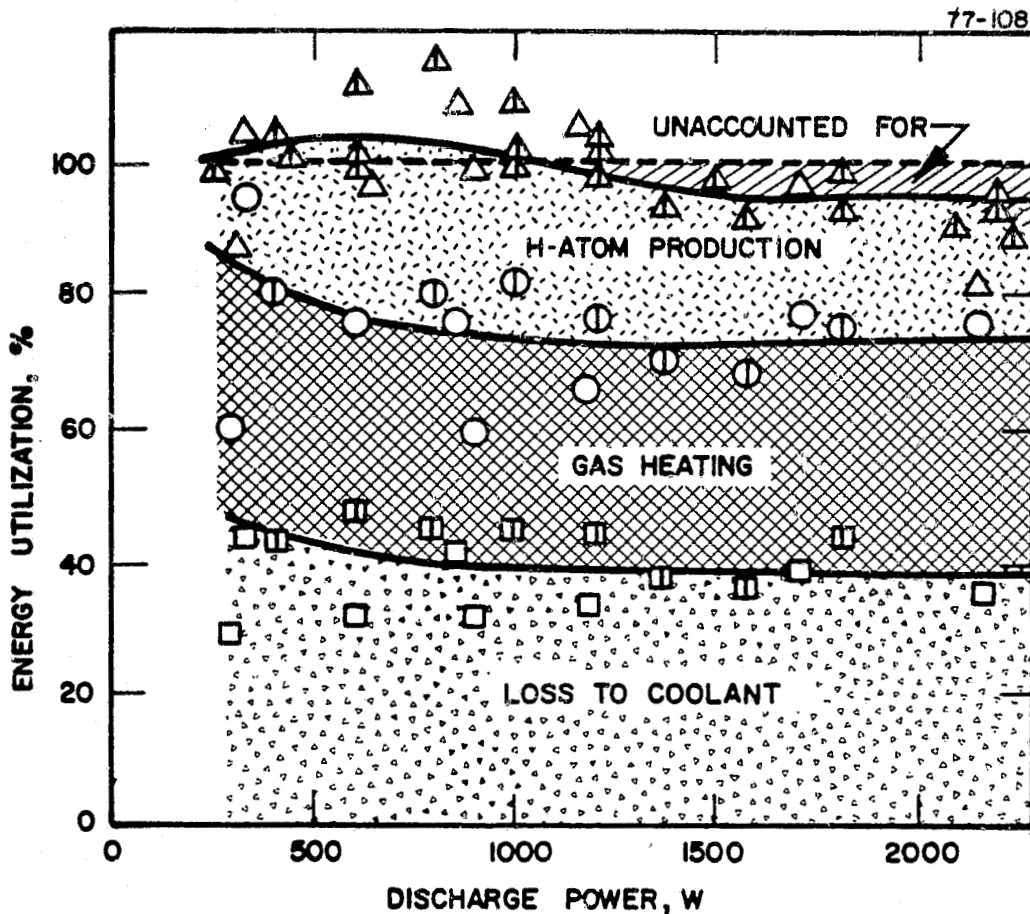


FIGURE 22 DISCHARGE ENERGY DISTRIBUTION

Nozzle no. 2, anode, $P_u = 50$ Torr; $P_d = 22$ Torr;
 $\dot{m}_{H_2} = 54 \text{ mmol s}^{-1}$.

Open symbols - data of runs 4, 6
 Closed symbols - data of runs 107-109

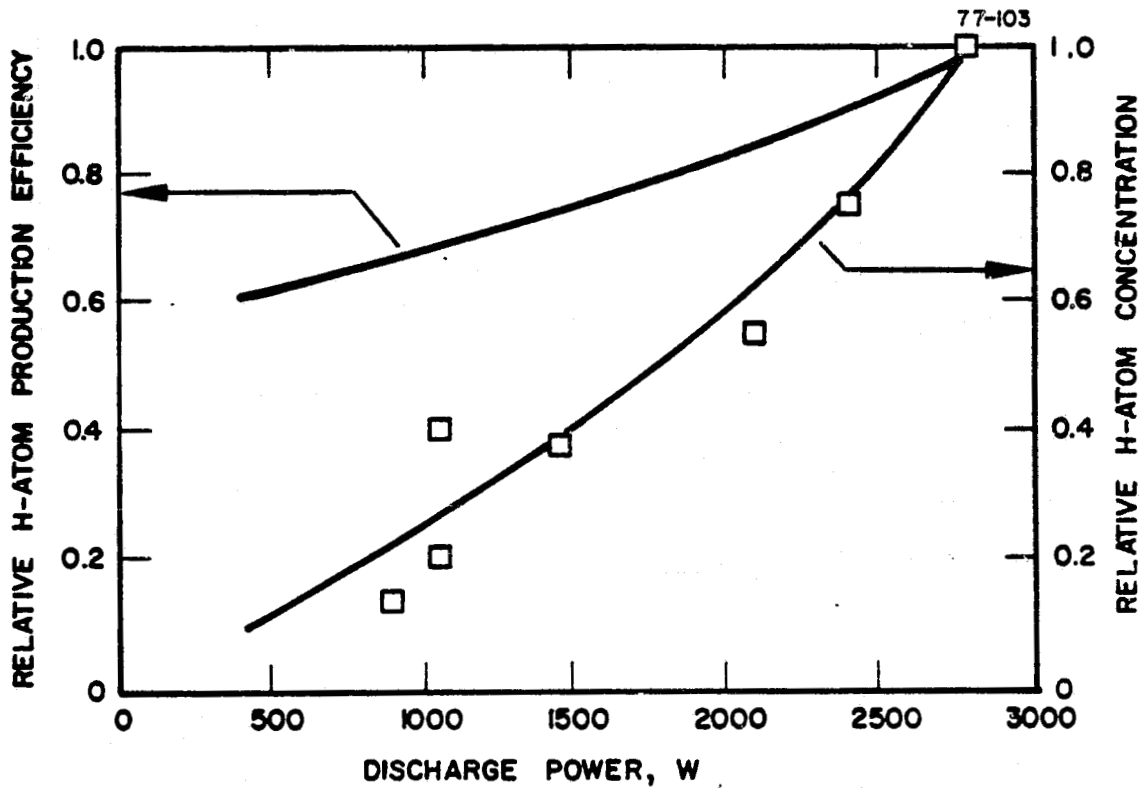


FIGURE 23 DISCHARGE ENERGY EFFICIENCY AND HYDROGEN ATOM YIELD

Nozzle no. 5, anode, angled injector tubes, $P_u = 140$ Torr;
 $P_d = 80$ Torr; $\dot{V}_{H_2} = 183 \text{ mmol s}^{-1}$.

C-2

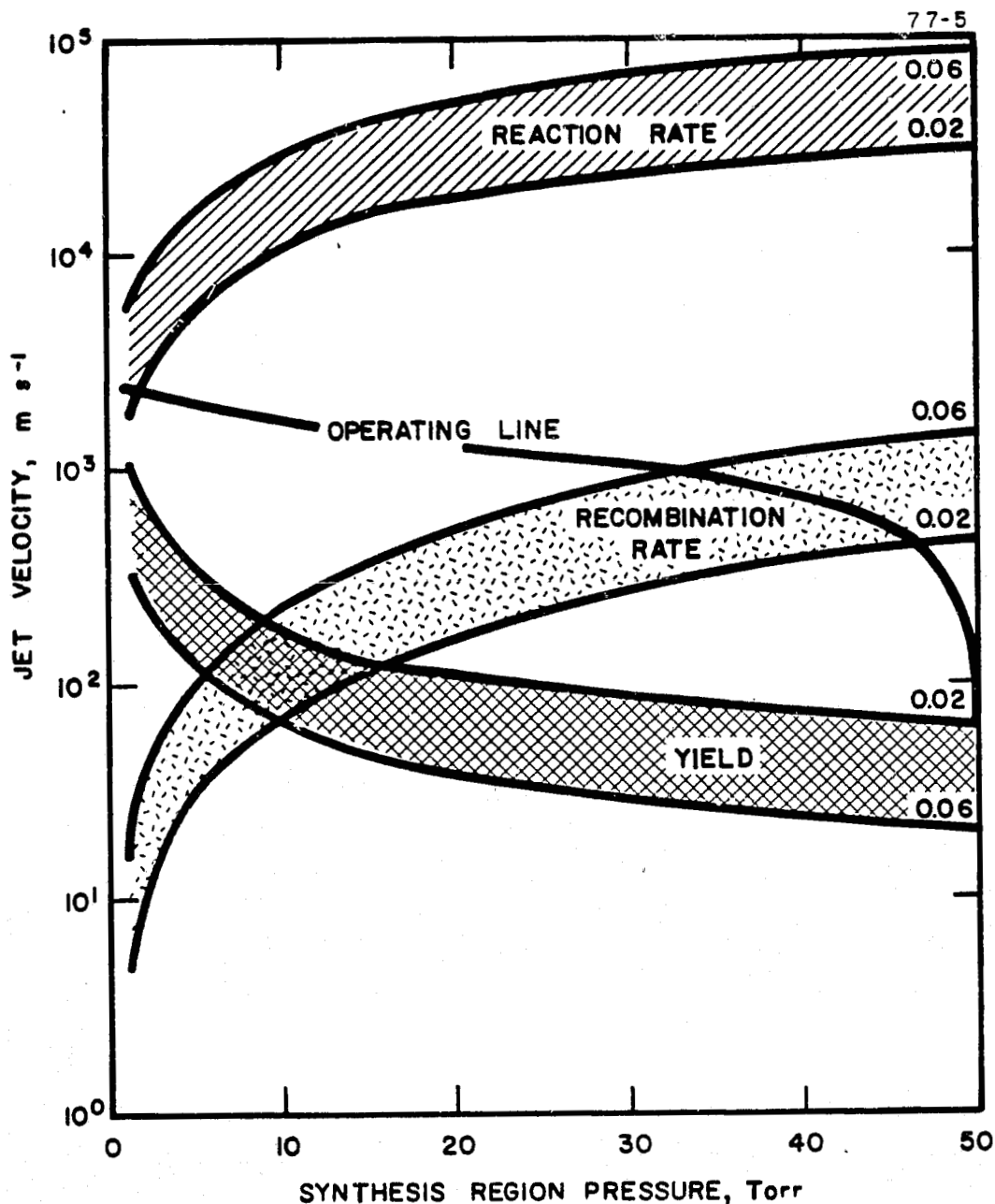


FIGURE 24 LIMITING PERFORMANCE CURVES

$P_U = 50$ Torr, $T_U = 300$ K; $k_R = 1 \times 10^{-11}$ ml s⁻¹;
 $X_H = 0.02$ and 0.06 indicated on curves.

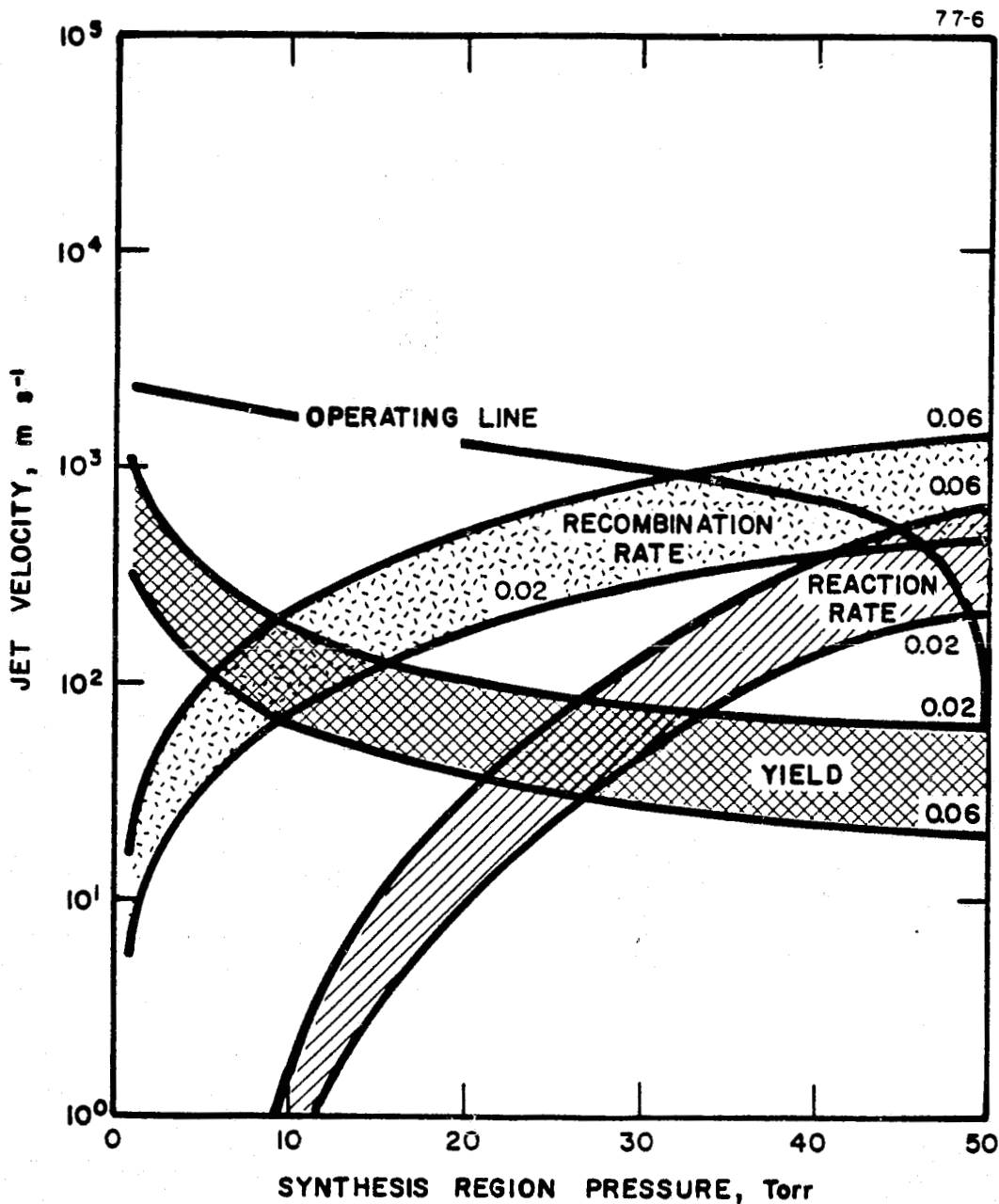


FIGURE 25 LIMITING PERFORMANCE CURVES

$P_u = 50$ Torr, $T_u = 300$ K; $k_R = 3 \times 10^{-10} \exp(-2500/T)$
 ml s^{-1} ; $X_H = 0.02$ and 0.06 indicated on curves.

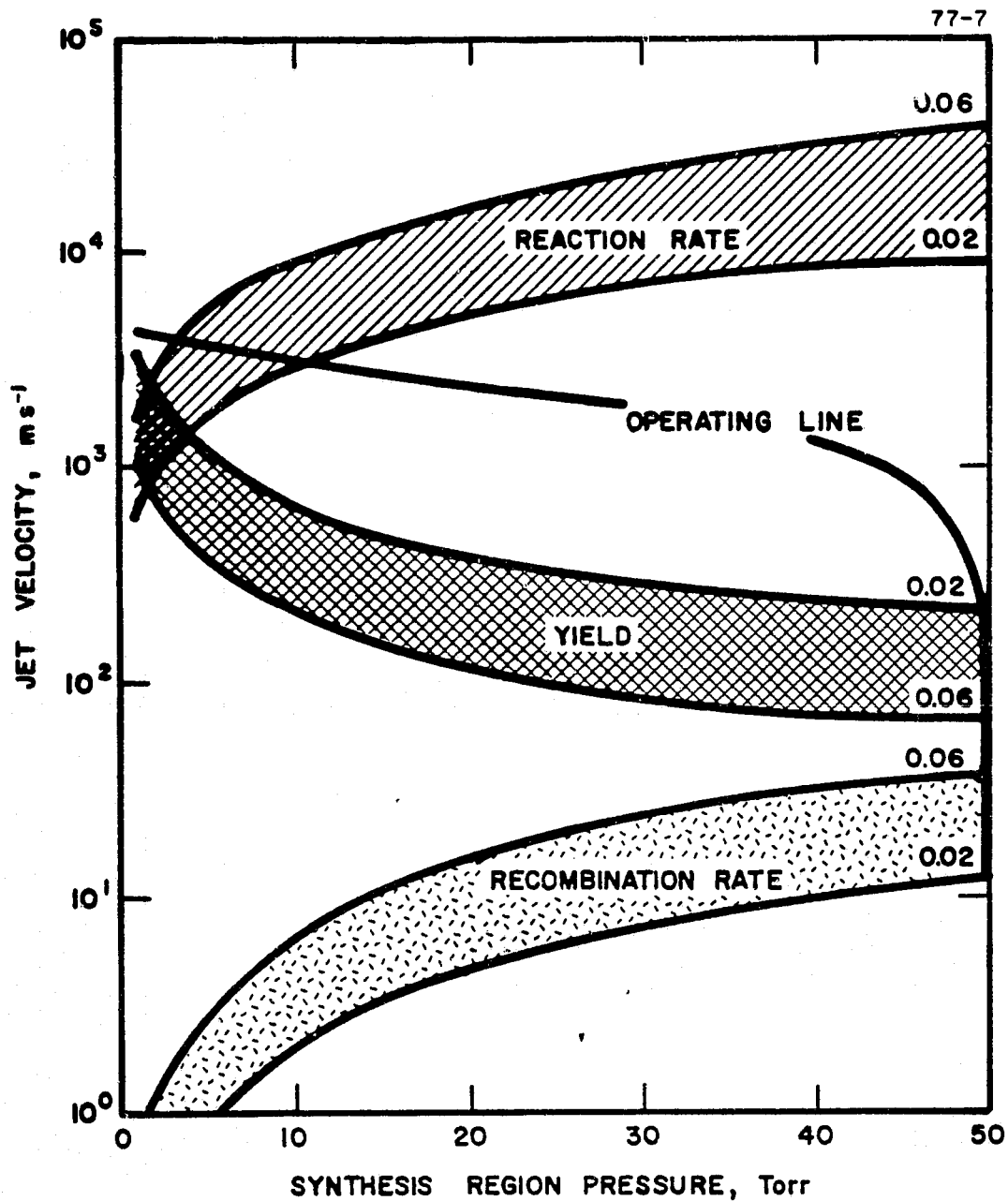


FIGURE 26 LIMITING PERFORMANCE CURVES

$P_u = 50$ Torr, $T_u = 1000$ K; $k_R = 1 \times 10^{-11}$ ml s^{-1} ;
 $X_H = 0.02$ and 0.06 indicated on curves.

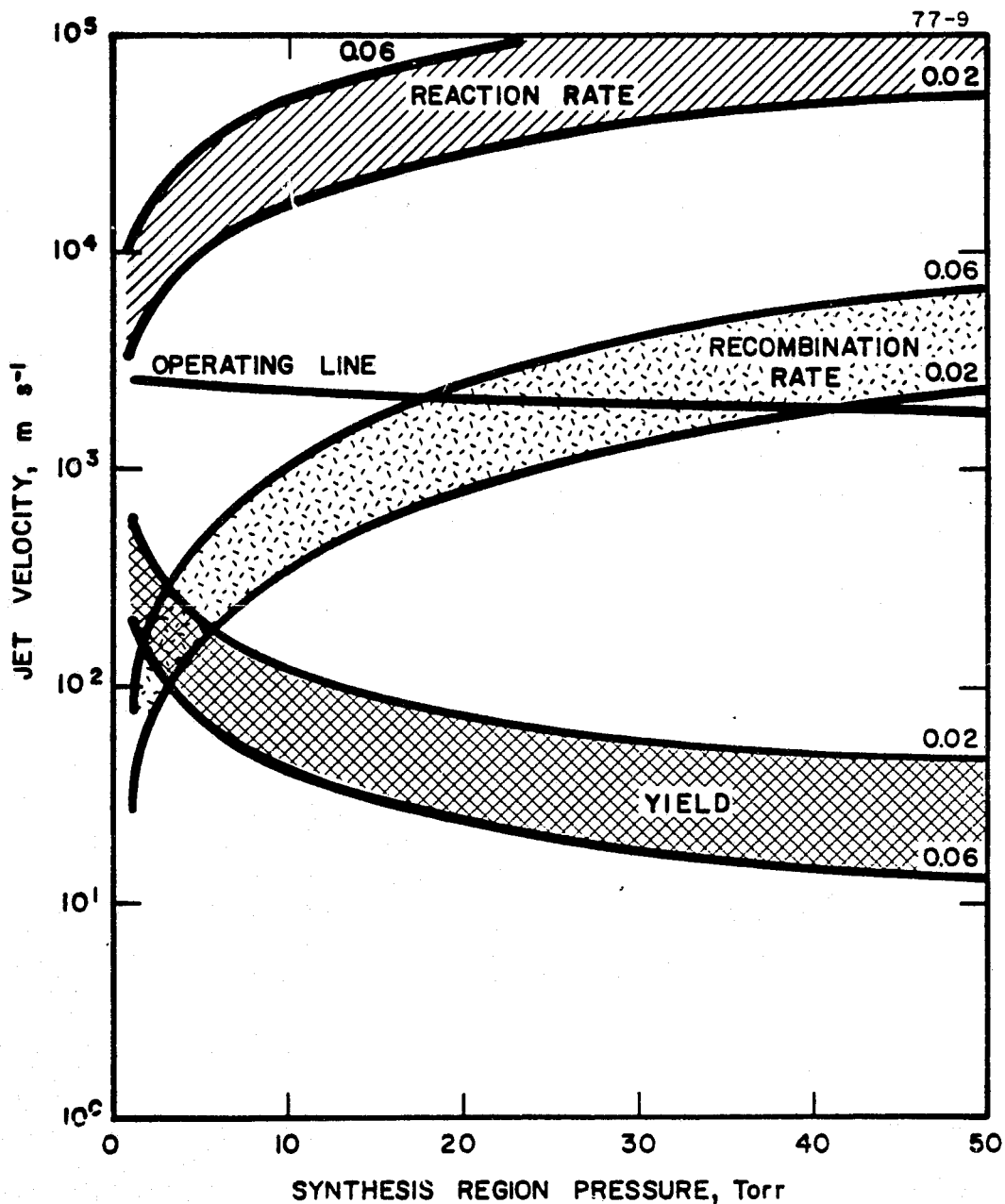


FIGURE 28 LIMITING PERFORMANCE CURVES

$P_u = 300$ Torr, $T_u = 300$ K; $k_R = 1 \times 10^{-11}$ ml s $^{-1}$;
 $X_H = 0.02$ and 0.06 indicated on curves.

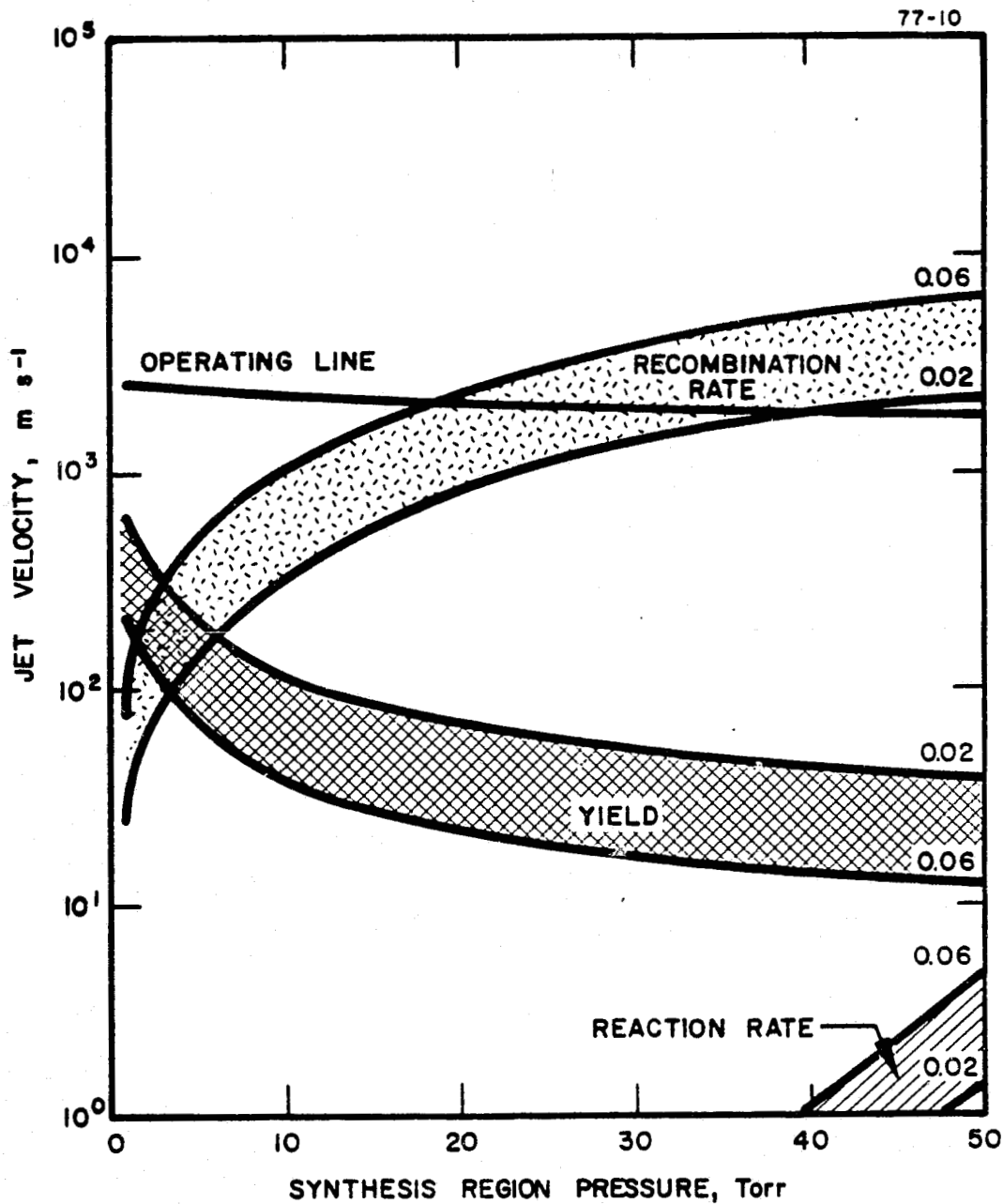


FIGURE 29 LIMITING PERFORMANCE CURVES

$P_u = 300$ Torr, $T_u = 300$ K; $k_R = 3 \times 10^{-10} \exp(-2500/T)$
 ml s^{-1} ; $X_H = 0.02$ and 0.06 indicated on curves.

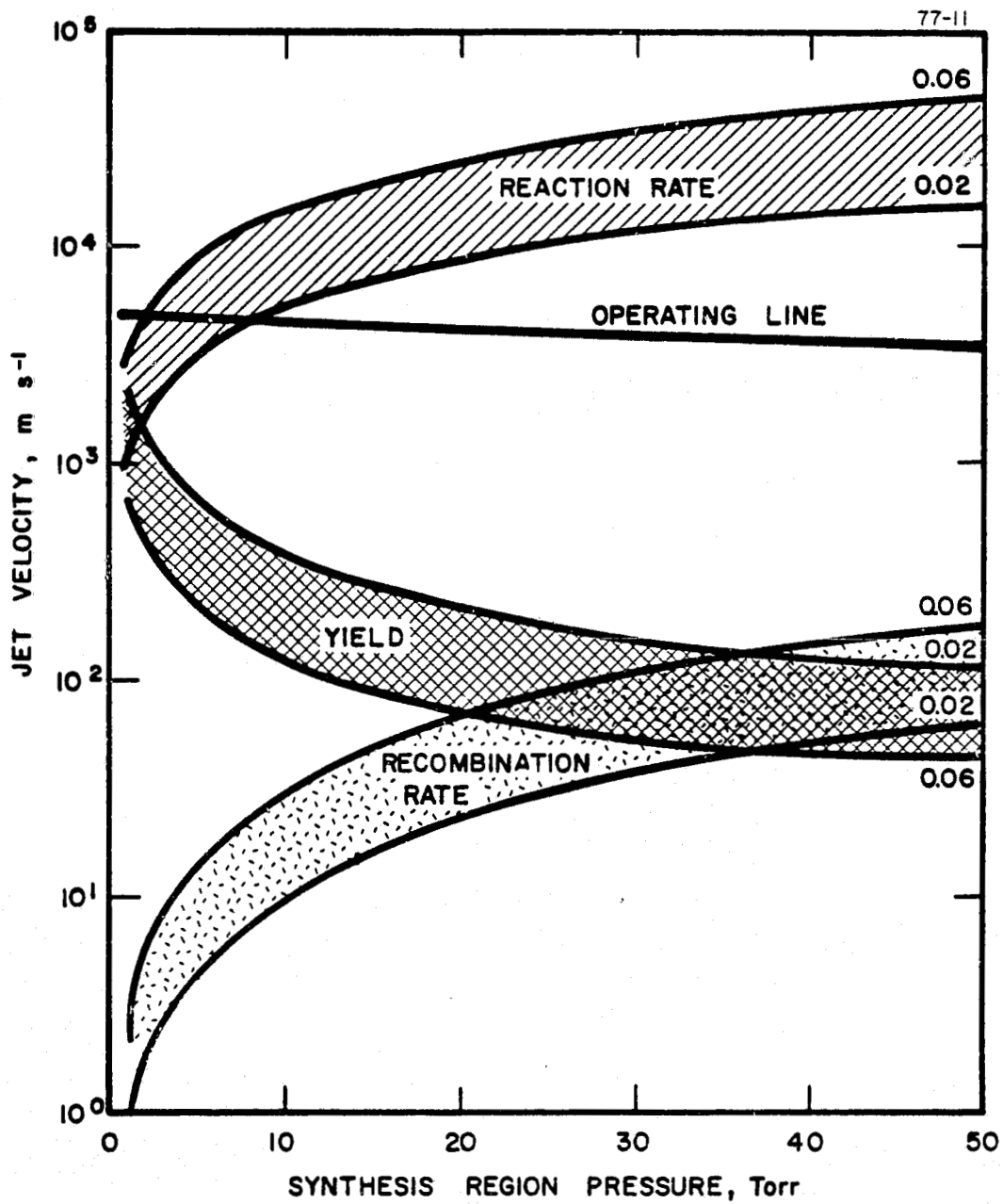


FIGURE 30 LIMITING PERFORMANCE CURVES

$P_u = 300$ Torr, $T_u = 1000$ K; $k_R = 1 \times 10^{-11}$ ml s⁻¹;
 $X_H = 0.02$ and 0.06 indicated on curves.

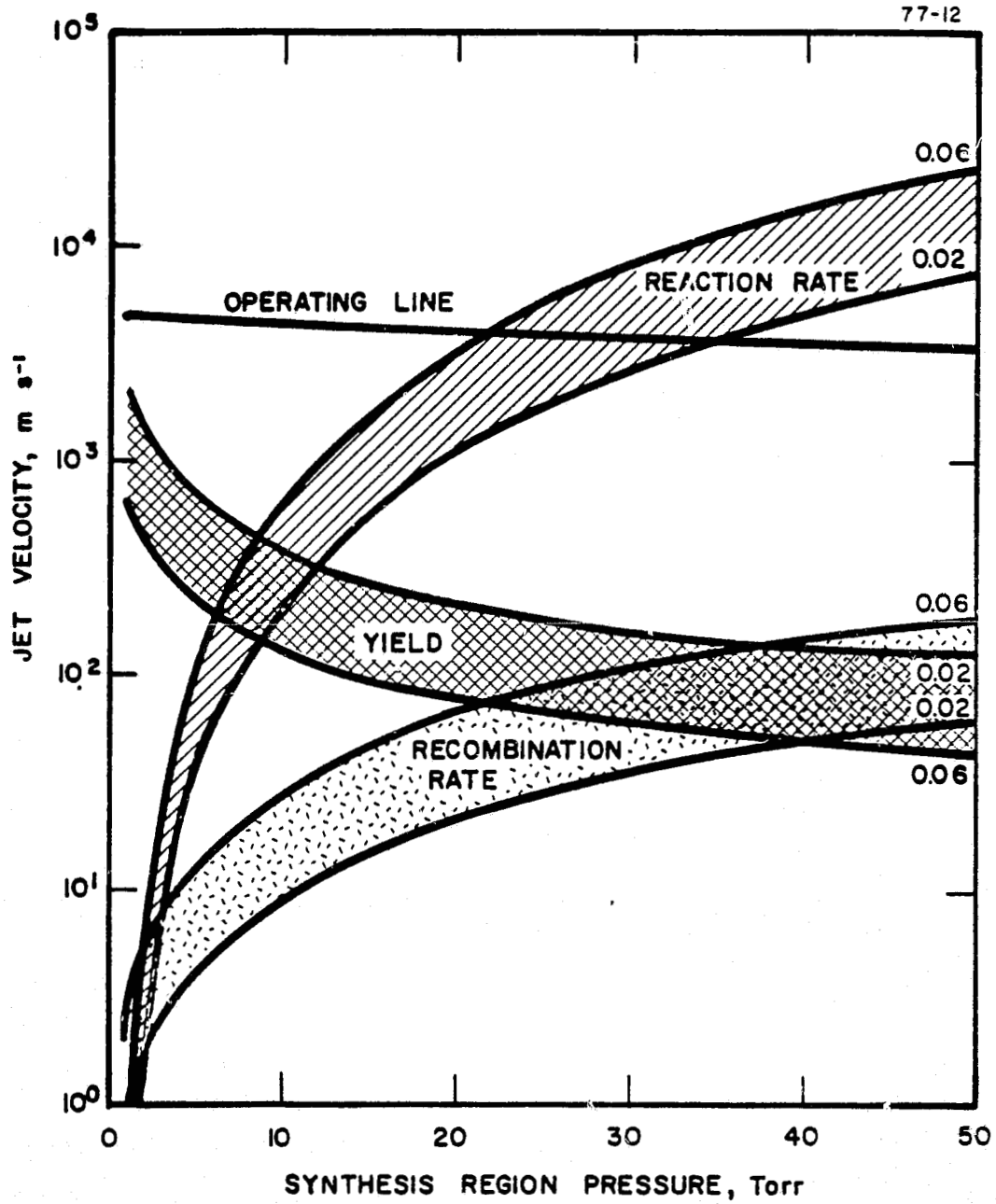


FIGURE 31 LIMITING PERFORMANCE CURVES

$P_u = 300$ Torr, $T_u = 1000$ K; $k_R = 3 \times 10^{-10} \exp(-2500/T)$
 $ml\ s^{-1}$; $X_H = 0.02$ and 0.06 indicated on curves.

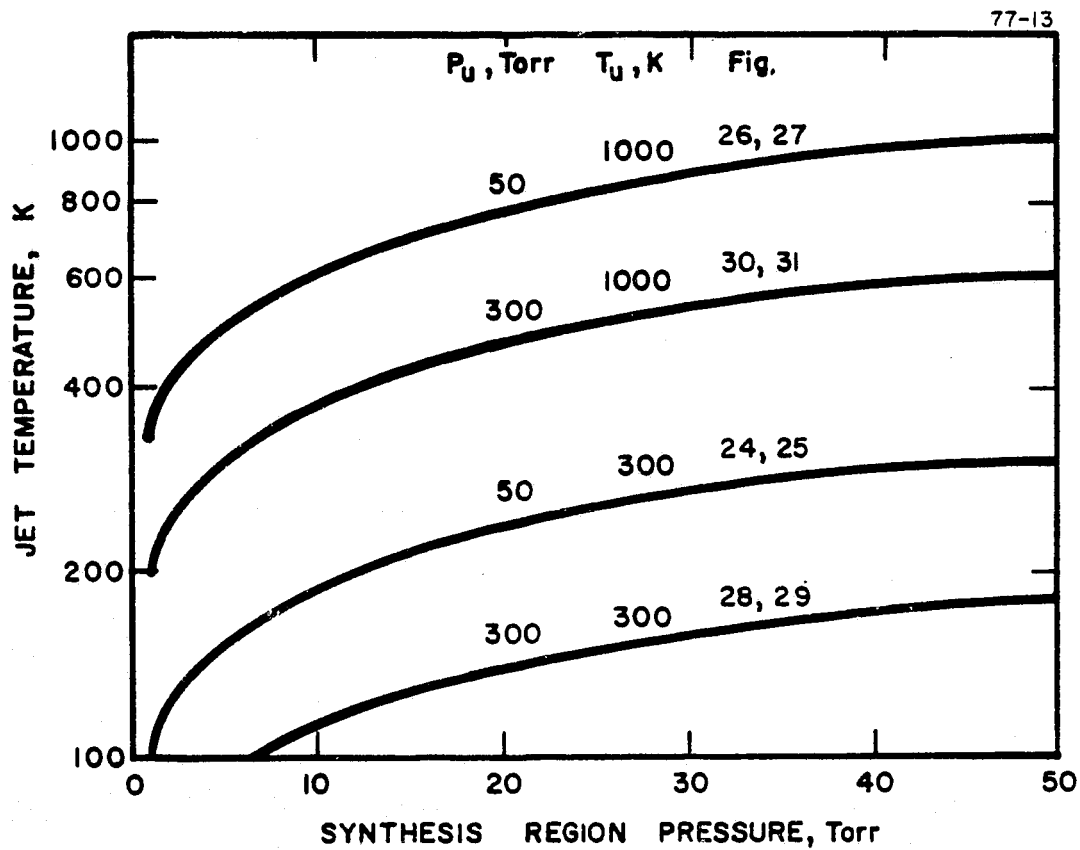


FIGURE 32 CALCULATED JET TEMPERATURES
 Conditions correspond to Figs. 24 through 31.

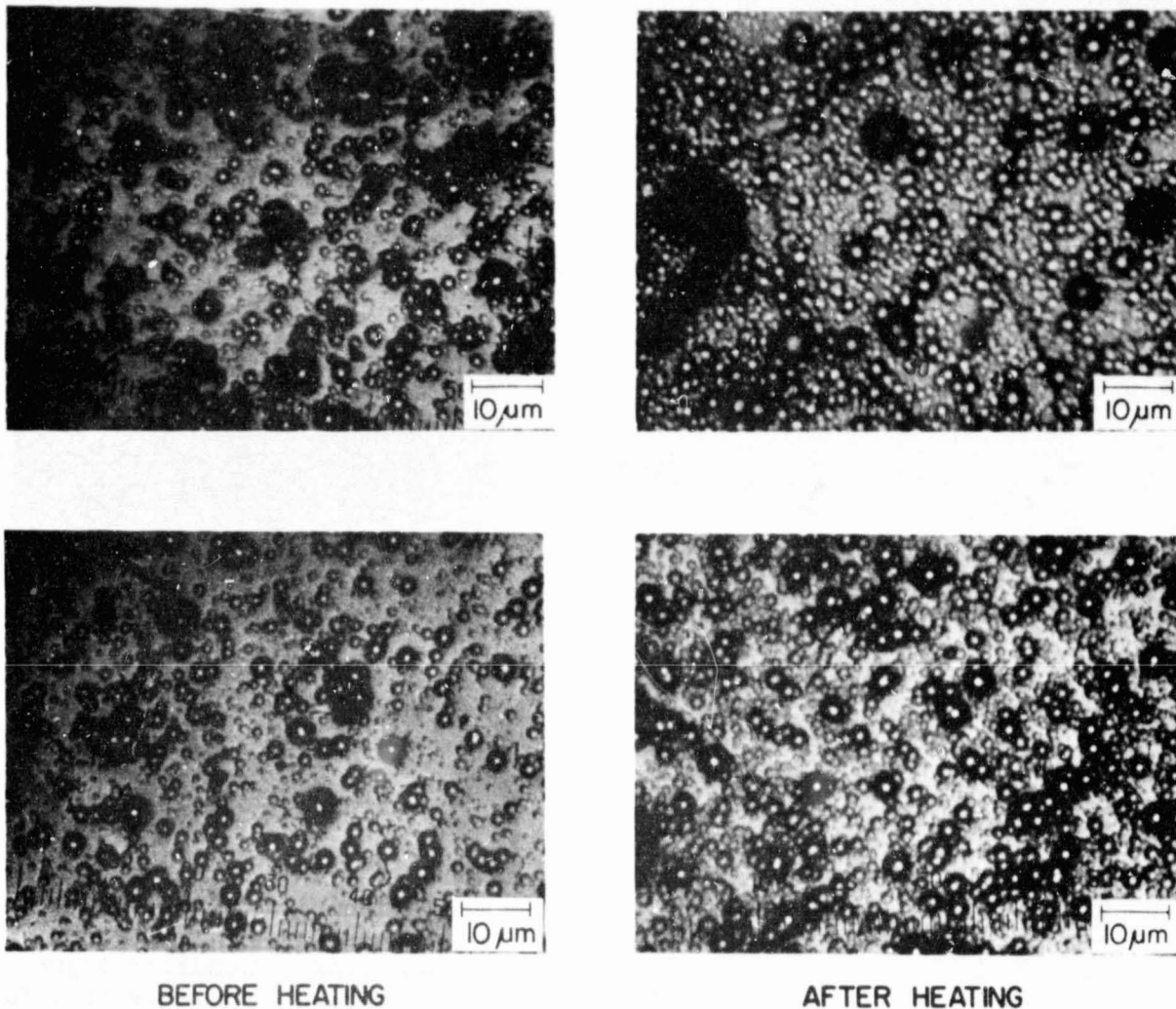
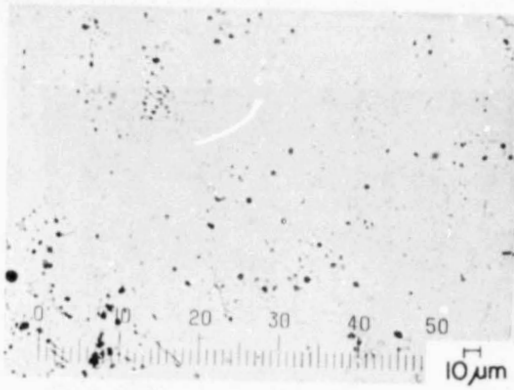


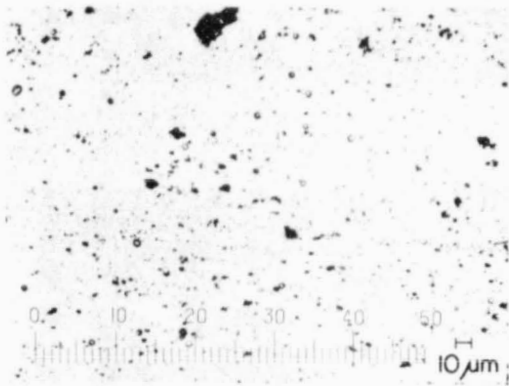
FIGURE 33 EFFECT OF HEATING SEMICONDUCTOR GRADE SiCl_4 DEPOSIT TO 820 K FOR 22 HR

Run 122
Front lighting
Two sets of photographs because part of deposit cracked and part did not.

ORIGINAL PAGE IS
OF POOR QUALITY

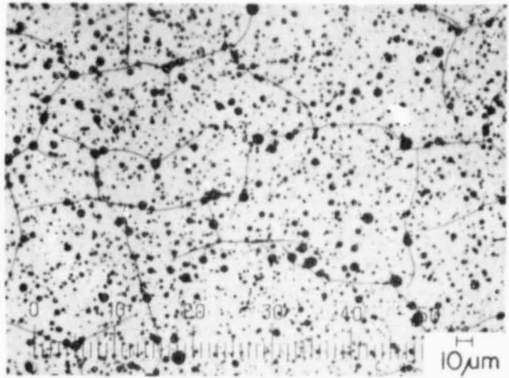
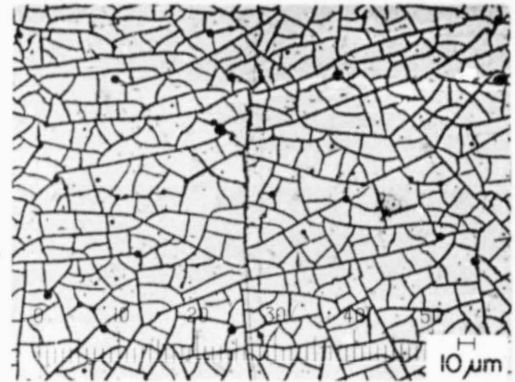


3 min

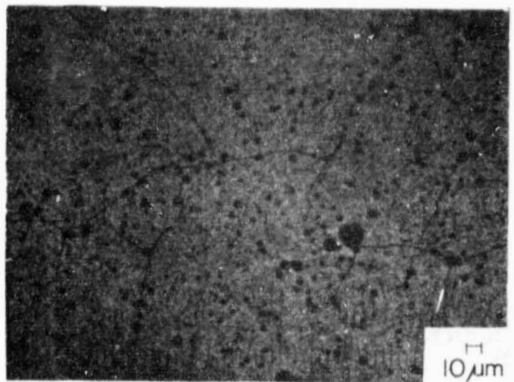


9 min

1220 K
for 2.5 hr



15 min



27 min

FIGURE 34 EFFECT OF EXPOSURE TIME ON SILICON FILMS DEPOSITED FROM SiCl_4

Runs 142, 143, 144, 145, 151

Reaction exposure period as indicated at each photograph. Bright field transmitted light. Same photographic exposure time for each photograph.

ORIGINAL PAGE IS
OF POOR QUALITY

78-27

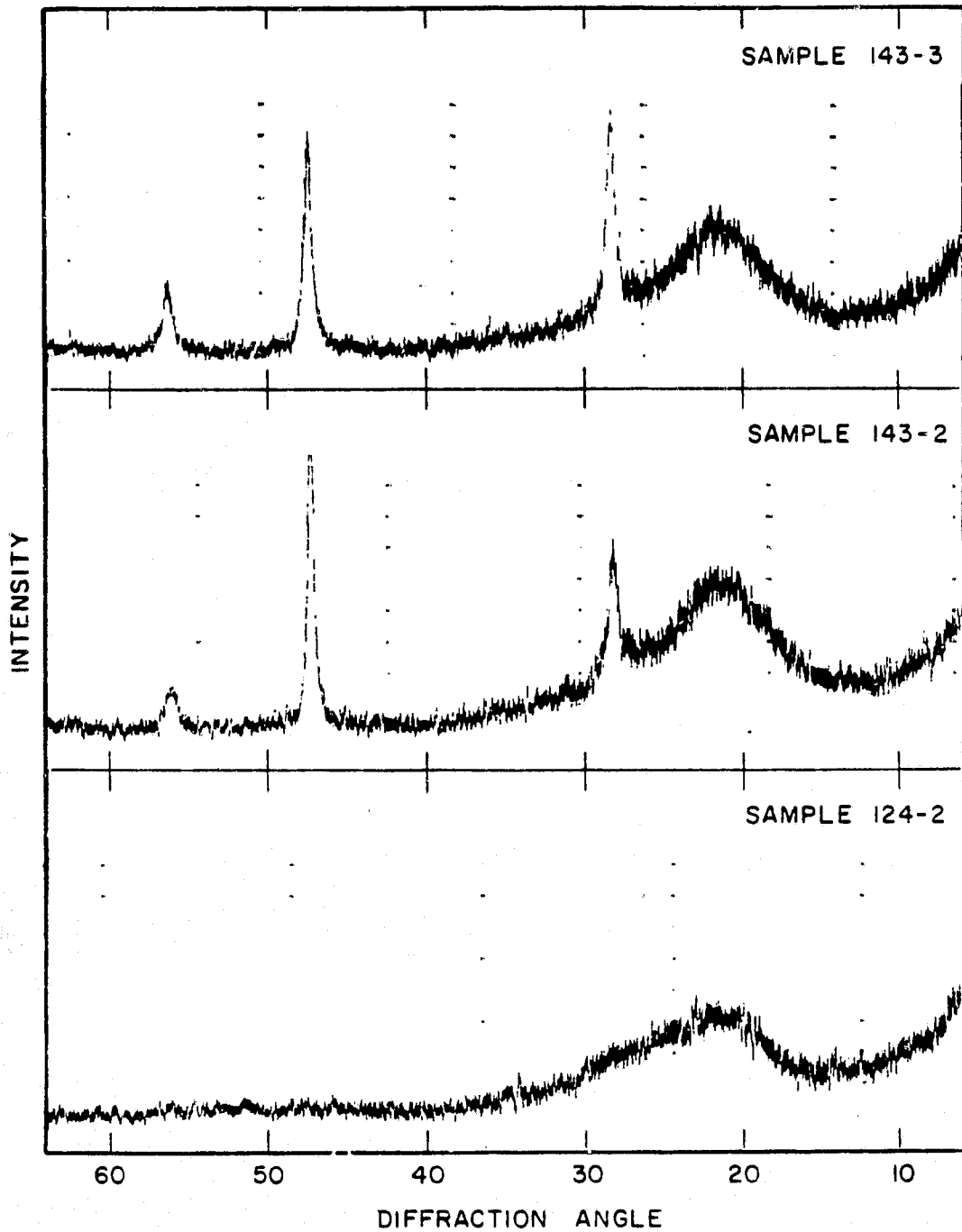


FIGURE 35 X-RAY DIFFRACTION PATTERNS FOR SILICON FILMS

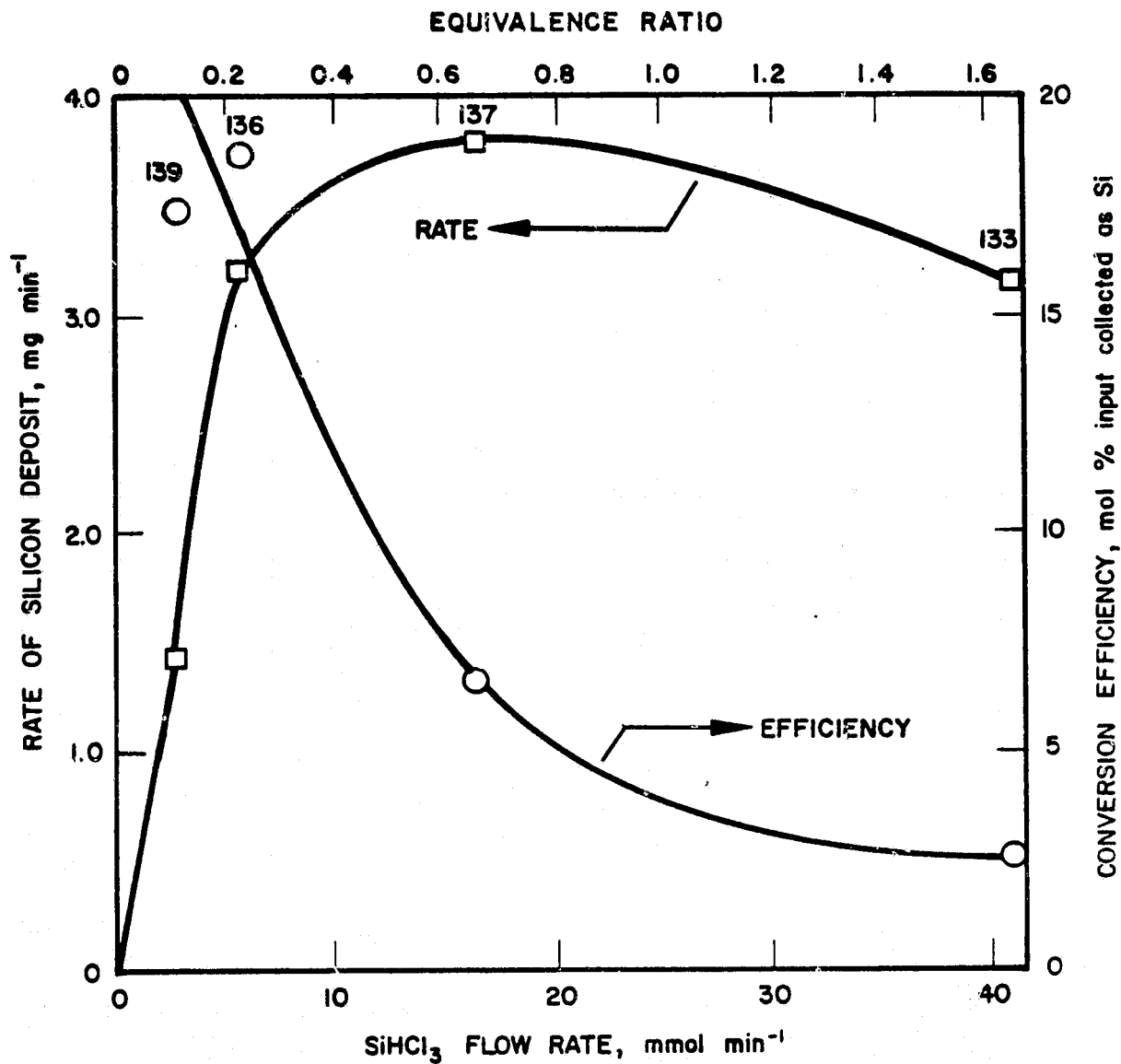


FIGURE 36 RATE OF SILICON DEPOSIT FROM SiHCl_3
Run numbers indicated above points.

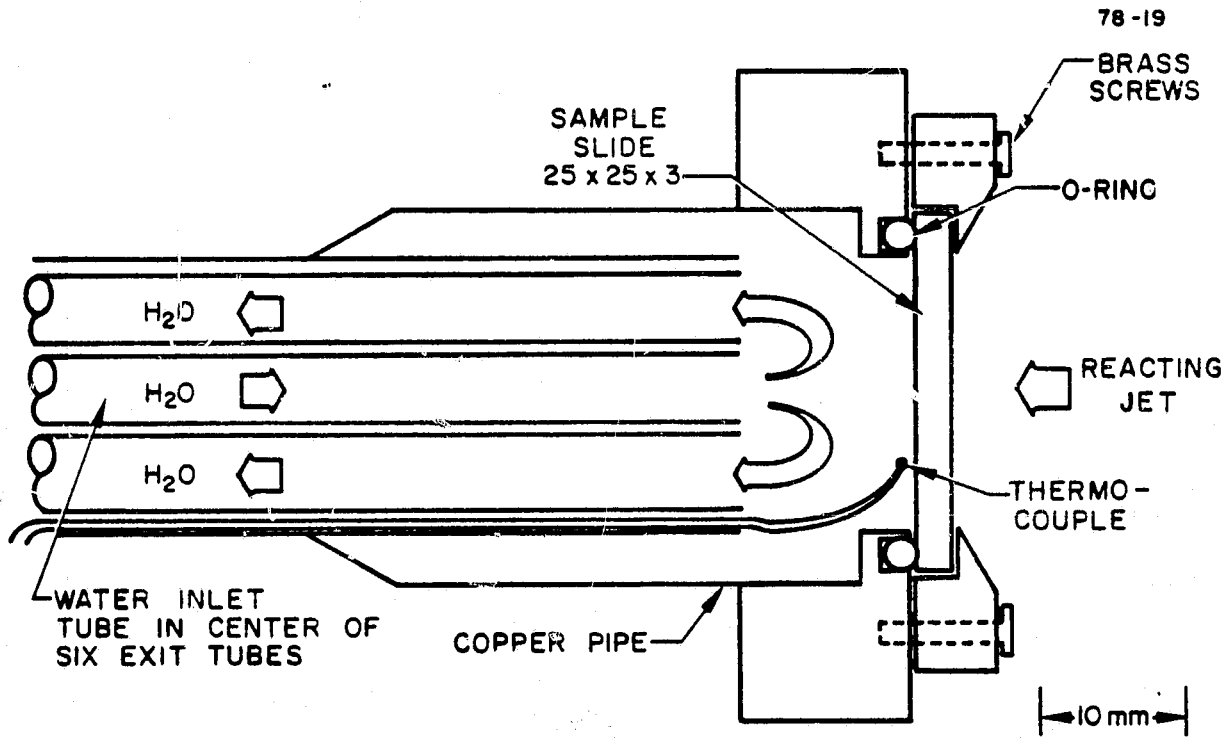


FIGURE 37 WATER-COOLED SAMPLE HOLDER

Dimensions in mm.

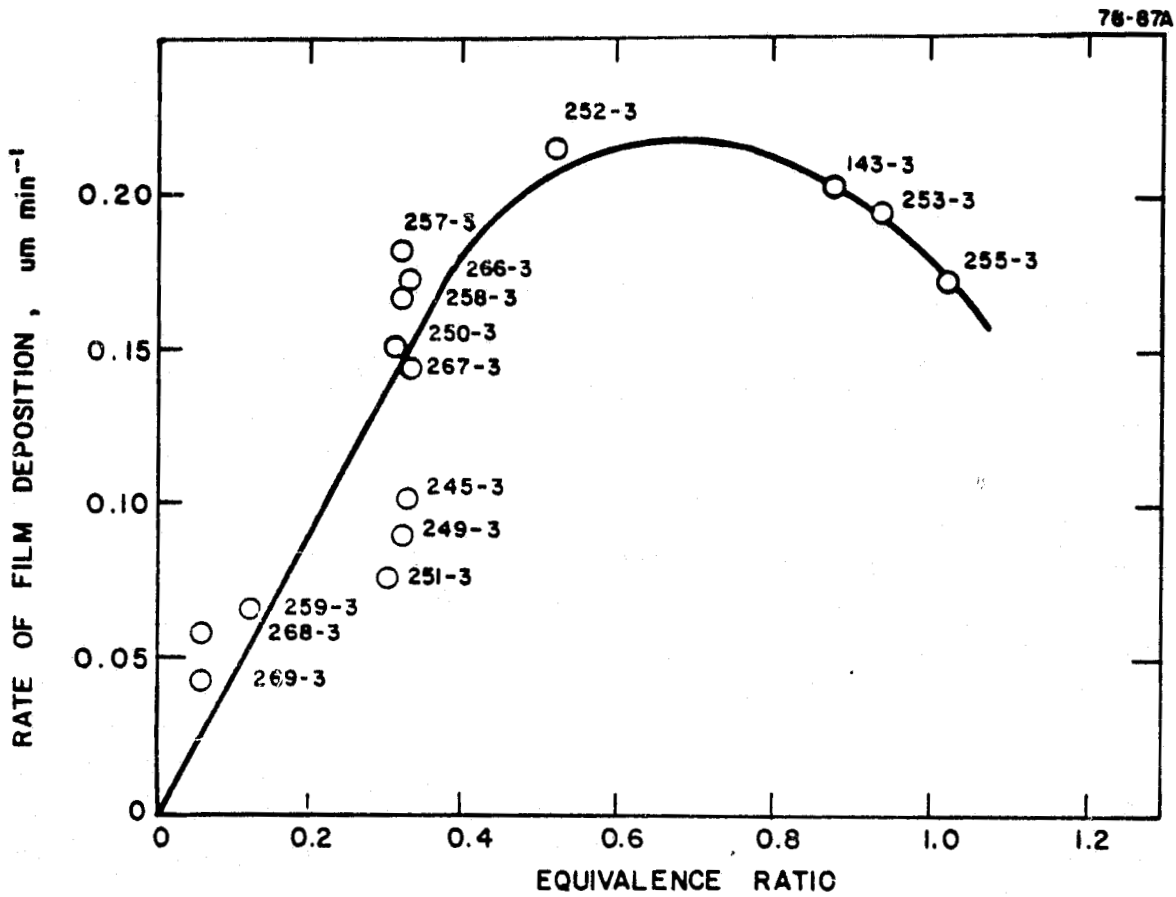


FIGURE 38 RATE OF FILM DEPOSITION FROM SiCl_4
 Run numbers indicated above points.

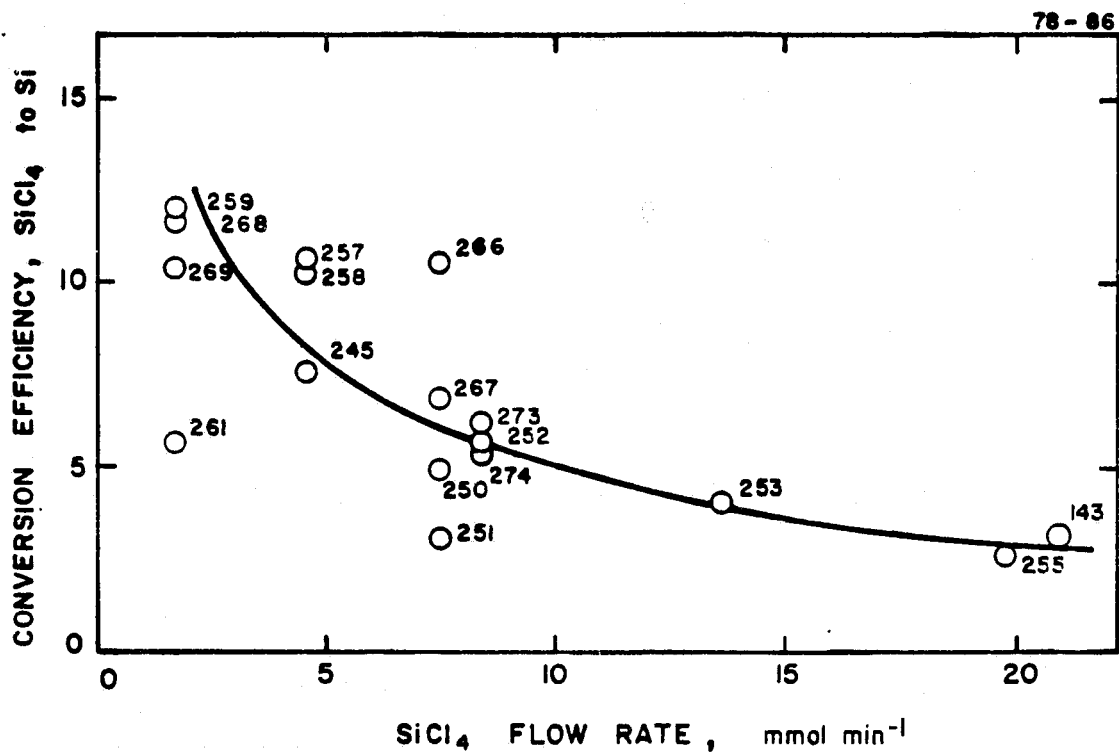


FIGURE 39 CONVERSION EFFICIENCY, SiCl_4 TO Si
Run numbers indicated above points.

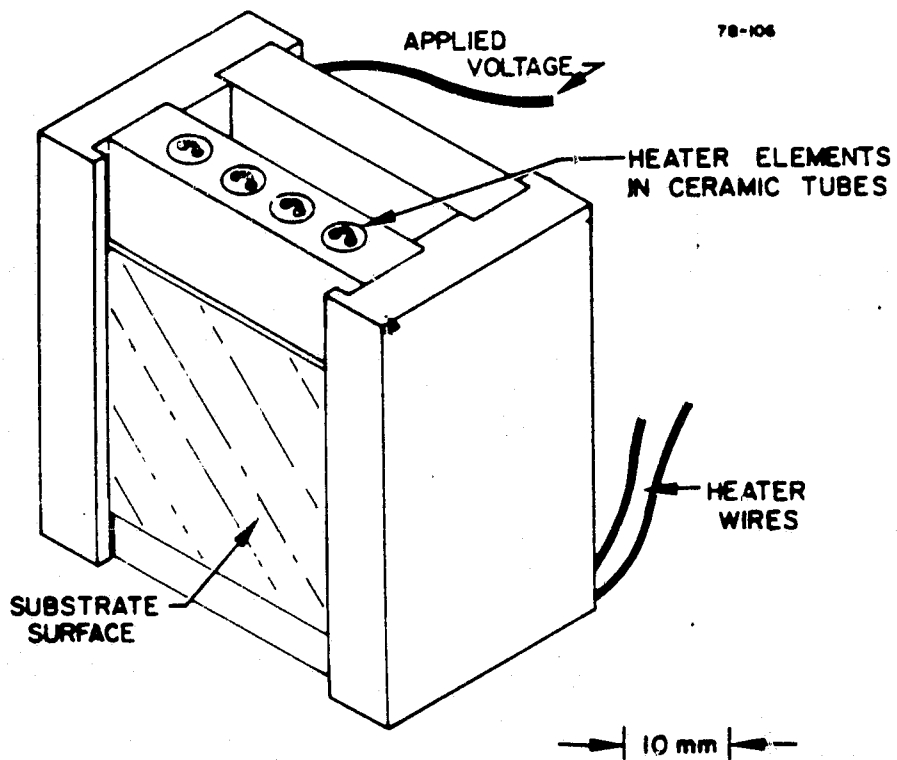
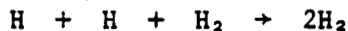


FIGURE 40 SUBSTRATE HOLDER

APPENDIX AH-ATOM DECAY

The rate of H-atom decay through the apparatus has been calculated assuming three-body recombination and reaction on the walls.

For the three-body recombination



with H_2 in excess:

$$\frac{C_{\text{H}}}{C_{\text{H}}^0} = (1 + C_{\text{H}_2}^0 k_{\text{H}} t)^{-1}$$

where:

- C_{H} = concentration of H atoms at any time t
- C_{H}^0 = initial concentration of H atoms at $t = 0$
- $C_{\text{H}_2}^0$ = concentration of H_2 , a constant
- k_{H} = recombination coefficient for H atoms, given by Kaufman²⁷ as

$$9.5 \times 10^{-33} \left(\frac{300}{T} \right) \text{ ml}^2 \text{ s}^{-1}$$

For recombination of H atoms on the wall the decay of H atoms is given by:

$$\frac{C_{\text{H}}}{C_{\text{H}}^0} = e^{-k_{\text{w}} t}$$

where k_{w} = the wall recombination rate. When the process is diffusion controlled, there are two conditions, given by solving the flow equation.³⁹

These are:

For plug flow:

$$k_{\text{w}}^{\text{p}} = \left(\frac{23.2}{d} \right) D_{\text{H}}$$

where:

- d = diameter of the duct
- D_{H} = diffusion coefficient for H atoms in H_2
- = $1 \times 10^3 \left(\frac{T}{300} \right)^{3/2}$ at 1 Torr estimated from the diffusion coefficient of Ar in H_2 .⁴⁰

For laminar flow:

$$k_w^L = \left(\frac{14.6}{d^2} \right) D_H$$

If the process is limited by recombination on the wall, i.e., if the flux of H atoms to the wall exceeds the wall recombination rate, the expression is⁴¹:

$$k_w = \frac{\gamma}{2d} \bar{c}$$

where:

- γ = wall recombination coefficient for H atoms
- = $\approx 10^{-3}$ (300-700 K) for quartz²⁶
- = 2×10^{-5} (300 K) to 5×10^{-4} (200 K) for Pyrex²⁶
- \bar{c} = molecular velocity $(8kT/\pi m_H)^{1/2}$

The time, t , to be used in these equations is given by:

$$t = \left(\frac{P_d}{\dot{m} RT} \right) \left(\frac{\pi d^2}{4} \right) l$$

where:

- P_d = pressure
- R = gas constant
- \dot{m} = molar flow rate of H₂
- l = length of duct.

For runs 11-18 (see Table VI, Section V.C) in which products were collected in liquid nitrogen traps, the decay of H atoms prior to reaching the traps can be estimated from the above. For these experiments (cf., Fig. 4),

- P = 35 Torr
- T = 380 K, calculated for the jet
- C_H^0 = 1%, $6.8 \times 10^{15} \text{ ml}^{-1}$
- \dot{m} = 64 mmol s⁻¹

To calculate the flow time it was assumed that the jet breaks up in about 15 cm and completely fills the tube. The flow time to the first liquid nitrogen trap then becomes about 70 ms. The reduction in H-atom concentration by the time the flow reaches the first liquid nitrogen trap is then, for each of the various decay processes, operating independently of the other:

	C_H/C_H^0
Three-body recombination	0.29
Recombination on the wall	
Plug flow	0.10
Laminar flow	0.19
Wall recombination limited	
Pyrex	0.86
quartz	0.19

Since silicon, polymers, and some SiO_2 are deposited on the wall, it may have a γ larger than any given above. The flow is probably more closely approximated by plug flow than by laminar flow. Thus by the time the first liquid nitrogen trap is reached the H-atom concentration has decayed to less than 20% of its initial value.

This means that the 10 to 15% conversion of SiCl_4 to SiHCl_3 suggested as occurring on the walls of the liquid nitrogen trap (Section V.C) took place after the H-atom concentration had decayed to $< 20\%$ of C_H^0 . Thus, greater yields should be obtainable by moving the traps closer to the nozzle.